EXPERIMENTAL AND ANALYTICAL INVESTIGATION OF TEMPERATURE SENSITIVE PAINTS.

H. D. Schultz

LOCKHEED MISSILES & SPACE COMPANY, INC.

F33615-71-C-1635

TECHNICAL REPORT AFFDL-TR-72-52

June 1972

USAF. Syst Com.

Air Force Flight Dynamics Laboratory
Air Force Systems Command
Wright-Patterson Air Force Base, Ohio

FOREWORD

The study "Experimental and Analytical Investigation of Temperature Sensitive Paints" was performed by Lockheed Missiles & Space Company, Inc., Sunnyvale, California. The work was accomplished under USAF Contract F33615-71-C-1635, Project 1366, "Aeromechanics Technology for Military Aerospace Vehicles," Task 136607, "High Speed Aerodynamic Heating to Military Flight Vehicles." The contract was administered by the Air Force Flight Dynamics Laboratory, Air Force Systems Command, Wright-Patterson Air Force Base, Ohio. Mr. M. E. Hillsamer (AFFDL/FXG) was the Air Force Project Engineer.

This report covers work performed between May 1971 and March 1972. The report was submitted by the author in April 1972.

The contributions of Mr. F. L. Guard, who served as Program Manager, and Messrs. R. C. Baker and M. C. Fong, who participated in data reduction and analysis, are gratefully acknowledged.

This technical report has been reviewed and is approved.

Philip P. Antonatos

Philip P. Antonatos
Chief, Flight Mechanics Division
Air Force Flight Dynamics Laboratory

ABSTRACT

This report presents the results of a study which consisted of two principal phases: (1) an analytical investigation to extend the validity of the temperature-sensitive coating technique for aerodynamic heating measurement to areas in which known theories do not apply, and (2) a combined analytical and experimental study to develop methods of predicting areas of high thermal gradients in an interfering flow field.

Two data reduction computer programs were developed to treat the general two-dimensional case of a finite-slab convectively heated on one or both sides. These programs provide an inverse solution to the two-dimensional transient heat conduction equation with surface heating gradients and variable thermal properties.

A three-dimensional shock interference wind tunnel model was designed, fabricated, and tested in the AFFDL High Temperature Facility. The model is basically a sharp flat plate, instrumented for pressure and phase-change coating heat transfer measurements, with a shock generator fin mounted perpendicular to the plate along the edge. Tests were performed at a nominal Mach number of 10 and Reynolds number of 0.3×10^6 per foot.

By use of the temperature-sensitive coating technique, heating distributions in the interaction region have been identified in greater detail than is possible by use of thermocouple-instrumented models. Pressure and heating data are compared with theory and a procedure for estimating peak heating rates in the interaction region is recommended.

CONTENTS

ILLUSTRATIONS

SYMBOLS

c	Specific heat (Btu/lb-^{o}F)
C	Constant of proportionality in linear viscosity-temperature relationship, $C = \mu_w T / \mu T_w$
C_d	Nose drag coefficient
C_f	Skin friction coefficient
C_p	Pressure coefficient
D	Leading edge diameter (ft)
g	Gravitational acceleration (32.17 ft/sec^2)
h	Heat transfer coefficient (Btu/ft^2-sec-^{o}F)
i	Enthalpy (Btu/lb-^{o}F)
J	Mechanical equivalent of heat (778 ft-lb/Btu)
K	Coefficient in pressure interaction theory
k	Thermal conductivity (Btu/sec-ft-^{o}F)
L	Slab thickness (ft)
M	Mach number
n	Exponent in pressure interaction theory
P	Pressure (lb/ft^2 or lb/in.^{2})
Pr	Prandtl number
Re	Reynolds number
r	Recovery factor
T	Temperature (^{o}F or ^{o}R)
$\bar{T}$	$(T_{pc} - T_i) / (T_{aw} - T_i)$
t	Time from start of heating (sec)

t_d	Thermal diffusion time (sec)
V	Velocity (ft/sec)
X	Distance from model leading edge (in. or ft)
Y	Distance from right edge of test insert (in. or ft)
Y'	Distance from windward face of fin measured in Y direction (in. or ft)
y	Normal distance from surface of slab (ft)
α	Thermal diffusivity, $k/\rho c$ (ft^2/sec)
β	Semi-infinite slab parameter, $h\sqrt{t}/\sqrt{\rho ck}$
γ	Ratio of specific heats
δ	Fin deflection angle (deg)
μ	Viscosity ($lb\text{-}sec/ft^2$)
ρ	Density (lb/ft^3)
$\bar{\chi}$	Viscous interaction parameter, $M^3\sqrt{C}/\sqrt{Re_x}$

Subscripts

aw	Adiabatic wall
e	Inviscid, sharp wedge properties
f	Fin
fp	Flat plate
i	Initial
m	Model or along peak heating ray
o	Reservoir or upstream of interaction
pc	Phase change
pk	Peak pressure or heat transfer
pl	Plateau

ref	Reference
w	Wall
x	Based on distance from plate leading edge
∞	Freestream

Superscript

*	Evaluated at Eckert's reference temperature

Section I

INTRODUCTION

The present study consisted of two principal phases: (1) an analytical investigation to extend the validity of the temperature-sensitive coating technique for aerodynamic heating measurement to areas in which known theories do not apply, and (2) a combined analytical and experimental study to develop methods of predicting areas of high thermal gradients in an interfering flow field.

Advantages of aerodynamic heating measurements using temperature-sensitive coatings are well known: i.e., model costs are significantly lower than metallic models required for thermocouple instrumentation, nearly complete coverage of the model surface is obtained as compared to measurements at discrete points, and data can be obtained on complex configurations which are difficult to instrument with thermocouples or for configurations subject to localized heating effects for which the desired placement of instrumentation is not known beforehand. As a result, a sizable portion of current wind tunnel aerodynamic heating tests are performed using temperature-sensitive paints. For thick model sections with small surface heating gradients, data reduction is performed by application of the one-dimensional semi-infinite slab heat conduction solution. In these areas, data accuracy is only slightly less than that obtained through the use of thermocouple-instrumented models.

Prior to the present study, comparatively little work had been done to extend the temperature-sensitive paint technique to areas where semi-infinite slab theory is inapplicable. Lack of suitable data reduction procedures has resulted in erroneous heating data, particularly from thin model sections which are heated on both sides, and from areas of high heating gradients where lateral conduction within the model material affects the surface temperature.

Two approaches were used to provide data reduction procedures for these cases. First, the classical finite-slab solution was plotted in a form suitable for heat transfer data reduction of a uniformly heated thin model section where the backface temperature increases with time. Two computer programs were then developed to treat the general two-dimensional case of a finite-slab convectively heated on one or two sides. These programs provide an inverse solution to the two-dimensional transient heat conduction equation with surface heating gradients and variable material thermal properties. The programs determine the surface heat transfer coefficient distribution required to produce the experimentally determined coating phase-change times. Validation of the programs was accomplished by comparisons with exact solutions for one-dimensional heat conduction, and by comparing experimental data from the present tests with theory.

The second phase of the program investigated heat transfer distributions in an interfering flow field. A three-dimensional shock interference wind tunnel model was designed, fabricated, and tested in the AFFDL High Temperature Facility. The

model consists of a sharp leading edge flat plate with shock generator fins mounted perpendicular to the plate surface along the edge. The flat plate accommodates either a stainless steel insert for pressure measurements, or a nonmetallic, low conductivity material insert for heat transfer testing. Heat transfer inserts were fabricated from Teflon and Stycast – a high-temperature castable plastic. A cylindrical model was also fabricated and tested to provide heat transfer data with known lateral conduction effects for validation of the data reduction program. This model consists of a 30 in. aluminum tube with 2.0 in. diameter and 0.25 in. wall swept 40 deg relative to the airstream.

A total of 27 pressure tests, 71 heat transfer tests, and 5 oil flow tests were accomplished. All tests were performed at a nominal freestream Mach number of 10 and Reynolds number of 0.3×10^6 per foot. Heating distributions on the two models were measured by the temperature sensitive coating technique, using Tempilaq as the surface temperature indicator. Heat transfer data reduction was accomplished using the methods described above. The resulting experimental data, along with similar data from the literature, were then used to develop a method for predicting peak heating in a region affected by three-dimensional shockwave-boundary layer interactions.

Extended data reduction techniques for temperature-sensitive paint heat transfer measurement are described in the following section. Sections III and IV describe the experimental program and methods developed for predicting interference heating distributions, respectively.

Section II

PHASE-CHANGE COATING HEAT TRANSFER DATA REDUCTION TECHNIQUES

A primary objective of this study was to develop methods for reducing phase-change coating heat transfer data in areas where known solutions, such as one-dimensional semi-infinite slab theory, do not apply. Specifically, a solution was required for areas where: (1) large thermal gradients exist across the model surface, and (2) the model backface temperature increases with time. Two computer programs were developed for data reduction in areas affected by lateral conduction. These programs are described below, following a discussion of semi-infinite slab and finite-slab solutions.

1. ONE-DIMENSIONAL SEMI-INFINITE SLAB SOLUTION

Data reduction by the semi-infinite slab solution consists of measuring the test time required for the surface to reach a known temperature, as indicated by the coating melt patterns, and calculating the corresponding heat transfer coefficient by the solution of the one-dimensional transient heat conduction equation:

$$\frac{\partial T}{\partial t} = \frac{k}{\rho c} \frac{\partial^2 T}{\partial y^2} \tag{1}$$

To solve this equation, a set of boundary conditions which best describe the actual tunnel test are used. In this case, the boundary conditions are:

$$T\ (y,\ 0) = T_i$$

$$T\ (\infty,\ t) = T_i$$

$$\frac{\partial T\ (0,\ t)}{\partial y} = \frac{h}{k} \left[T_{aw} - T\ (0,\ t) \right]$$

It is assumed that the coating temperature and model surface temperature are identical. The solution of the above equation yields the test time required for the surface temperature to reach T_{pc}, the temperature at which the coating melts. Other assumptions are:

a. The depth of heat penetration into the model is small compared with the wall thickness so that the model acts like a semi-infinite slab.

b. The model is initially isothermal.

c. The surface is subjected to an instantaneous step in aerodynamic heating at time zero and the heat transfer coefficient does not vary with time.

d. The model thermal conductivity, density, and specific heat do not vary with temperature.

The solution of Equation (1) with stated boundary conditions is:

$$\overline{T} \equiv \frac{T_{pc} - T_i}{T_{aw} - T_i} = 1 - e^{\beta^2} \operatorname{erfc} \beta \qquad (2)$$

where

$$\beta \equiv \frac{h\sqrt{\alpha t}}{k} = \frac{h\sqrt{t}}{\sqrt{\rho c k}}$$

Figure 1 plots the semi-infinite slab solution in the form of β versus $\overline{T}$. For semi-infinite slab theory to be applicable, the time required for the phase change to occur must be small compared with the thermal diffusion time of the model wall. The thermal diffusion time depends only on the thermal diffusivity and wall thickness, and is given approximately by the equation (Ref. 1):

$$t_d \approx \frac{0.2\, L^2}{\alpha} \qquad (3)$$

This relation was obtained by assuming a cubic distribution of temperature with depth in a slab subjected to an instantaneously applied heat transfer coefficient at one surface, and solving for the time for which a significant change in backface temperature occurs. If the time required for the phase change to occur is greater than the thermal diffusion time, data reduction must be based on finite-slab analysis.

2. ONE-DIMENSIONAL FINITE-SLAB SOLUTION

One-dimensional finite-slab solutions can be used to extend data reduction to the case of a uniformly heated thin model section which is adiabatic at its backface. These solutions involve infinite series which are tedious to evaluate, and are therefore commonly presented in graphical form. Figure 2 shows the finite-slab solution for the case of an adiabatic backface plotted in terms of Biot number (h L/k) versus Fourier number ($\alpha t/L^2$) with $\overline{T}$ a parameter. The straight, parallel lines on the left side of Figure 2 have a slope of -0.5 and represent the semi-infinite slab solution. The lines begin to curve at $\alpha t / L^2 \approx 0.2$, which confirms the validity of Equation (3) as the criterion for the limit of applicability of semi-infinite slab theory. For large values of Fourier number, the slope of the lines approaches -1, which indicates that the temperature gradient through the slab is negligible and the "thin skin" assumption is valid.

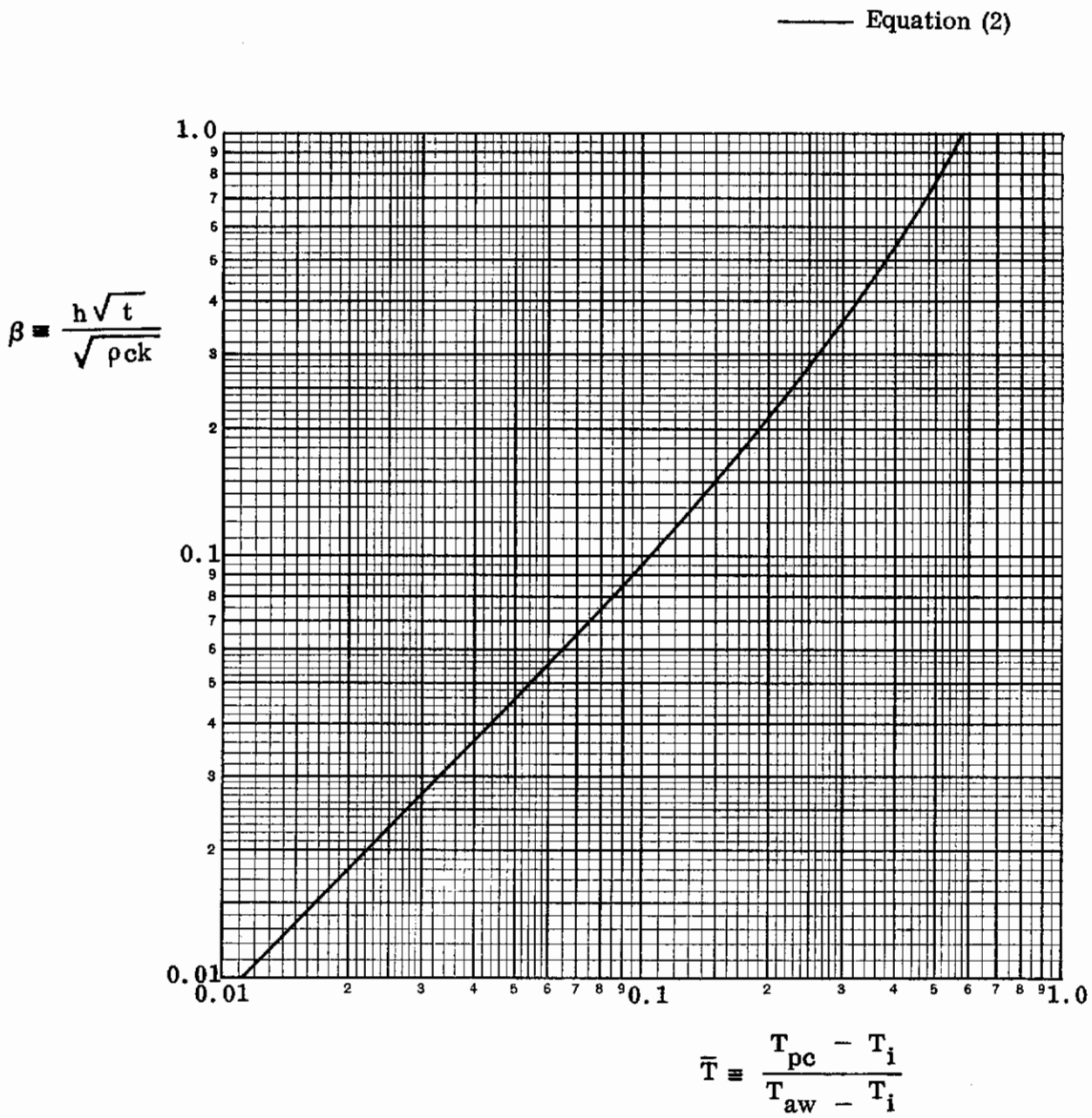

Fig. 1 Solution of One-Dimensional Semi-Infinite Slab Heat Conduction Equation

Reproduced from Reference 19

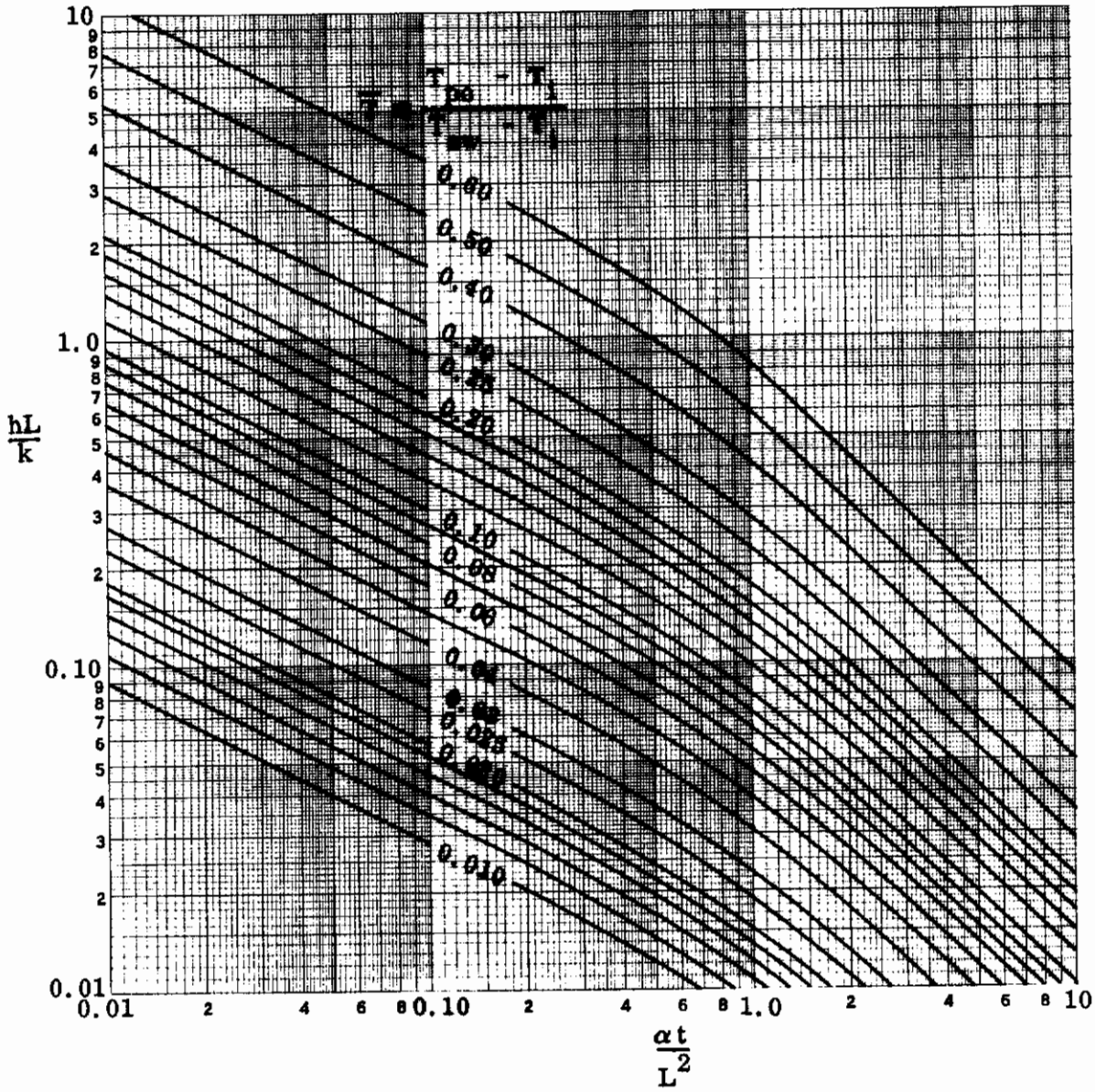

Fig. 2 Solution of One-Dimensional Finite-Slab Heat Conduction Equation

3. TWO-DIMENSIONAL FINITE-SLAB SOLUTION

Two computer programs were developed to reduce phase-change coating heat transfer data in areas where semi-infinite slab theory is inapplicable. Program I determines the surface heat transfer coefficient distribution on a slab which is convectively heated on one side and adiabatic on the backface. Program II determines the heat transfer coefficient distribution on a slab which is convectively heated on both sides. It is assumed that the slab is initially at a uniform temperature, that the surface experiences an instantaneous step in heat transfer coefficient at time zero, and that the coefficient and adiabatic wall temperature do not vary with time. Both programs account for the effects of lateral conduction and temperature-dependent specific heat and thermal conductivity.

The solution employed is similar to that used for many Thermal Analyzer Programs. A two-dimensional nodal network is generated and the transient heat conduction equations are solved by a finite-difference procedure. The program constructs the nodal network; sets all node temperatures equal to the input initial temperature; estimates the surface heat transfer coefficients; computes resistors, capacitors, and time constants; and performs heat balances on each node in discrete time steps until the temperature of each surface node exceeds the phase-change temperature. The time required for each node to reach the phase-change temperature is compared with the experimental phase-change time and, if they do not all agree within a specified tolerance, the heat transfer coefficients are adjusted and the process is repeated.

Input data for Program I are supplied on two cards. The first card describes the network dimensions, initial temperature, phase-change temperature, adiabatic wall temperature, and desired printout interval for surface temperature histories. The second card lists the experimental phase-change times for each surface node. Input data for Program II are supplied on four cards. The first card describes the network dimensions, initial temperature, phase-change temperatures, adiabatic wall temperatures, and printout interval. The second card lists the slab thickness as a function of X distance. The third and fourth cards list the experimental phase-change times at each surface node. Both programs accept restarts so that any number of cases may be run consecutively.

Program I generates a two-dimensional nodal network based on the following quantities, which are supplied on the first data input card:

NX = Number of nodes in the X direction (parallel to the heated surface)
NY = Number of nodes in the Y direction (normal to the heated surface)
X = Width of slab, i.e., distance between node 1 and node NX in inches
Y = Thickness of slab in inches

Figure 3 illustrates the network generated, using NX = 5 and NY = 6 as an example. Node thicknesses in the Y direction are graduated and are roughly inversely proportional to the heating gradient. Edge nodes are half the size of adjacent nodes to accommodate problems with a symmetrical melt pattern. The program will reduce the input value of NY if the resulting computing interval is less than 0.5 percent of the maximum melt time, or if the Fourier number ($\alpha t/L^2$) based on minimum melt time

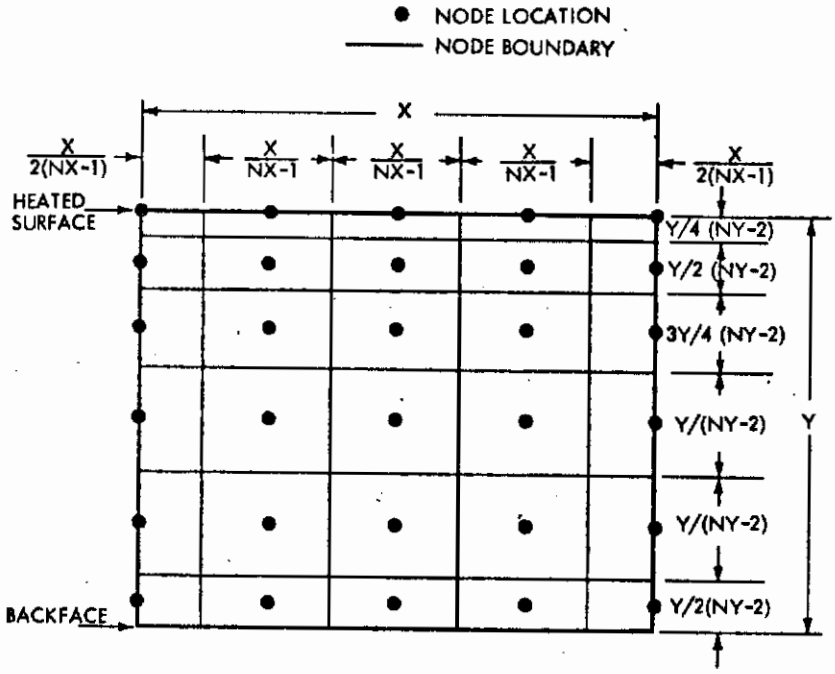

Fig. 3 Typical Nodal Network for Data Reduction Program I

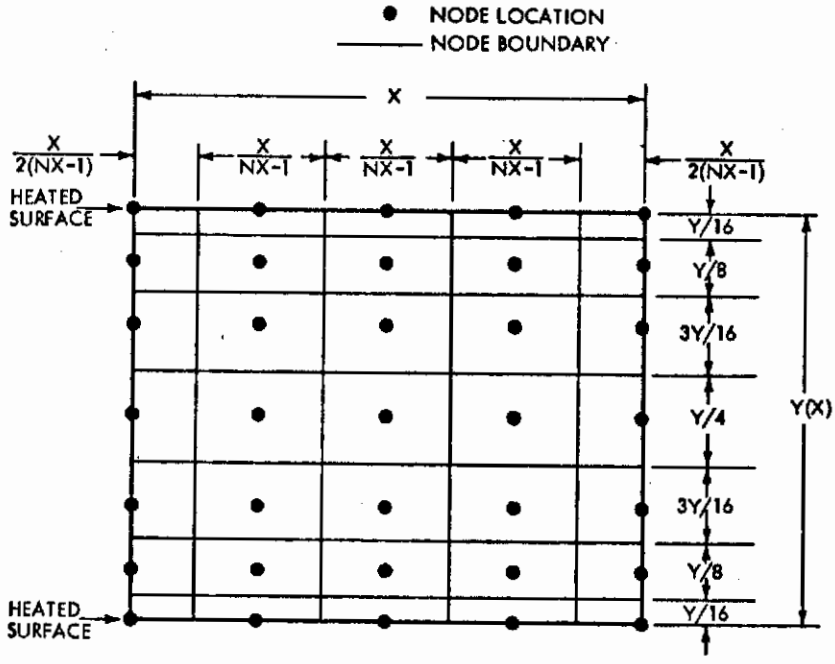

Fig. 4 Typical Nodal Network for Data Reduction Program II

is so large that the small temperature gradient through the slab does not justify use of the input number of nodes. Also, if finite-slab effects are negligible, the program revises the input slab depth (Y) based on the depth required to assure negligible back-face temperature rise, i.e., the program sets $Y = \sqrt{5\alpha t}$, where α is the thermal diffusivity and t is the maximum melt time. This is done to avoid excessive node spacings and placement of nodes in regions where temperature rise is insignificant. The above value of Y is also automatically assigned if Y is input as zero.

Program II generates a two-dimensional nodal network based on the following quantities, which are supplied on the first and second data input cards:

NX = Number of nodes in the X direction (parallel to the heated surface)

X = Width of slab, i.e., distance between node 1 and node NX in inches

Y (X) = Thickness of slab as a function of X distance in inches

The number of nodes in the Y direction (NY) is fixed at seven. Figure 4 illustrates the network generated, using NX = 5 as an example.

The method of solution is identical for Programs I and II. After constructing the network, the surface heat transfer coefficient distribution is estimated, using an approximation to finite-slab theory. Next, the program computes the capacitor and resistor values based on the equations

$$C = \rho V c$$

$$R = \frac{L}{k A}$$

where

ρ = Material density
V = Node volume
c = Specific heat
L = Distance between node centers
k = Thermal conductivity
A = Cross-sectional area for heat conduction

Specific heat and thermal conductivity are assumed to be temperature-dependent and described by equations of the form $c = A + BT + CT^2$ and $k = D + ET + FT^2$, where T (in ^{o}F) is local temperature (the node temperature for specific heat calculations and the average temperature of the two connecting nodes for resistor calculations). If the coefficients of the temperature terms are all zero, the capacitors and resistors are computed only at time zero; otherwise, they are computed each cycle, prior to the heat balance calculations.

The program also computes the time constant, or RC product, of each node. The RC product is the capacitance of a node multiplied by the equivalent resistance of the node. The latter is defined as the parallel combination of all resistors connected to the node, i.e.,

$$(RC)_k = \frac{C_k}{\sum_j \frac{1}{R_j}}$$

The program searches the network to find the minimum RC product, and multiplies this value by 0.5 to determine the computing interval Δt . The constant 0.5 is somewhat arbitrary and is based on experience with Thermal Analyzer Program usage. If the computing interval exceeds the RC product, instability problems may result, i.e., temperatures may oscillate above and below the correct value during successive computing cycles. If necessary, the computing interval is reduced early in a run to assure at least 20 computing cycles prior to the earliest phase-change.

The next step is to perform heat balances on each node and to determine a new set of network temperatures by the equation:

$$T_{k,t+\Delta t} = T_{k,t} + \frac{\Delta t}{C_k}\left[\sum_j \frac{T_{j,t} - T_{k,t}}{R_j} + hA\,(T_{aw} - T_{k,t})\right]$$

where

$T_{k,t+\Delta t}$ = Temperature of node k after time increment Δt

$T_{k,t}$ = Temperature of node k at time t

C_k = Thermal capacitance of node k

$T_{j,t}$ = Temperature of adjacent node j at time t

R_j = Thermal resistor connecting nodes j and k

hAT_{aw} = Heat transfer coefficient, heated surface area, and adiabatic wall temperature

The heat balances are repeated in time increments Δt until all surface temperatures exceed the phase-change temperature. The time required for each node to reach the phase-change temperature is compared with the experimentally determined time and, if they do not all agree within a specified tolerance, the heat transfer coefficients are adjusted and the process is repeated.

Program output includes a listing of all input data; capacitors, resistors, and RC products based on the initial temperature; and surface temperature histories for each iteration. The program then tabulates, for each surface node, the X location; slab depth (Program II only); computed phase-change time; experimental phase-change time; computed heat transfer coefficients; and ratio of computed to semi-infinite slab heat transfer coefficients.

Reference 2 describes the programs in detail, including the solution of sample problems. Program listings are contained in the Appendix of this report.

4. VALIDATION OF DATA REDUCTION TECHNIQUES

Heat transfer data reduction techniques developed during this study are validated by comparisons with analytical solutions, and by comparing heating data from the shock interference and swept cylinder models with theory.

Heat transfer coefficients computed by the data reduction programs have been compared with exact solutions for one-dimensional semi-infinite slabs and finite-slabs. Figure 5 compares surface temperature histories computed by Program I with exact solutions (Fig. 1) for two semi-infinite slab cases. Comparisons are shown for a large heat transfer coefficient which results in a surface temperature rise of $320^{\circ}F$ in 2 sec, and for a small heat transfer coefficient which results in a surface temperature rise of $45^{\circ}F$ in 20 sec. Figure 6 compares surface temperatures computed by Program I with exact solutions (Fig. 2) for two finite-slab cases. Slab thicknesses were selected so the ratio of melt time to thermal diffusion time is five for the high heating rate case and ten for the low heating rate case. For all examples, the program results are virtually identical to the exact solutions.

Figure 7 compares surface temperature histories computed by Program II with exact solutions (Fig. 2) for a slab which is convectively heated on both sides. Uniform heating is assumed on the two faces; consequently, the midplane is adiabatic and heat transfer coefficients may be determined by finite-slab theory based on half the slab thickness. As shown, Program II results are also in excellent agreement with theory.

Additional validation of the data reduction techniques was accomplished by comparing phase-change coating heat transfer data from the present test program with theory. Without side fins, thermal gradients are negligible on the shock interference model and the laminar heat transfer distribution can be accurately predicted. Consequently, data from tests without fins are useful in validating the finite- slab data reduction solution plotted in Fig. 2. Undisturbed flat plate heating data were obtained using the 0.04 in. Teflon and 0.05 in. Stycast inserts which are backed with 2 lb/ft^3 polyurethane foam (see Section 3.1). For these tests, coating melt times ranged from 23 to 36 sec, whereas the thermal diffusion time (Eq. 3) is only 1.7 sec for the Teflon insert and 0.63 sec for the Stycast insert.

Figure 8 compares the undisturbed flat plate heating data with Eckert's reference enthalpy method (Ref. 3). Bluntness and viscous-induced pressures are based on Creager's method (Ref. 4) and the heat transfer coefficients are corrected for pressure gradient by the Bertram-Feller solution (Ref. 5). As shown, data from the Stycast insert are in excellent agreement with laminar flat plate theory, whereas the Teflon data are overpredicted by about 35 percent. The Teflon data for this run are believed to be affected by a room-temperature transition in crystal structure (see Section 3.4) and are therefore erroneous. The excellent correlation of the Stycast data substantiates the one-dimensional finite-slab data reduction solution and also demonstrates that the polyurethane foam provides an essentially adiabatic backface for the thin heat transfer inserts. It should be noted that experimental surface pressures from the tests without side fins are 10 to 20 percent higher than predicted (see Figure 42). If the experimental data were used for theory evaluation, the theoretical heating distribution plotted on Figure 8 would increase by about seven percent.

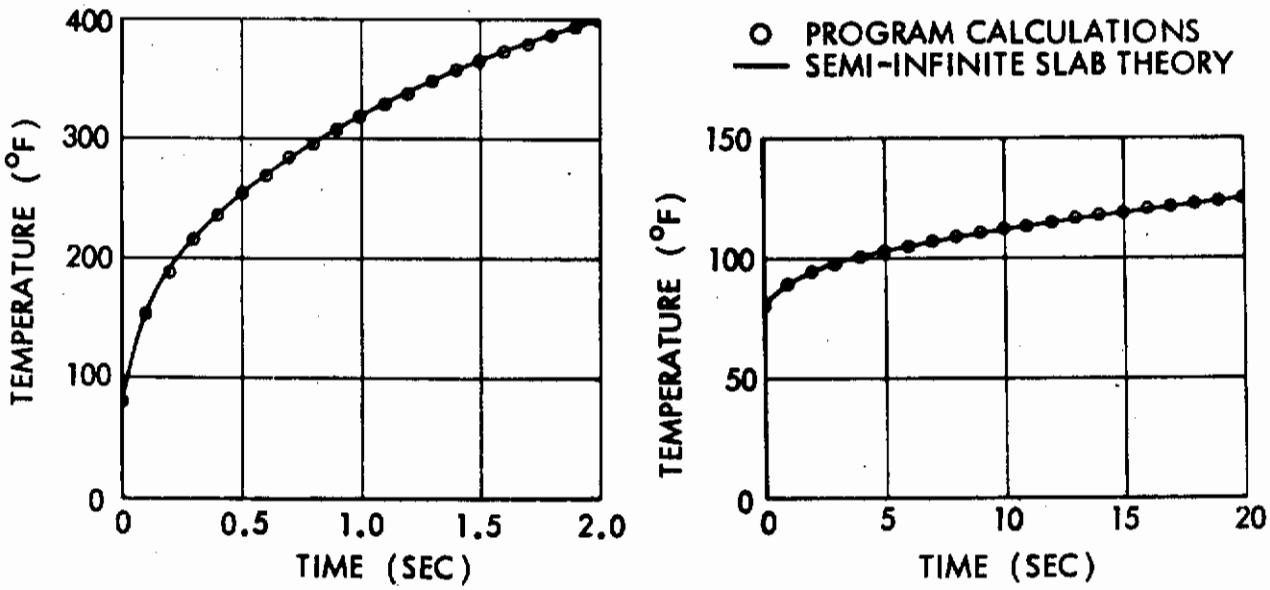

(a) $h = 0.00629$ Btu/ft^2 sec $^\circ$F
$t_d = 2.4$ sec

(b) $h = 0.000235$ Btu/ft^2 sec $^\circ$F
$t_d = 24$ sec

Fig. 5 Comparison of Computer Program I Calculations With Semi-Infinite Slab Theory

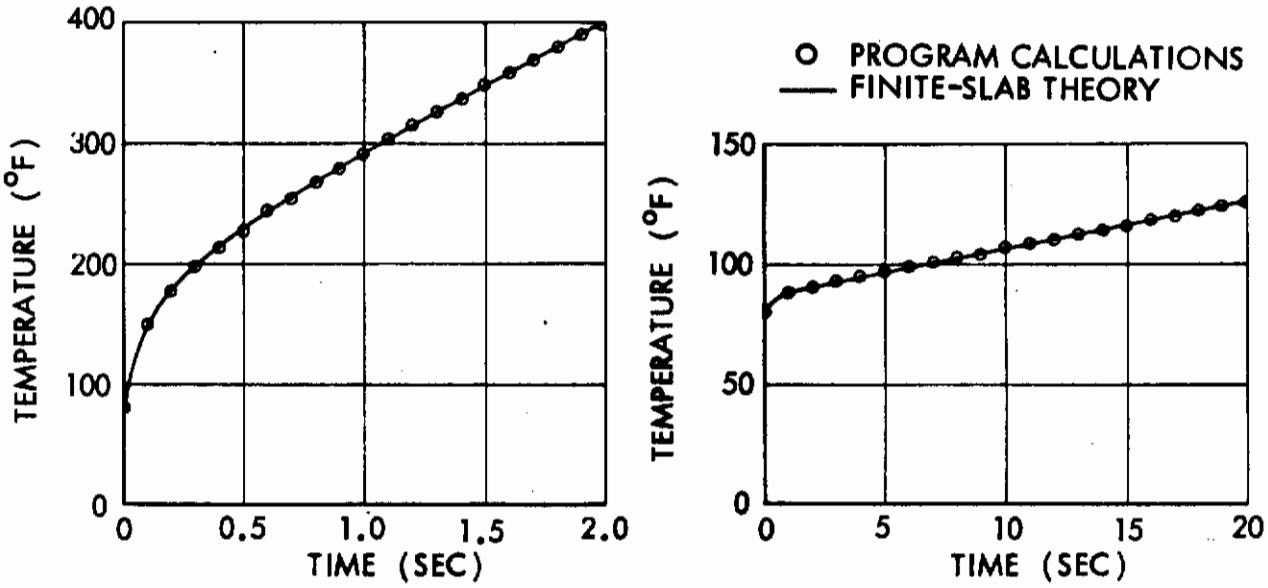

(a) $h = 0.00521$ Btu/ft^2 sec $^\circ$F
$t_d = 0.40$ sec

(b) $h = 0.000161$ Btu/ft^2 sec $^\circ$F
$t_d = 2.0$ sec

Fig. 6 Comparison of Computer Program I Calculations With Finite-Slab Theory

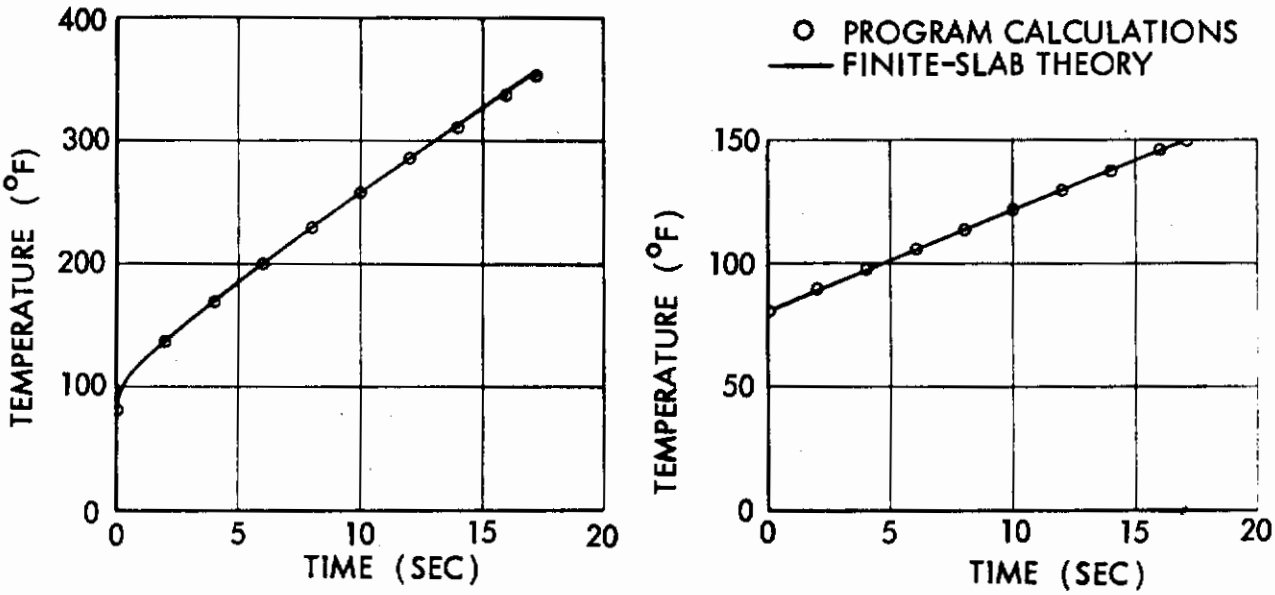

(a) $h = 0.00142$ Btu/ft^2 sec $^\circ$F
$t_d = 0.79$ sec

(b) $h = 0.000151$ Btu/ft^2 sec $^\circ$F
$t_d = 0.17$ sec

Fig. 7 Comparison of Computer Program II Calculations With Finite-Slab Theory

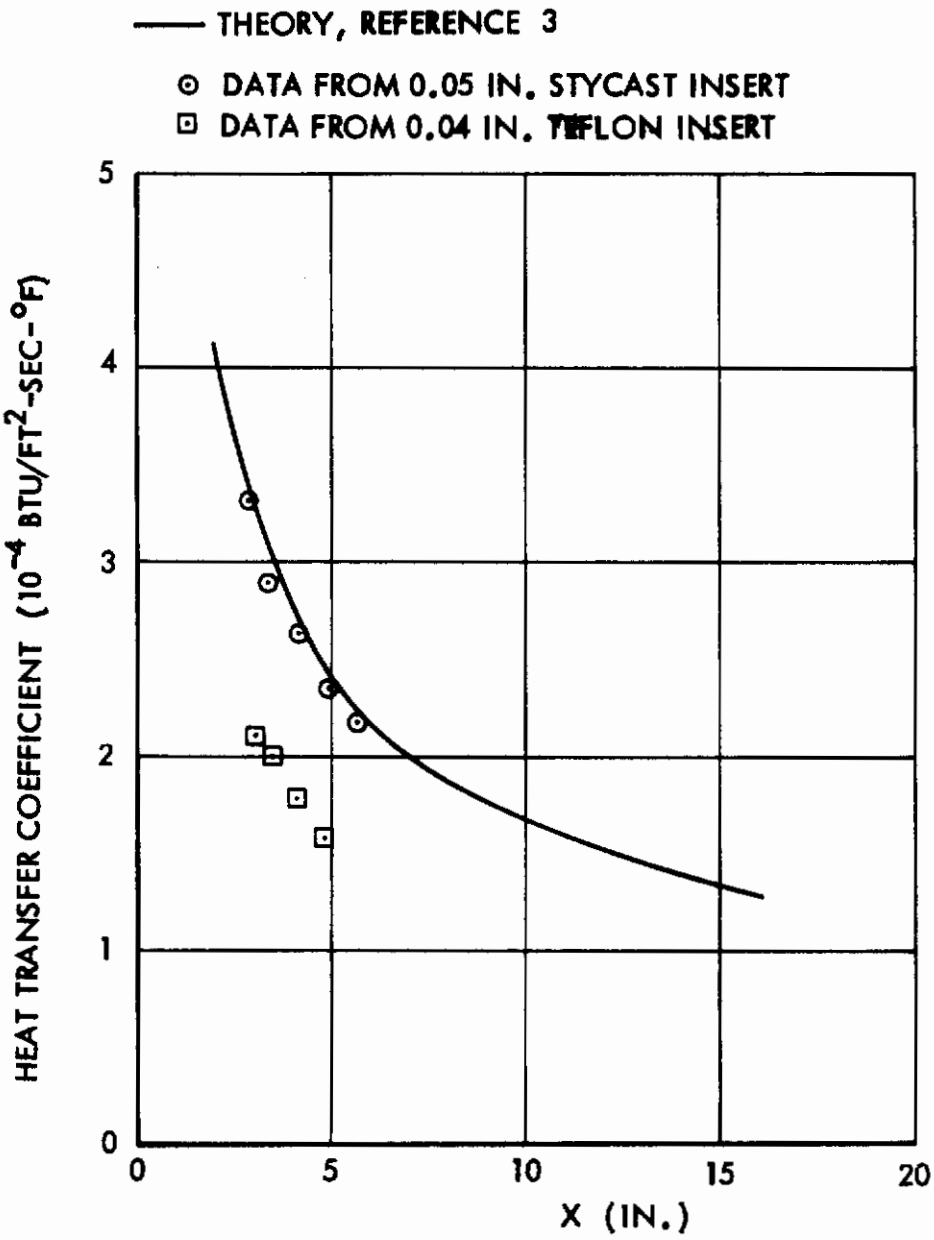

Fig. 8 Correlation of Undisturbed Flat Plate Heat Transfer Data

The aluminum swept cylinder model was designed and tested specifically to obtain data on a configuration with predictable heating characteristics to validate data reduction procedures developed for the case of a finite-slab with large lateral heating gradients. The thermal diffusion time for the 0.25 in. wall is 0.13 sec. Coating melt times ranged from 9.7 sec at the stagnation line to 20 sec at a circumferential angle of 90 deg.

Data reduction for cylinder model tests was performed using computer Program I. The experimental heating distribution is in good agreement with swept cylinder theory, as shown in Figure 9. It should be noted that lateral conduction and backface temperature rise for this problem are more significant than for the shock interference model. If, for example, data reduction were based on finite-slab theory, ignoring lateral conduction, the heat transfer coefficient would be low by 37 percent at the stagnation line and high by 41 percent at $\theta = 90$ deg. The good agreement between data and theory demonstrates the ability of the data reduction program to accurately solve problems involving a finite-slab with large lateral heating gradients.

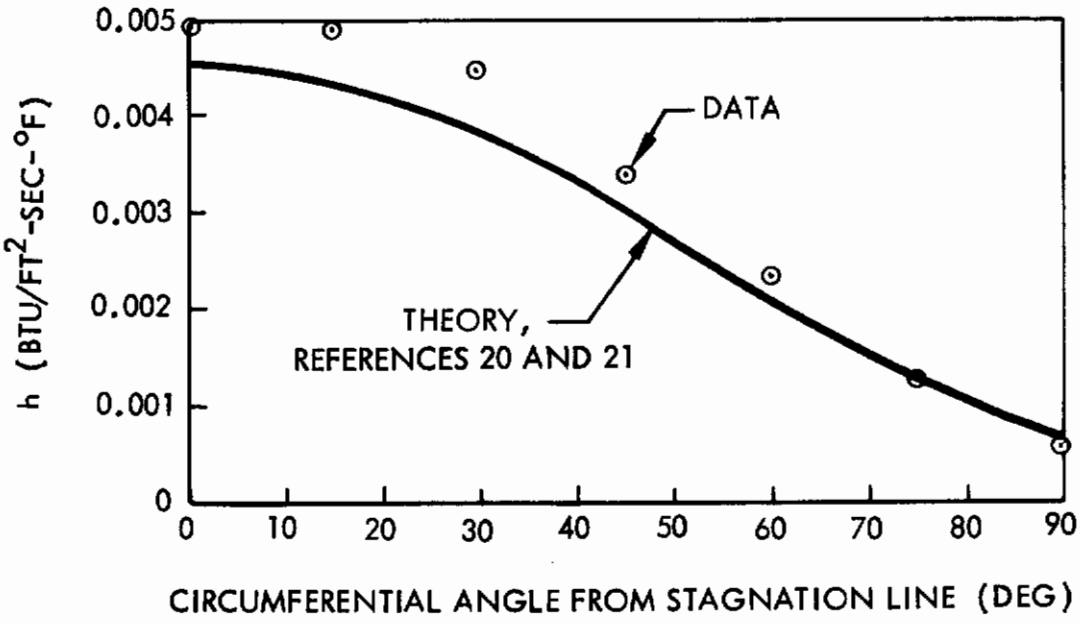

Fig. 9 Correlation of Swept Cylinder Heat Transfer Data

Section III

WIND TUNNEL TEST PROGRAM

A wind tunnel test program was conducted to measure pressure and heat transfer distributions in a region affected by three-dimensional shockwave-boundary layer interactions, and to obtain data to confirm the data reduction techniques developed under this contract. Primary results of these tests are presented below. Additional information, such as model design drawings and heat transfer measurements from individual runs, is contained in the test report (Ref. 6).

1. MODELS

Two wind tunnel models were fabricated for testing in the AFFDL High Temperature Facility. The shock interference model, shown in Fig. 10, is basically a flat plate with a shock generator fin mounted perpendicular to the plate along the edge. All instrumentation is on the flat plate, which accommodates either a stainless steel insert instrumented with 50 pressure taps or a low thermal conductivity insert for phase-change coating heat transfer tests.

The model base plate is 16 in. long and 12 in. wide, and separates 8 in. from the right side to change aspect ratio. A removable leading edge is provided for both the 8 in. and 12 in. spans. The leading edges are sharp with a 20-deg bevel angle, and clamp the forward edge of the instrumented inserts to the baseplate. Three impact pressure probes are permanently installed on the beveled leading edge to aid in determination of freestream flow properties.

The fin shock generators also have sharp leading edges with 20-deg bevel, and are 6 in. high, 16 in. long, and 0.50 in. thick. The left fin, which is not shown in Fig. 10, is positioned at zero incidence angle and was used for only five tests. The right fin can be positioned at incidence angles of 5, 10, and 15 deg, and at lateral displacements of 0.125, 0.200, and 0.300 in. Both fins can be attached to the baseplate at axial positions of 0, 2.0, 4.0, 6.0, 8.0, and 10.0 in.

Six heat transfer inserts were fabricated from TFE Teflon and two were fabricated from Stycast 2762FT. The thickness of the Teflon and Stycast slabs varied, as shown in Table I.

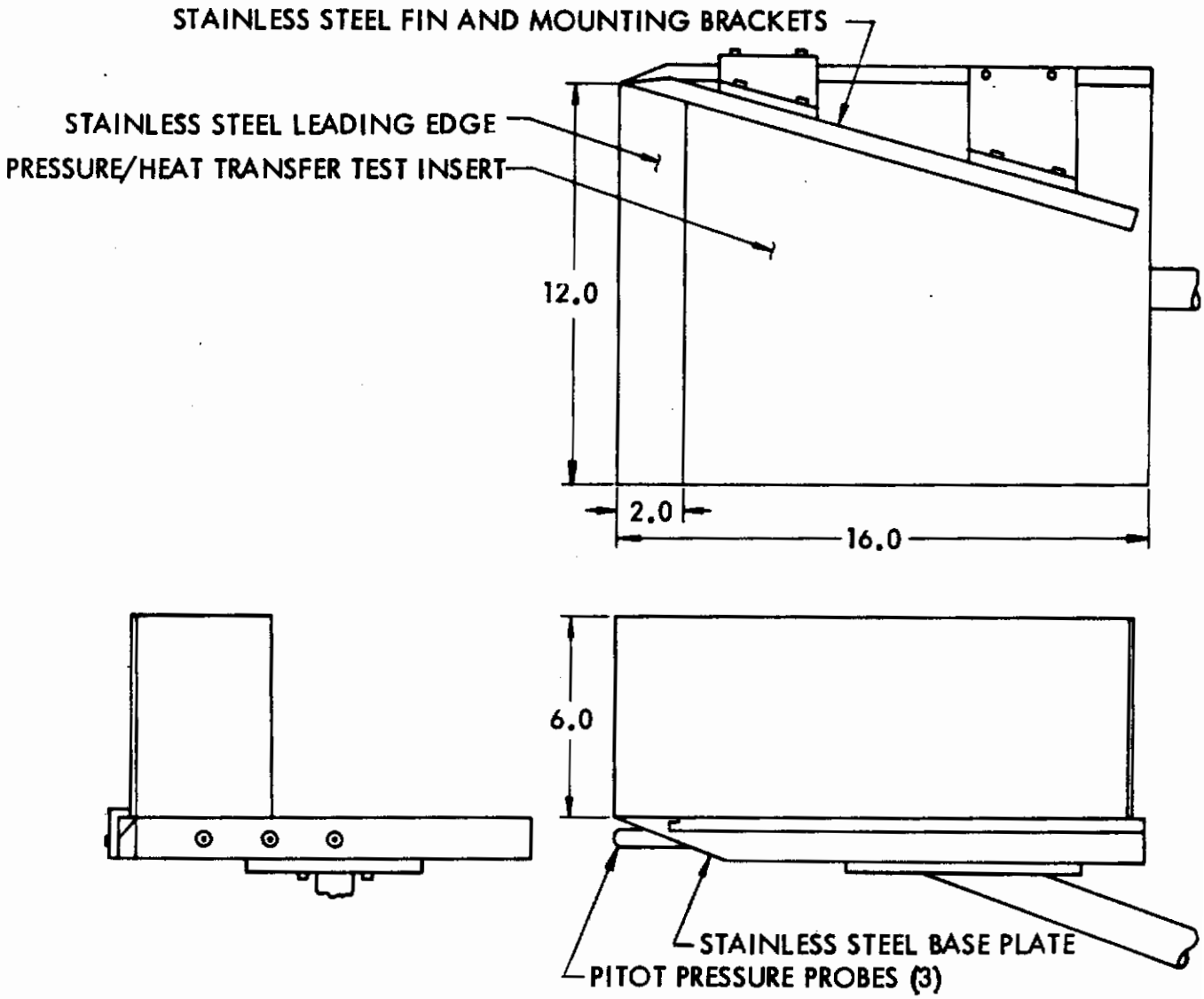

Fig. 10 Shock Interference Model

Table I

HEAT TRANSFER INSERTS

Quantity	Material	Width x Length (in.)	Thickness (in.)	Thermal Diffusion Time (sec)
3	Teflon	12 x 14	0.250	67.6
1	Teflon	8 x 14	0.250	67.6
1	Teflon	8 x 14	0.060	3.9
1	Teflon	8 x 14	0.040	1.7
1	Stycast	12 x 14	0.250	15.7
1	Stycast	8 x 14	0.050	0.6

All inserts have an overall thickness of 0.375 in. The 0.250 in. slabs are bonded directly to a 0.125 in. steel backup plate. The thinner inserts utilize a sandwich of 2 lb/ft^3 rigid polyurethane foam between the test material and the backup plate to provide a nearly-adiabatic backface. Each slab is instrumented with five iron-constantan thermocouples to measure backface temperature.

The second model tested during this program is the swept cylinder shown in Fig. 11. This model is fabricated from a 6061-T6 aluminum tube with 2.0 in. diameter and 0.25 in. wall. The tube is filled with fibrous insulation to minimize internal heat transfer, and is attached to the support sting at an acute angle of 50 deg to form a 40-deg swept cylinder relative to the airstream. As discussed in Section II, data from this model were used to validate data reduction procedures developed for the case of a finite-slab with large surface heating gradients.

Tempilaq, a material which undergoes a phase-change from an opaque solid to a clear liquid at known temperatures, was used as the surface temperature indicator for heat transfer tests.

2. FACILITY AND TEST PROCEDURES

The AFFDL High Temperature Facility is a hypersonic blowdown wind tunnel which uses an alumina pebble bed heater as the heat source. The tunnel has an open jet test section and can be operated at a nominal Mach number of 9, 10, or 11 at stagnation temperatures up to 4000°R. An axisymmetric 150 in. long contoured Mach 10 nozzle with 24 in. exit diameter was used during this program. Vacuum capability consists of a 60,000 ft^3 sphere with three stages of pumping to provide run times up to three minutes. For the flow conditions of this program, maximum run time was about 90 sec.

The test procedure for heat transfer runs was to adjust the fin location, clean the test surface with alcohol, apply the phase-change coating, start the tunnel, and rapidly inject the model into the airstream. Test time generally ranged from 15 to 60 sec, after which the model was retracted from the airstream and the tunnel was shut down. The shock interference model was intermittently cooled between runs with CO_2.

Coating melt patterns were recorded on 35 mm color film using a camera mounted directly above the model. Lighting was provided by two strobe lamps which were sequenced with the camera. The camera speed was four frames per sec. Typical results are

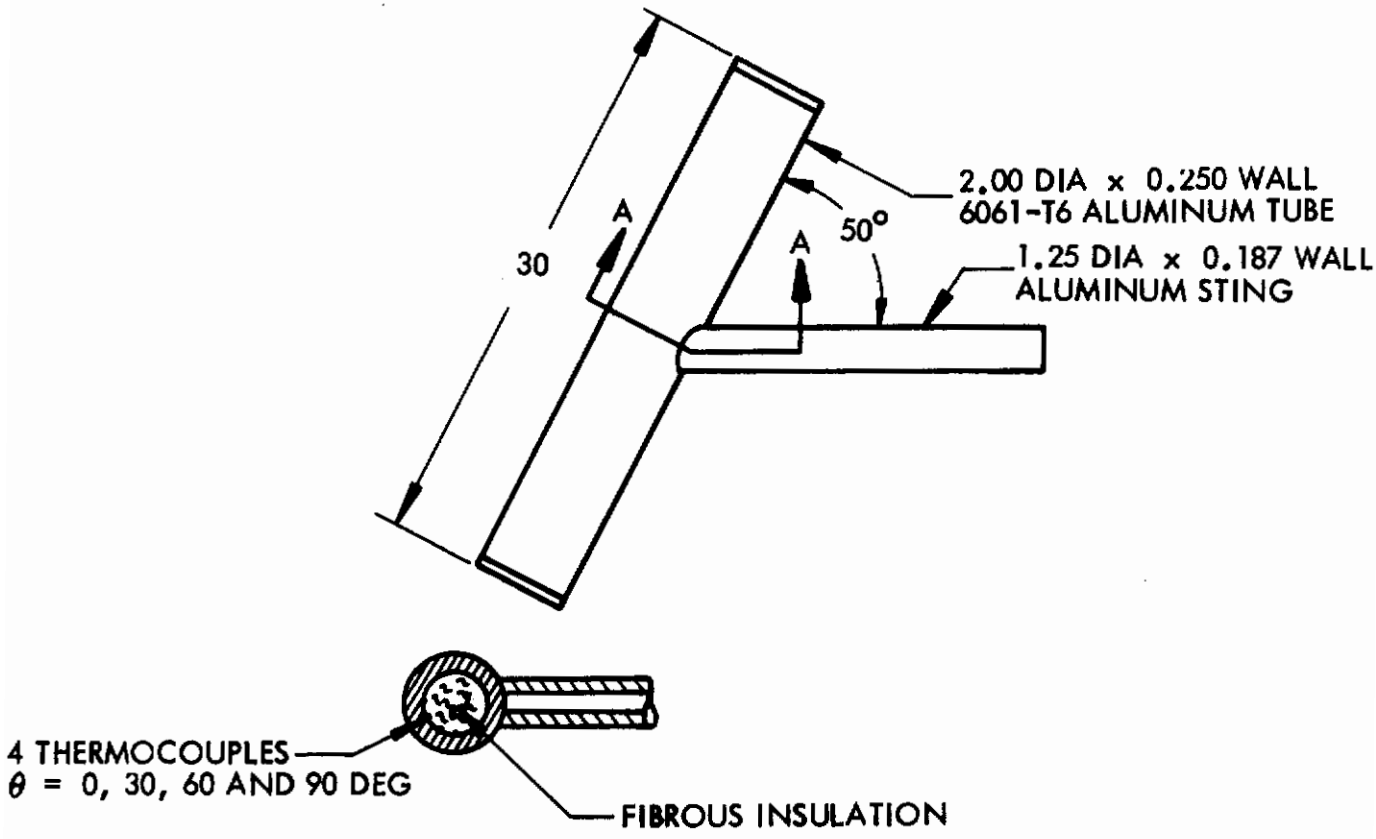

Fig. 11 Swept Cylinder Model

illustrated in Figs. 12, 13, and 14, which show coating melt pattern histories for three representative runs. These tests were performed using a black Stycast insert which appears as a dark region when the coating melts and becomes transparent. All of the Tempilaq coatings used during this program were dyed green to improve contrast between the coating and substrate.

For pressure tests, the tunnel was evacuated approximately 30 min prior to each run to allow time for model pressure tubing to pump down. Pressure tests lasted about 90 sec, and data were generally taken at 10 sec intervals after the flow stabilized.

A total of 27 pressure tests, 71 heat transfer tests, and 5 oil flow tests were accomplished during a three-week test period. Nominal reservoir conditions were P_o = 300 psia and T_o = 2100°R, which results in a freestream Reynolds number of 0.3 x 10^6 per foot at Mach 10. Four heat transfer tests were performed on the swept cylinder and the remainder were performed on the shock interference model. Fin deflections of 0, 5, 10, and 15 deg and axial positions of 0, 4, and 8 in. were tested, with the instrumented flat plate always at zero angle-of-attack.

3. EXPERIMENTAL PRESSURE DISTRIBUTIONS

As shown in Fig. 15, the shock interference model pressure insert contains 50 pressure taps at stations 10 and 12 in. aft of the model leading edge. The taps are spaced at 0.25-in. intervals starting at Y = 1.0 in. and ending at Y = 7.0 in.; however, the two taps at Y = 7.0 in. were not monitored.

Figures 16 through 27 show the pressure data from the shock interference model. The data are plotted in terms of local-to-freestream pressure versus distance from the windward face of the fin, Y', which is defined in Fig. 15. The distance from the edge of the model can be easily determined because the last data point plotted on each figure is located at Y = 6.75 in. Most of the pressure plots are a composite of data from two runs, which are identical except for a nominal one-eighth in. difference in the fin lateral position.

4. EXPERIMENTAL HEAT TRANSFER DISTRIBUTIONS

The procedure used to reduce heat transfer data was to project the test film on a sheet of vellum, trace the model outline, and then at selected times trace the coating melt patterns to form a composite map showing lines of constant heating rate. Where possible, the interference region peak heating location and magnitude were identified. The data were reduced to heat transfer coefficient form using the procedures outlined in Section II. In areas where lateral heating gradients are negligible, data reduction was performed using the semi-infinite slab solution for the 0.25 in. heat transfer inserts, and the finite-slab solution for the 0.04, 0.05, and 0.06 in. inserts. In areas where heating gradients are large, i.e., in the peak interference heating region, data reduction was performed using the computer program described in Section 2.3. Detailed coating melt-time distributions are required to account for lateral heating gradients; consequently, the program was used only for runs where the melt times, including the time when melting first occurred, could be accurately determined.

Figure 28 illustrates the procedure used to account for lateral heating gradients, using run 338 as an example. This test was performed using the 0.25-in. Stycast insert coated with 200°F Tempilaq, with the right fin positioned at X_f = 8 in.,

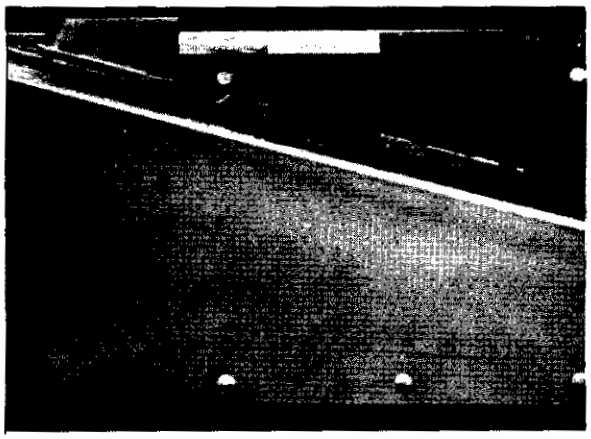

1.25 sec

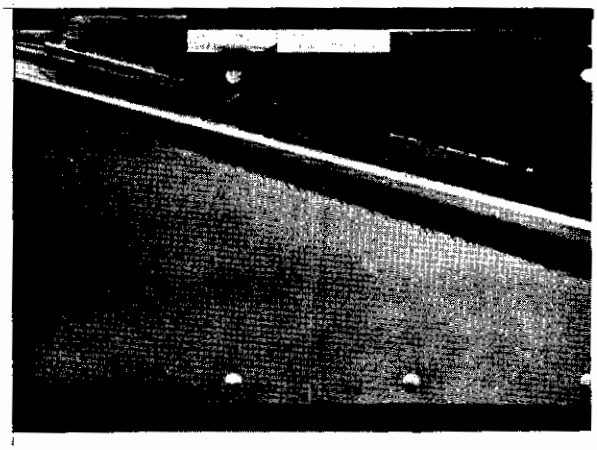

5.75 sec

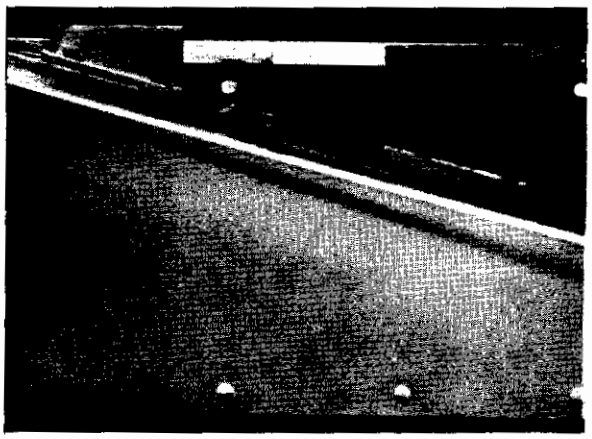

2.25 sec

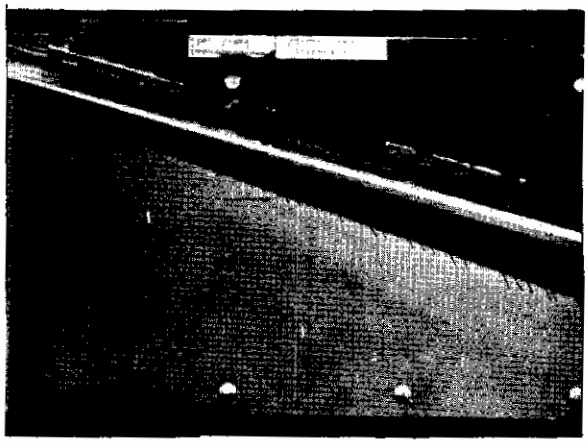

10.2 sec

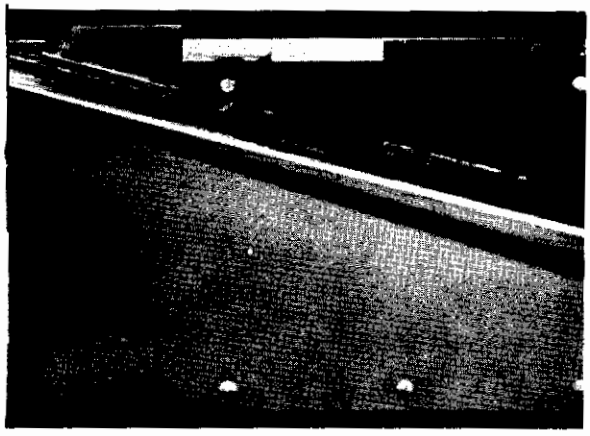

3.75 sec

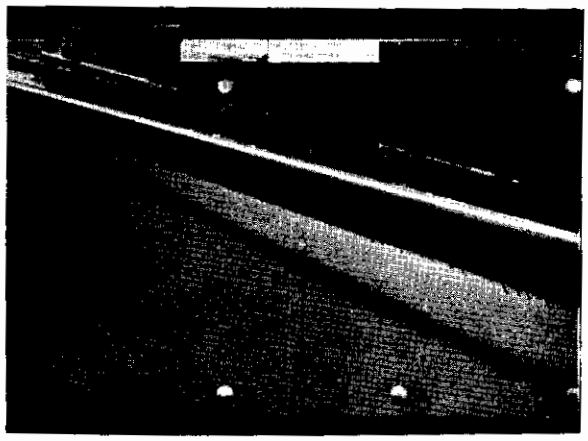

16.5 sec

Fig. 12 Coating Phase – Change Patterns for Run 323 (X_f = 0 in., δ = 15 deg)

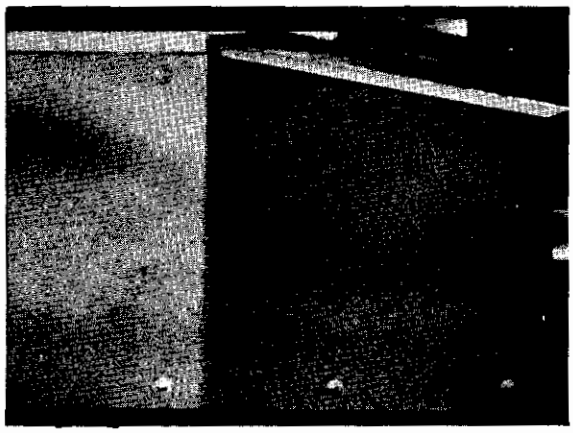

3.70 sec

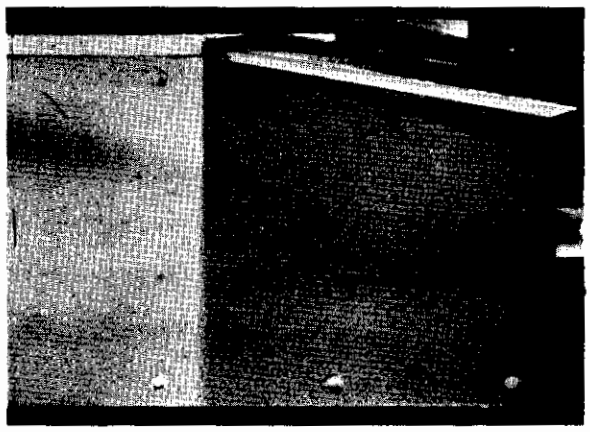

9.70 sec

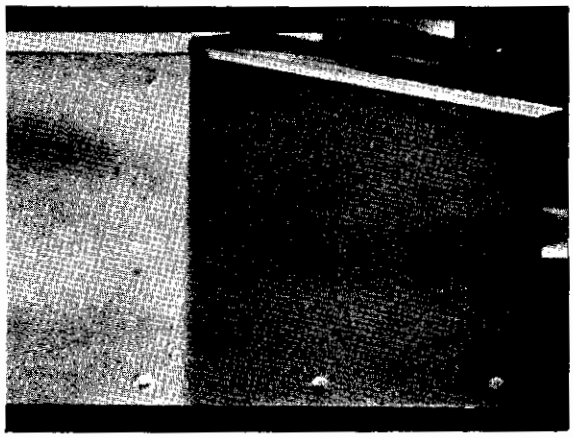

5.20 sec

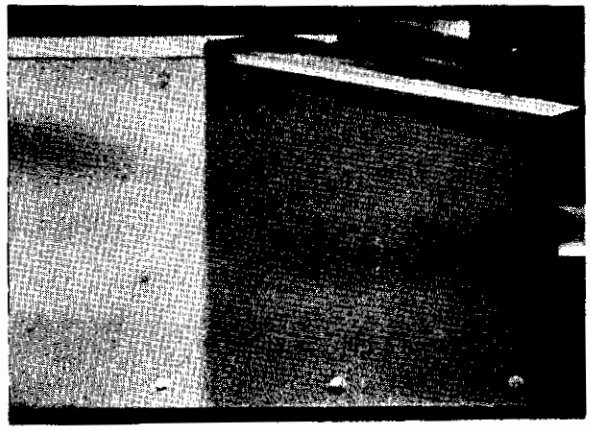

12.7 sec

7.20 sec

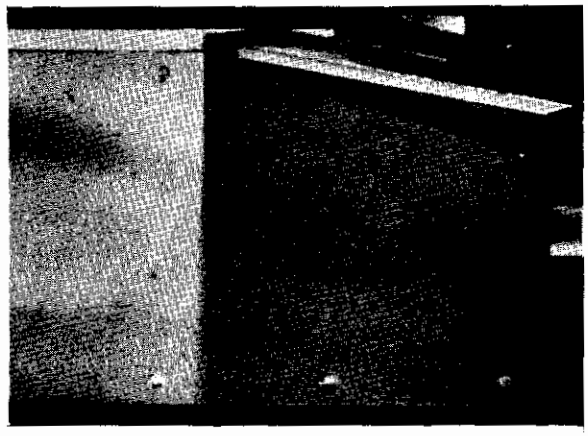

17.7 sec

Fig. 13 Coating Phase – Change Patterns for Run 321 (X_f = 8 in., δ = 10 deg)

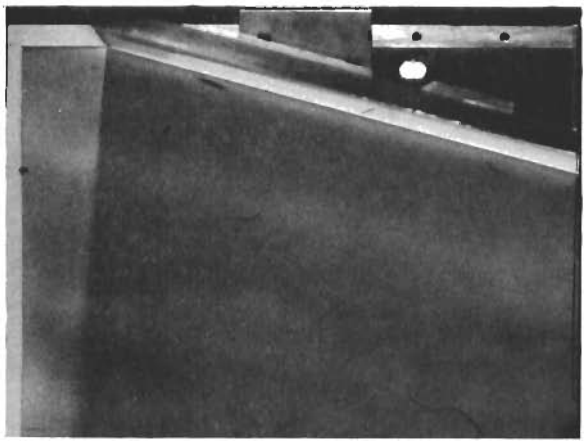

1.20 sec

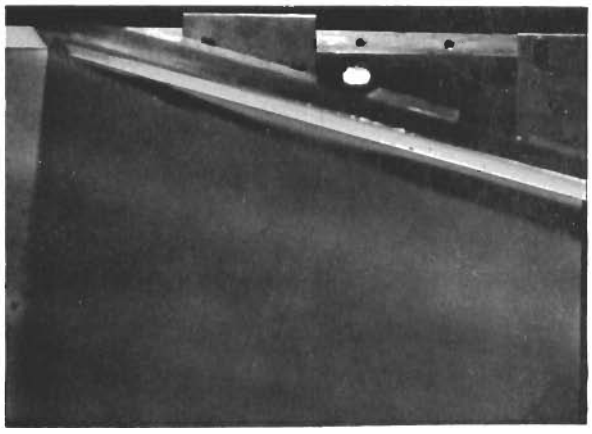

8.20 sec

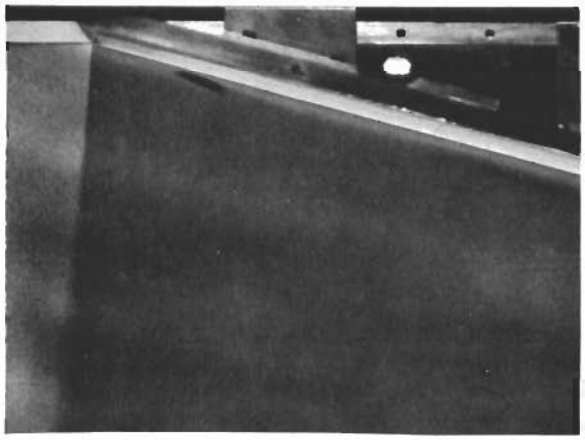

2.70 sec

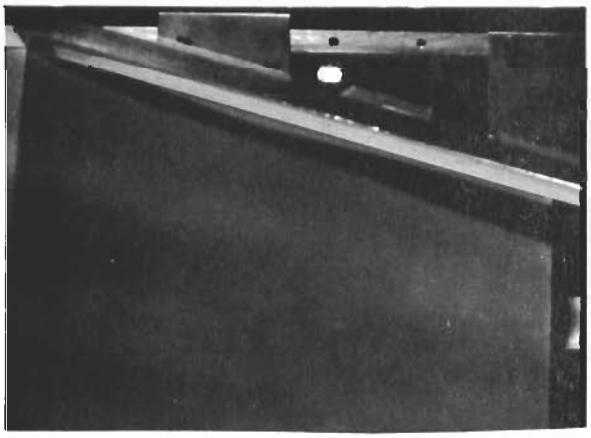

12.7 sec

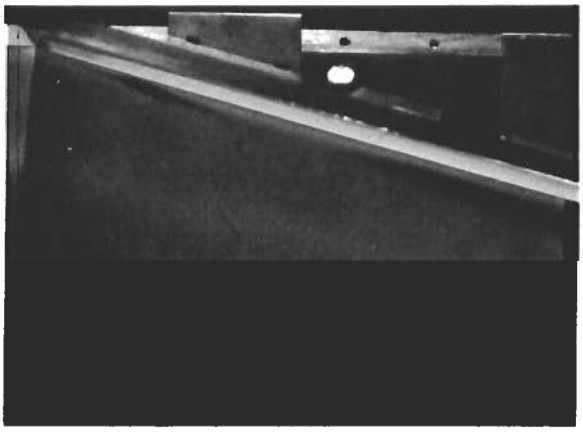

4.70 sec

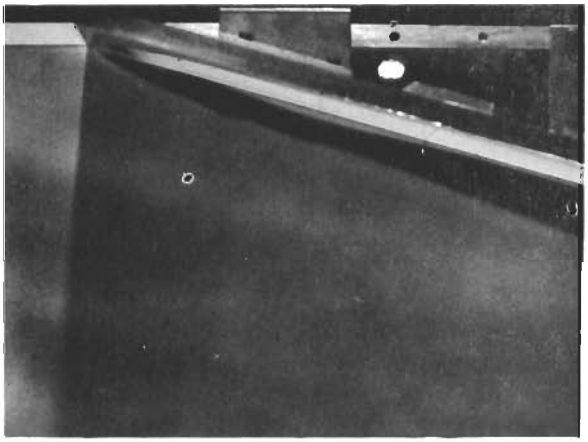

22.7 sec

Fig. 14 Coating Phase – Change Patterns for Run 337 (X_f = 4 in., δ = 15 deg)

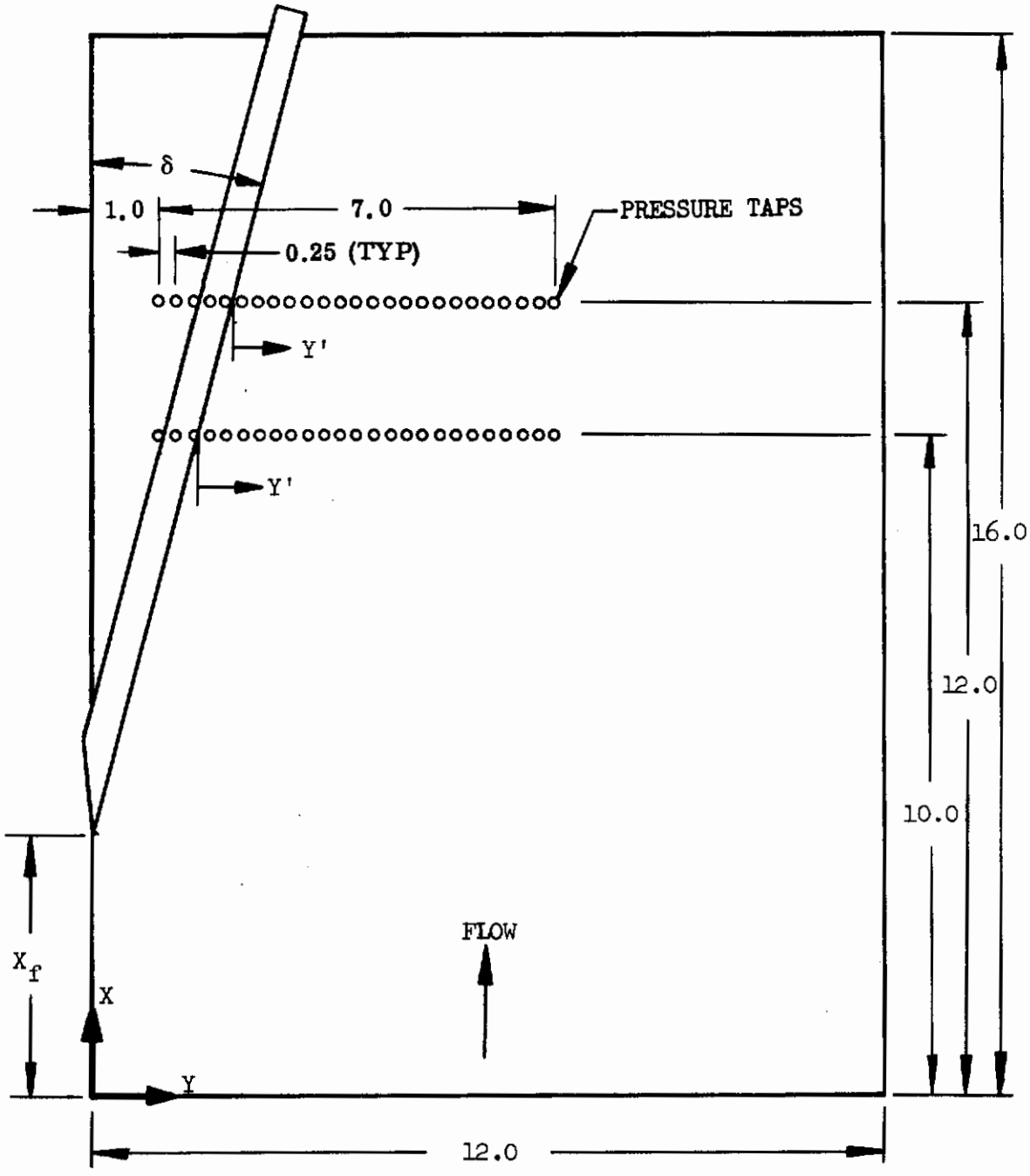

Fig. 15 Shock Interference Model Pressure Insert

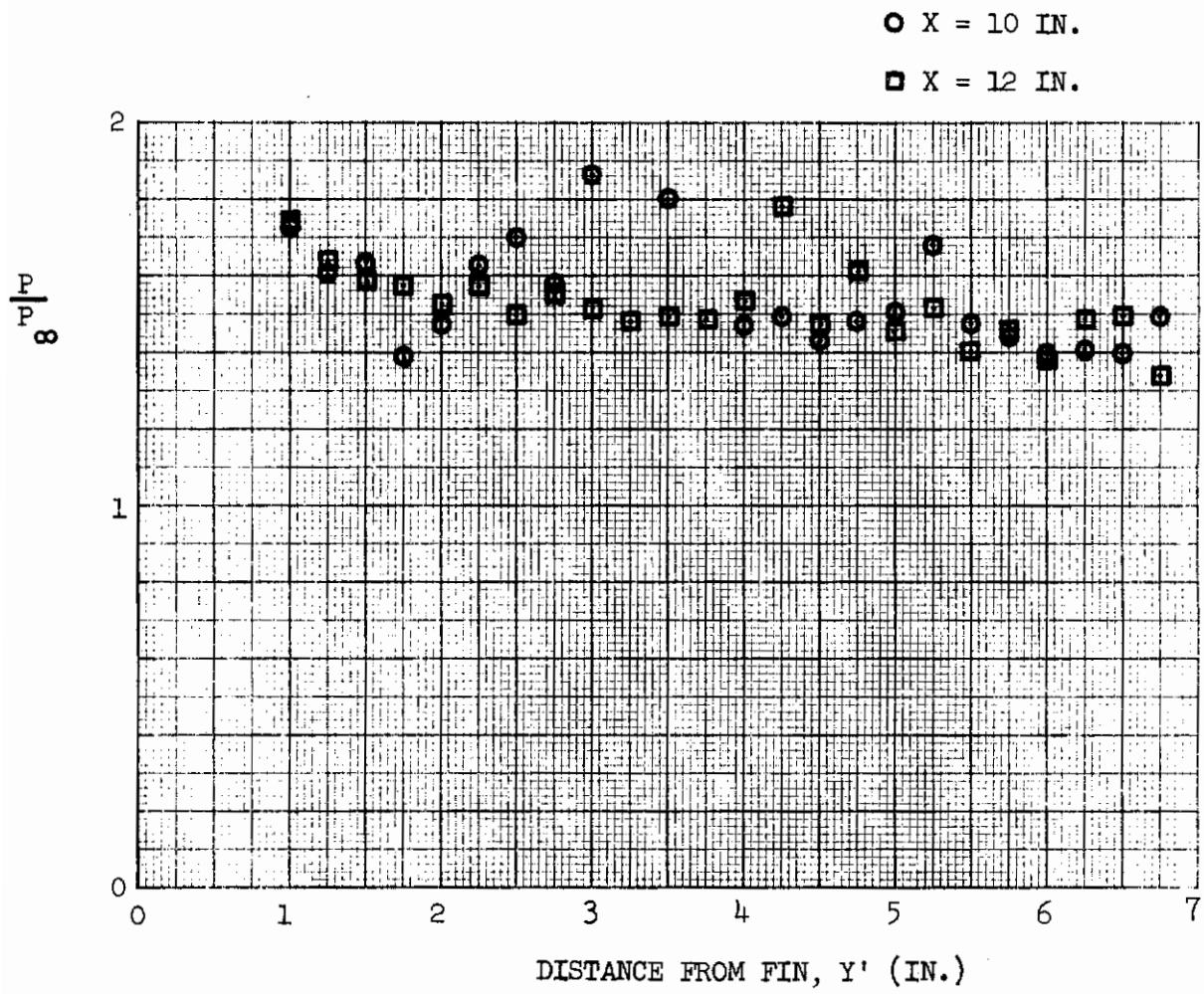

Fig. 16 Pressure Distributions Without Side Fins

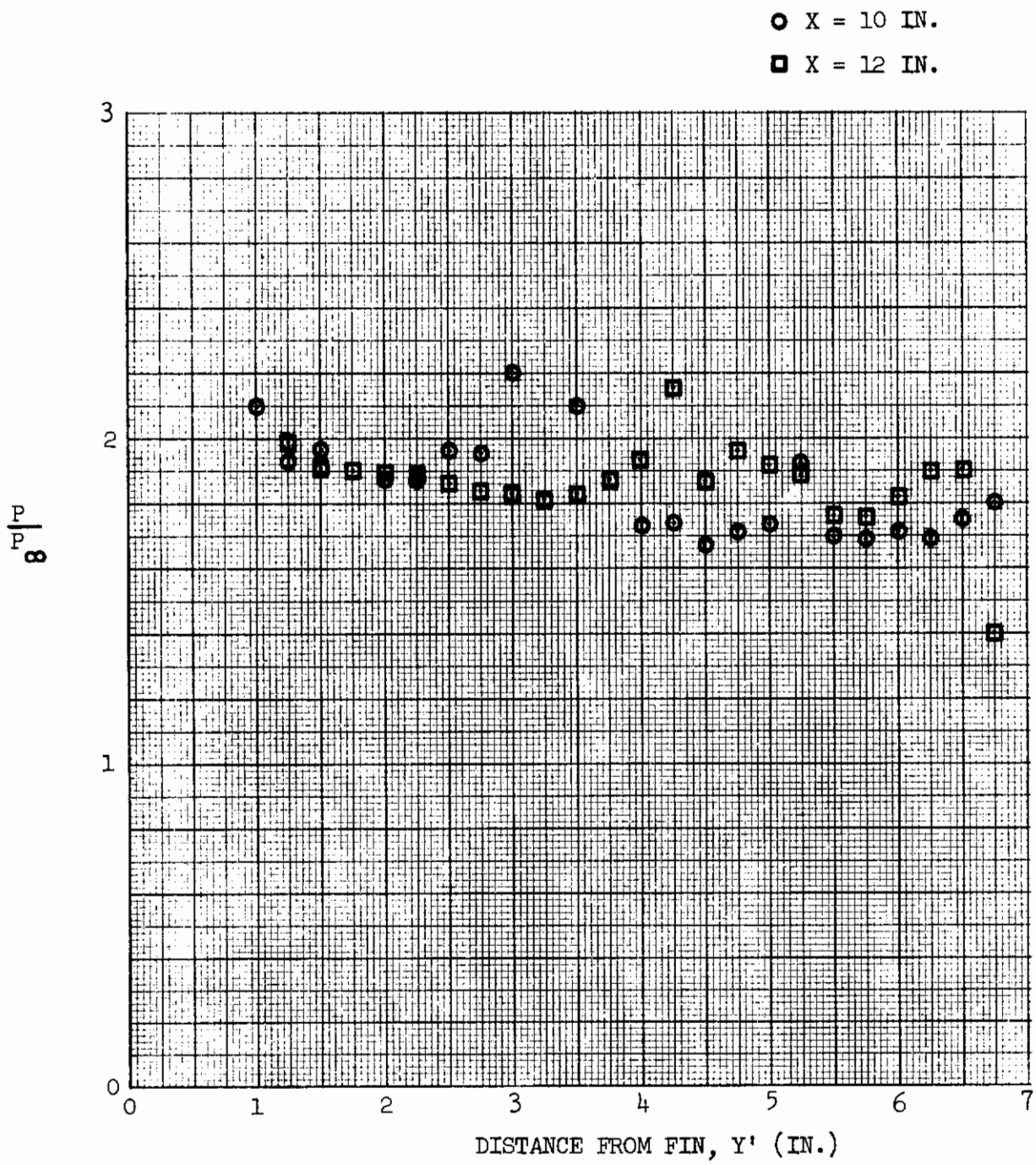

Fig. 17 Pressure Distributions With Both Side Fins at X_f = 0 in., δ = 0 deg.

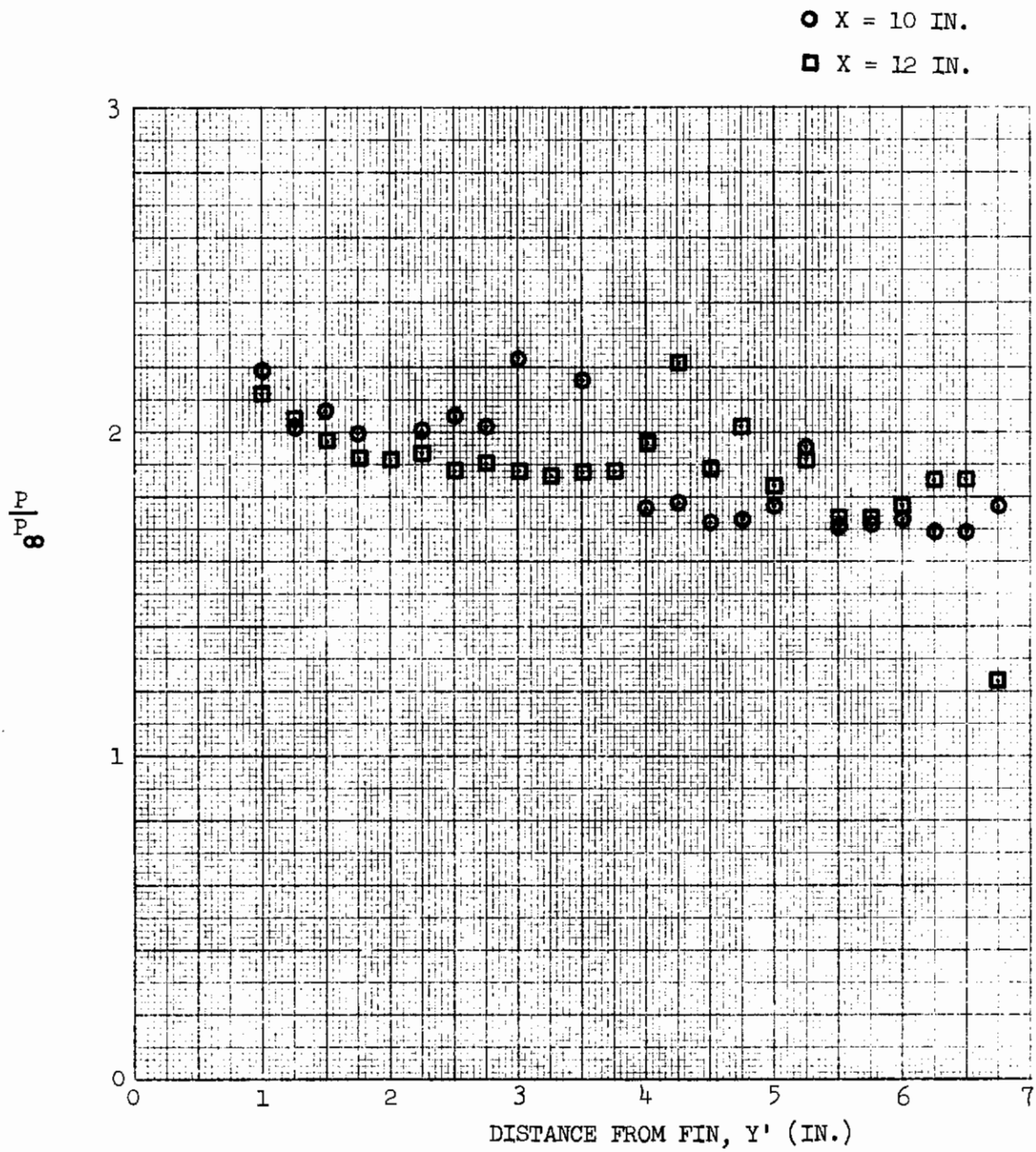

Fig. 18 Pressure Distribution for X_f = 0 in., δ = 0 deg.

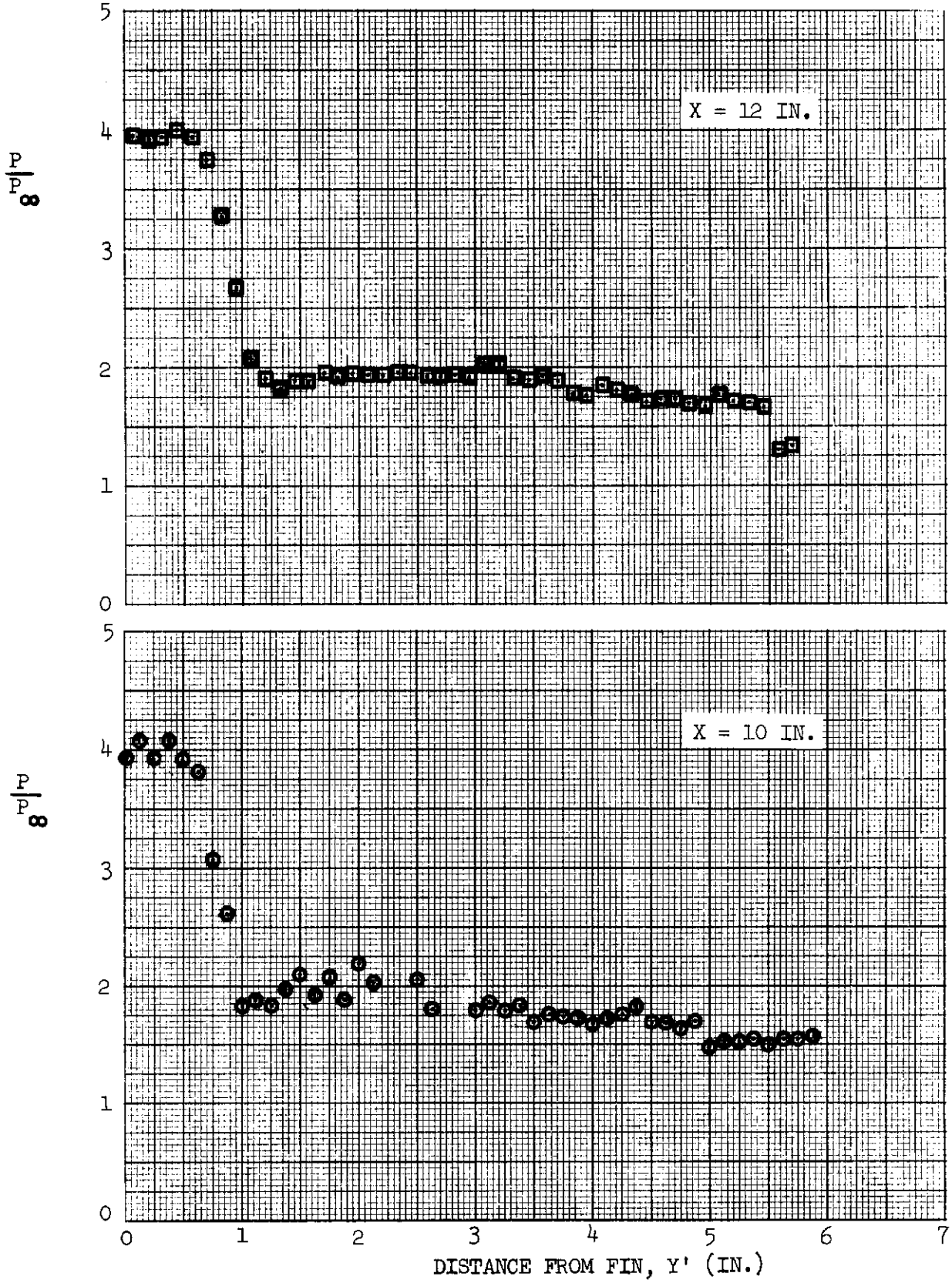

Fig. 19 Pressure Distribution for $X_f = 0$ in., $\delta = 5$ deg.

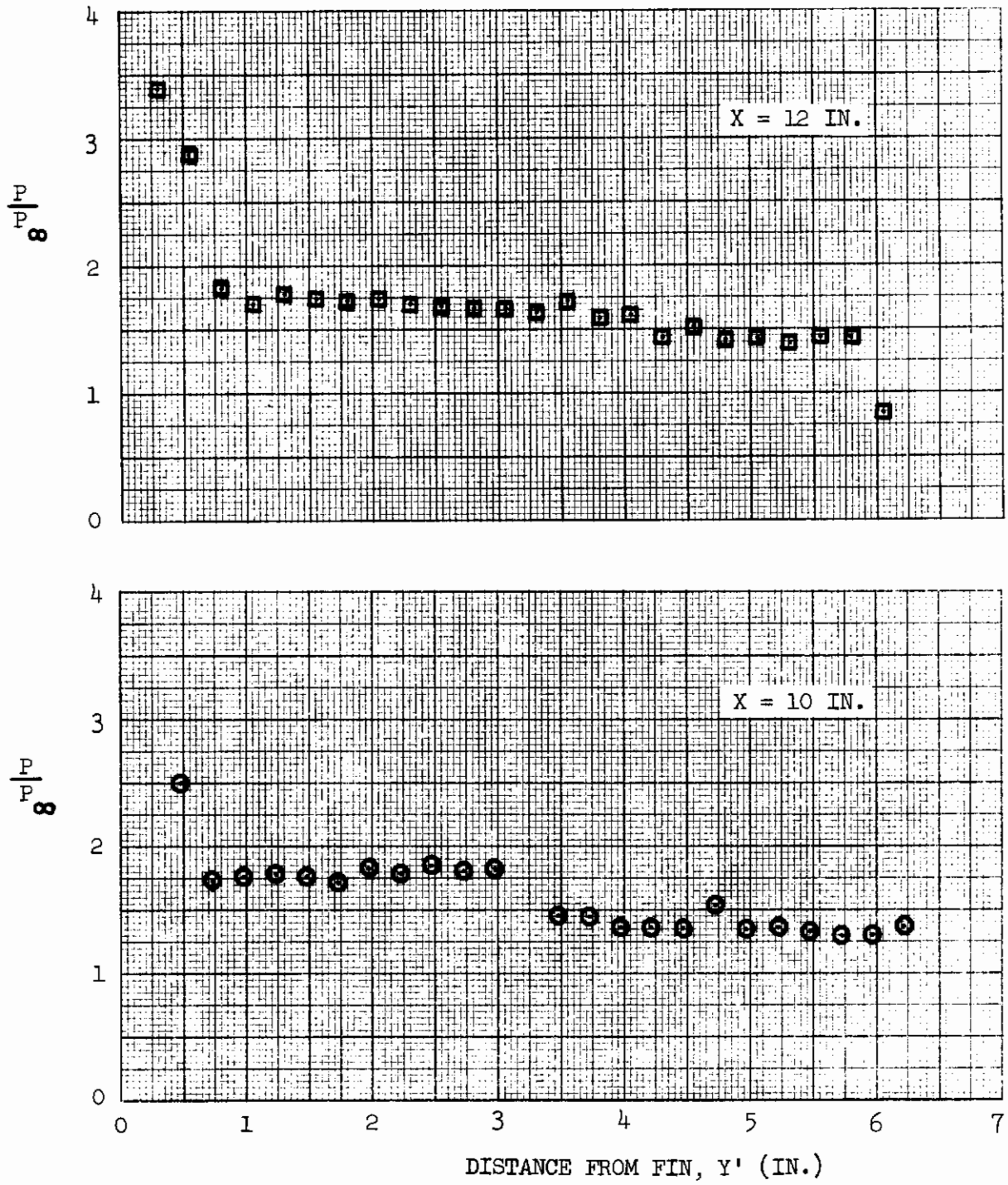

Fig. 20 Pressure Distribution for X_f = 4 in., δ = 5 deg.

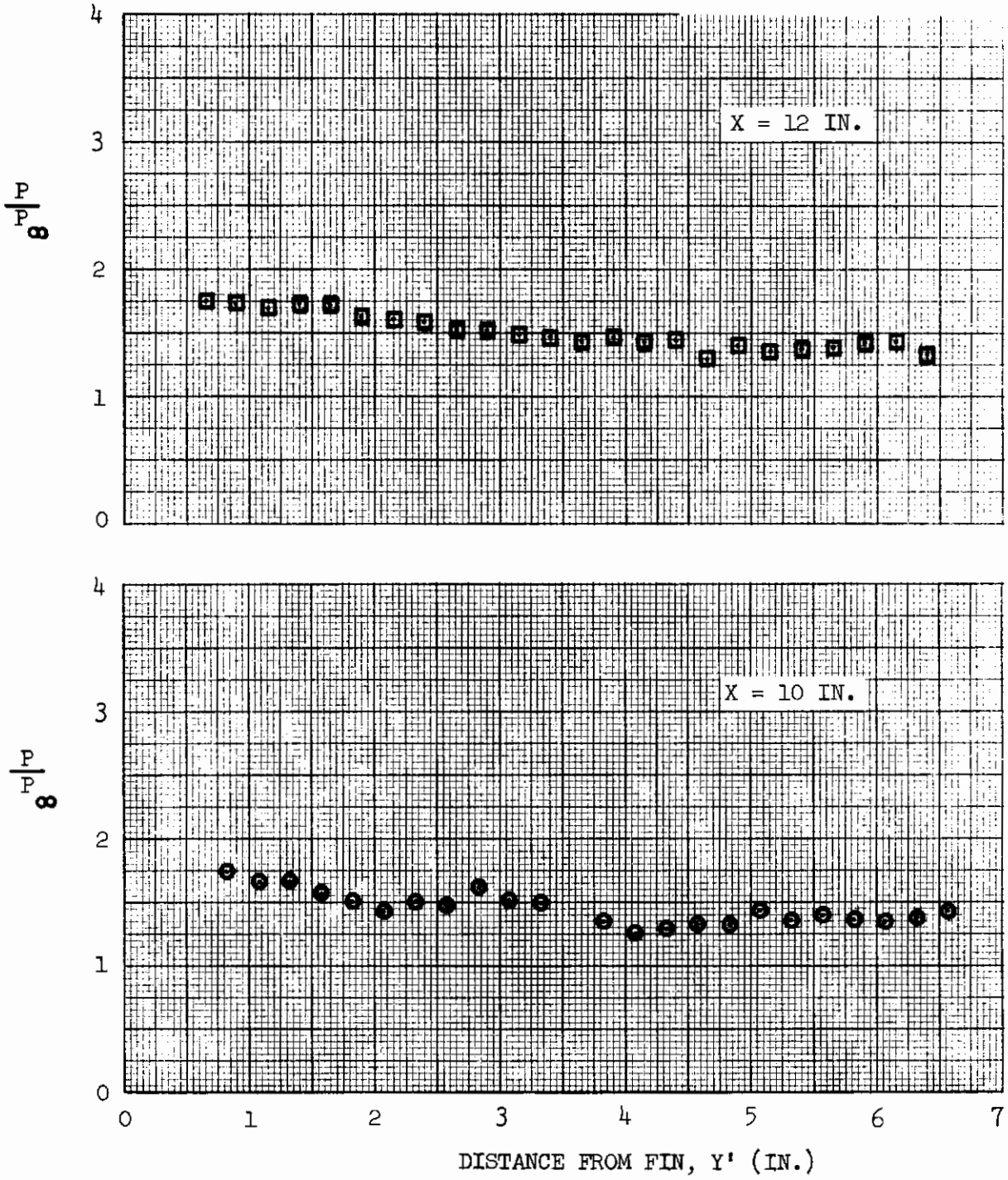

Fig. 21 Pressure Distribution for X_f = 8 in., δ = 5 deg.

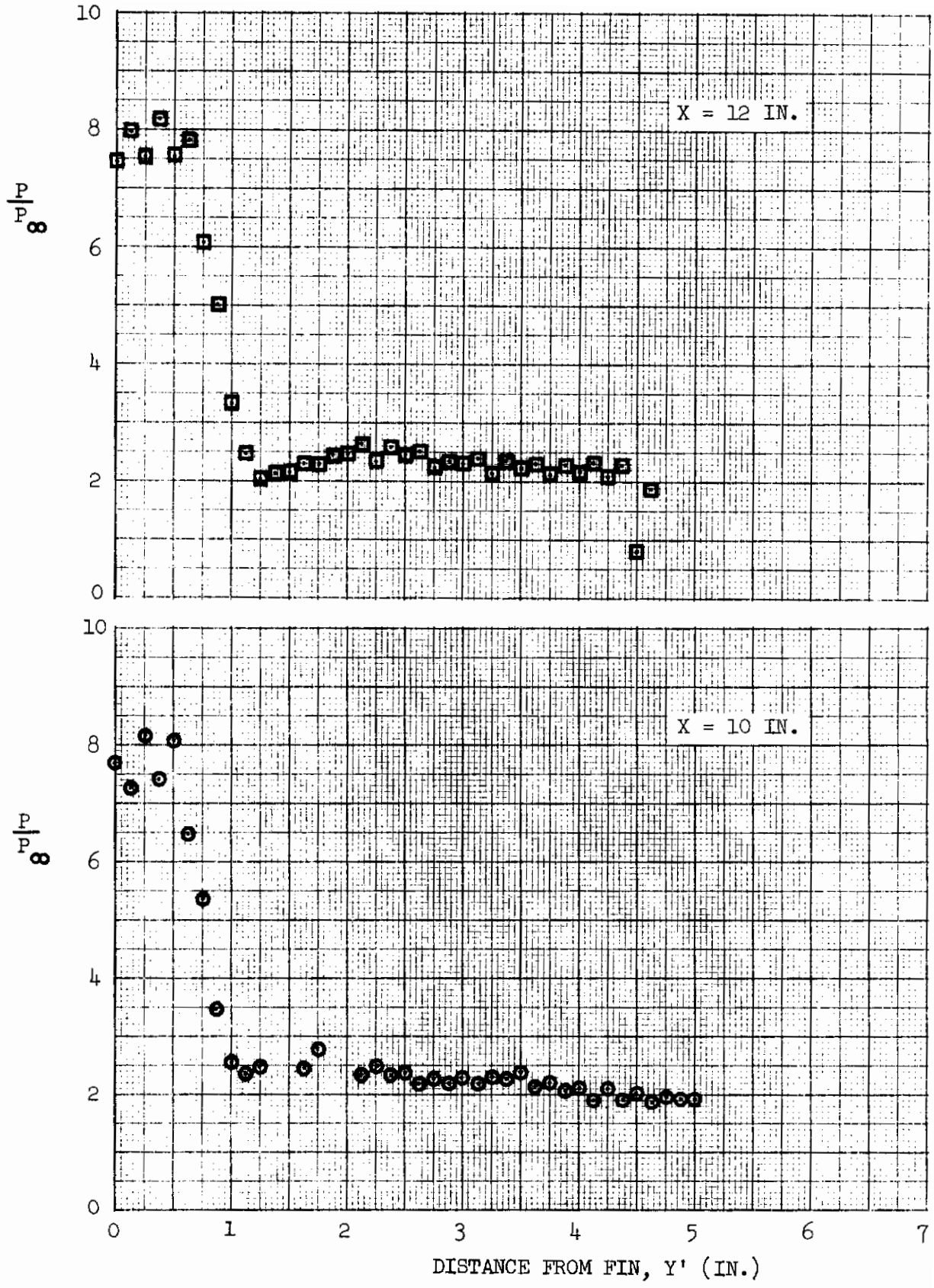

Fig. 22 Pressure Distribution for X_f = 0 in., δ = 10 deg.

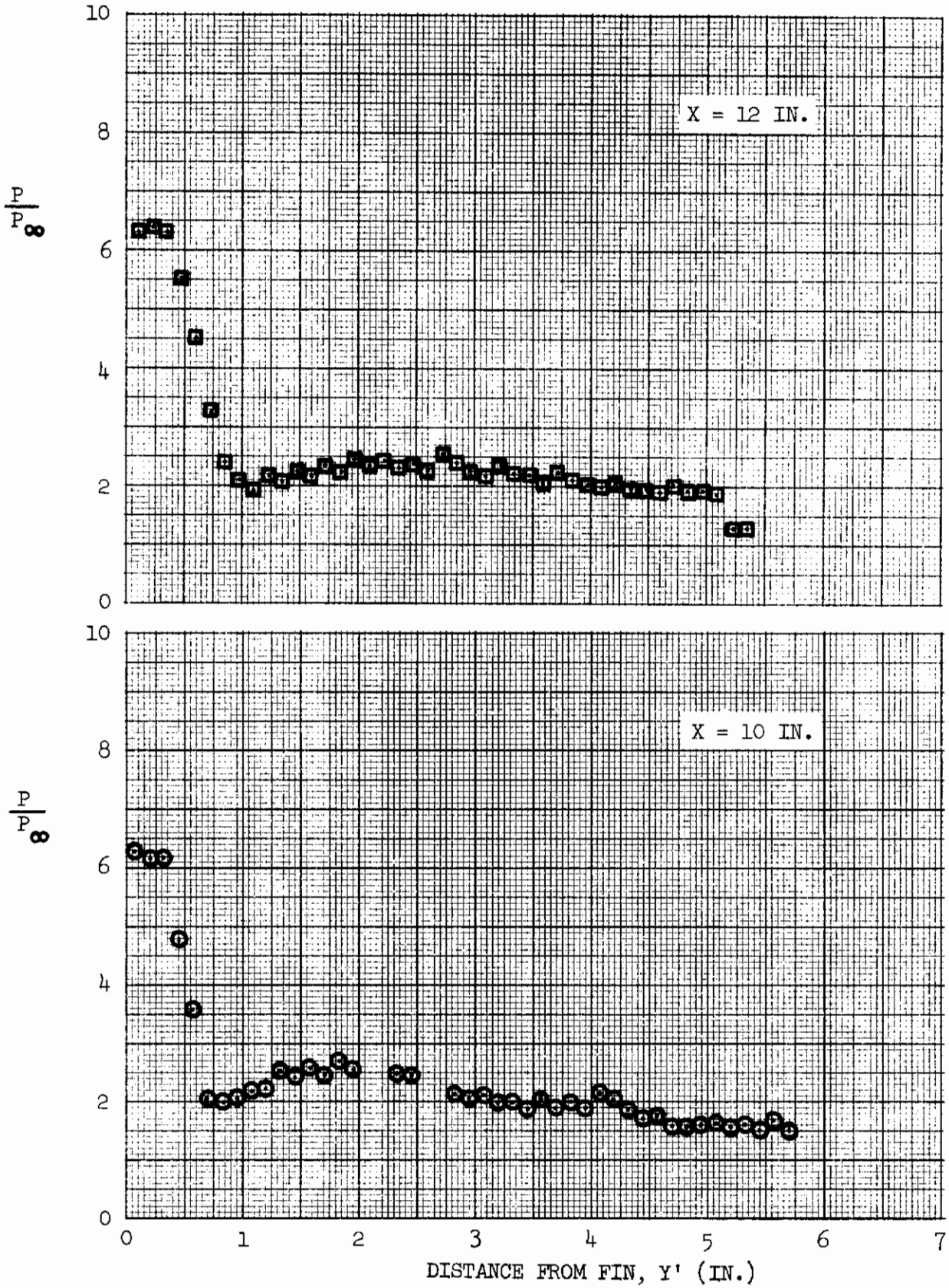

Fig. 23 Pressure Distribution for X_f = 4 in., δ = 10 deg.

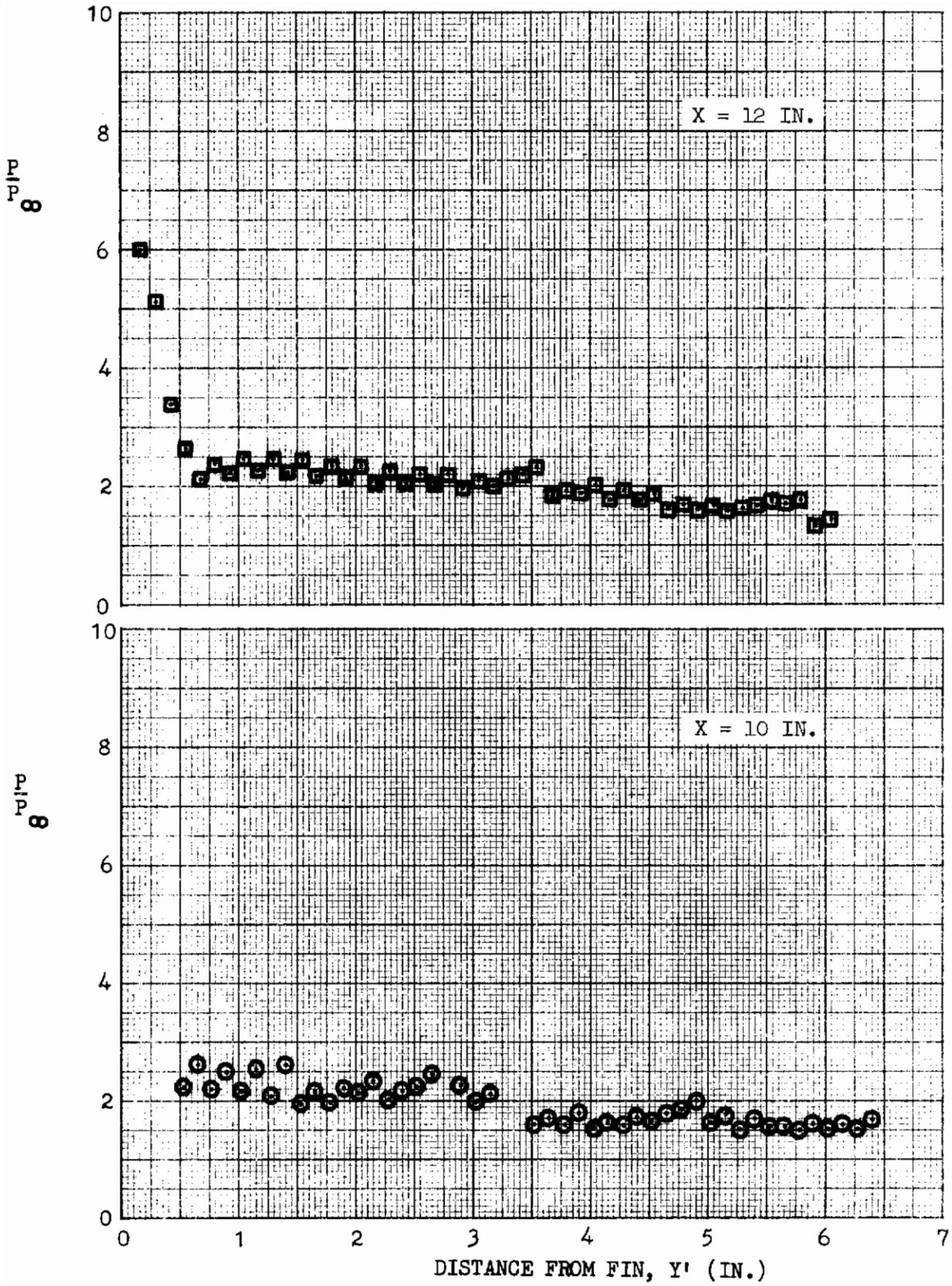

Fig. 24 Pressure Distribution for X_f = 8 in., δ = 10 deg.

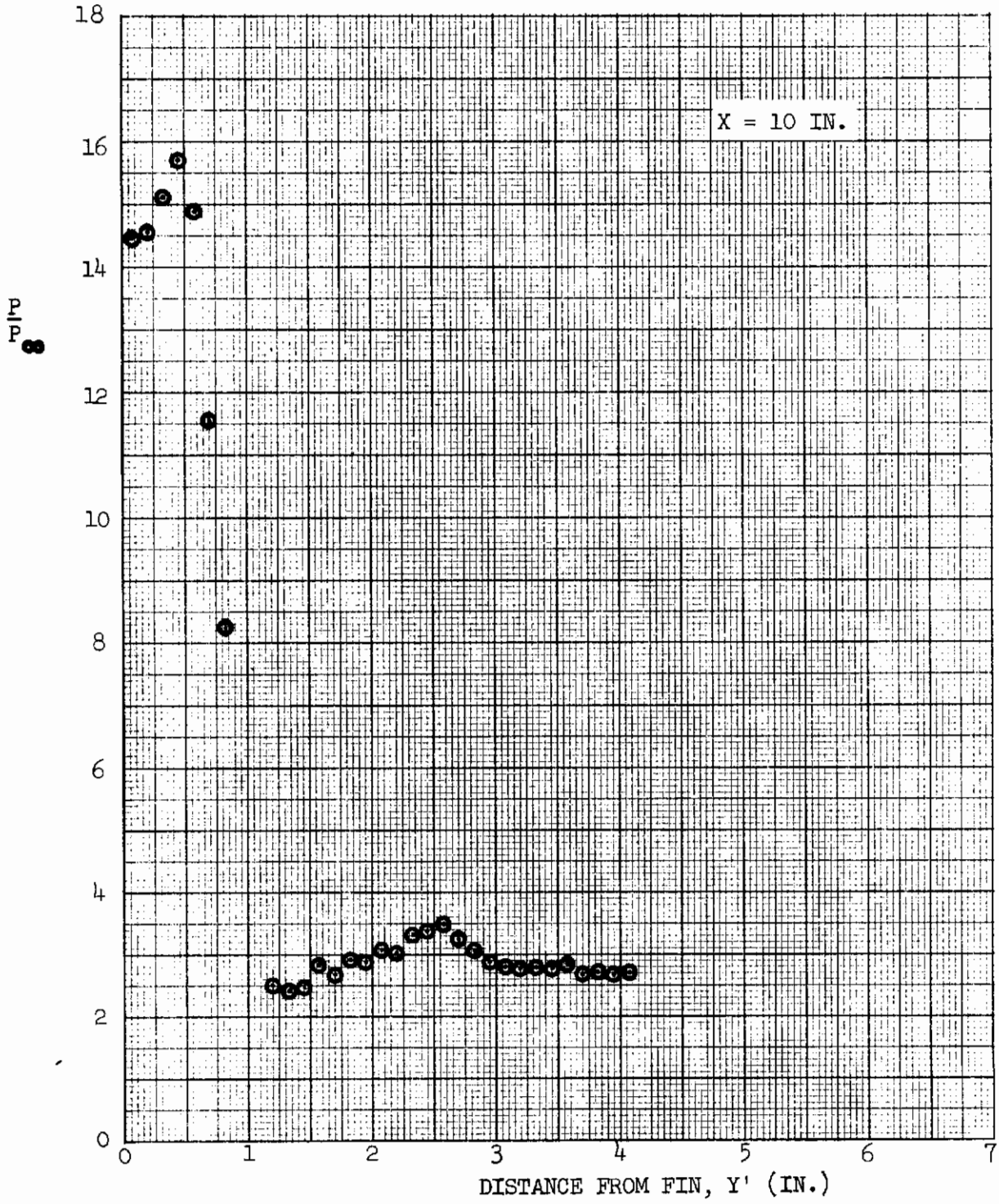

Fig. 25 Pressure Distribution for X_f = 0 in., δ = 15 deg.

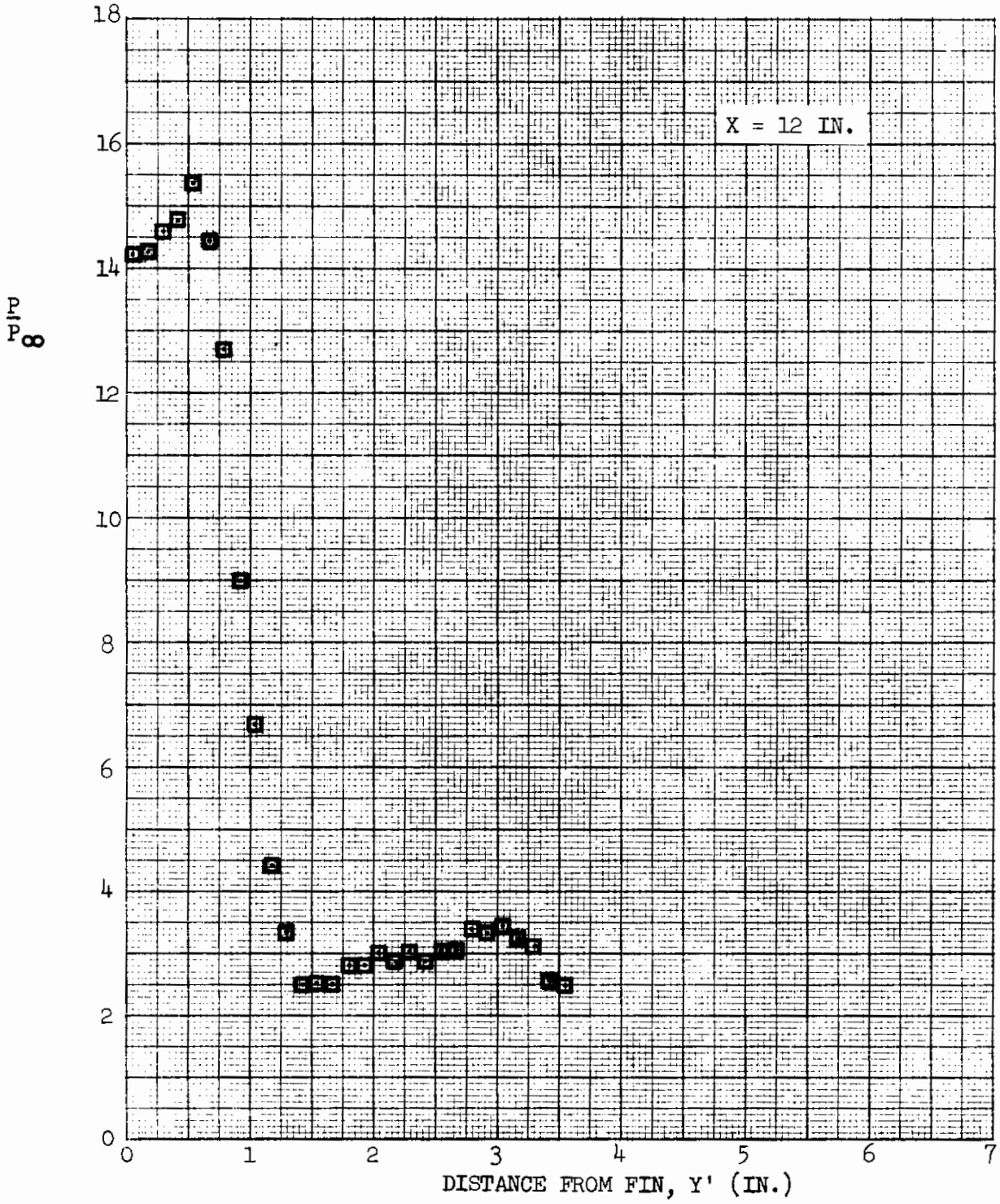

Fig. 25 Pressure Distribution for X_f = 0 in., δ = 15 deg. (Concluded)

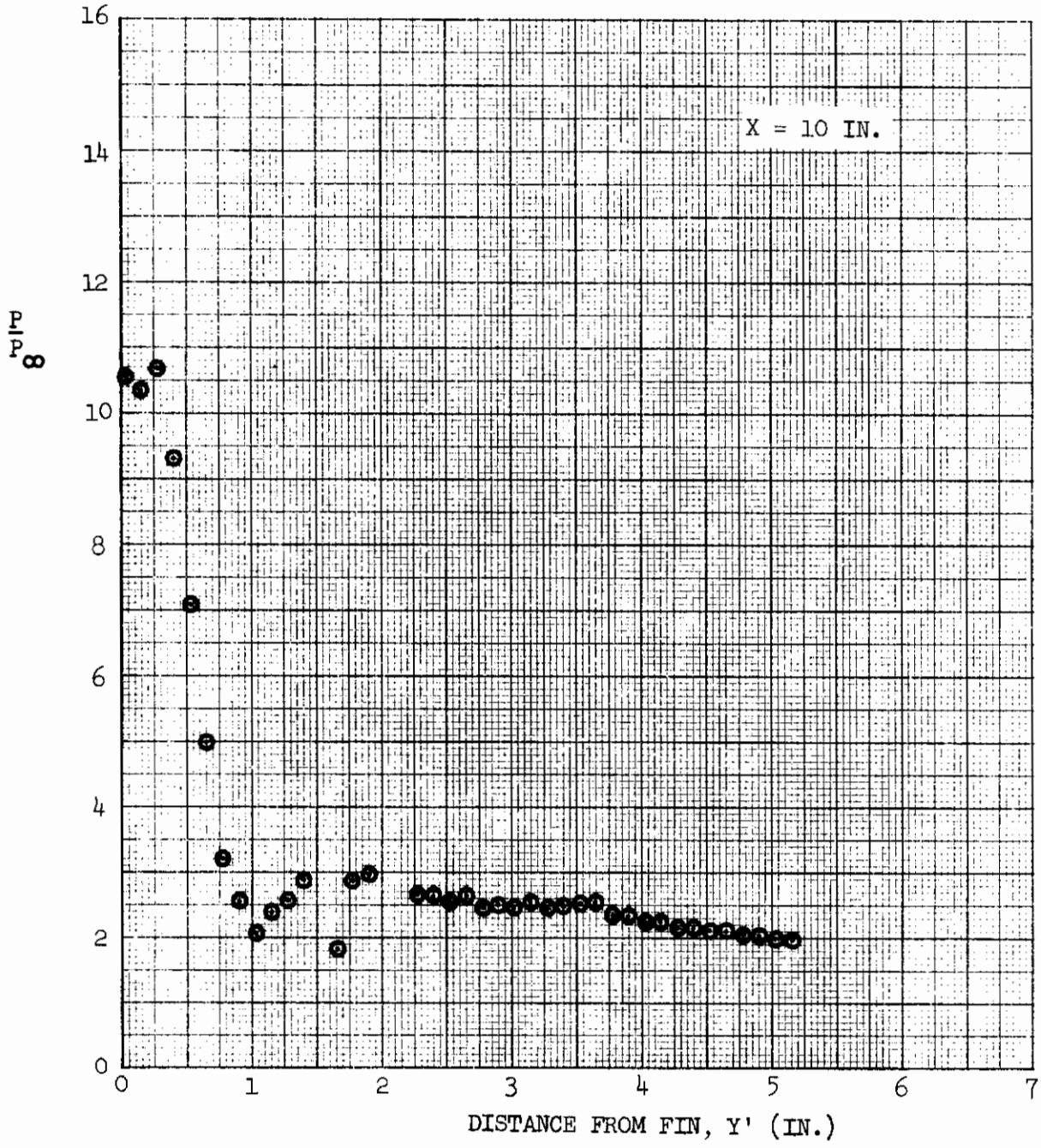

Fig. 26 Pressure Distribution for X_f = 4 in., δ = 15 deg.

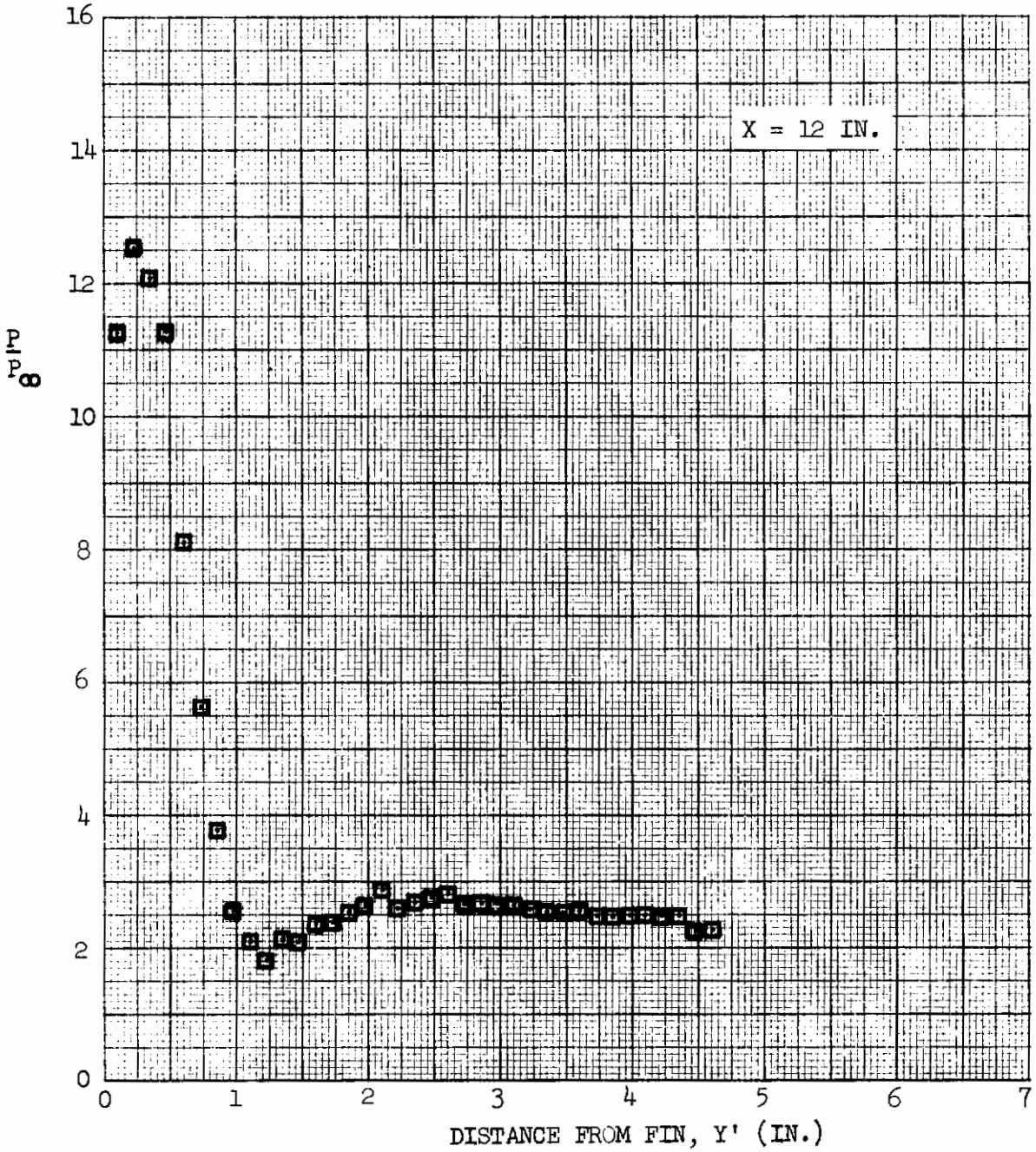

Fig. 26 Pressure Distribution for X_f = 4 in., δ = 15 deg. (Concluded)

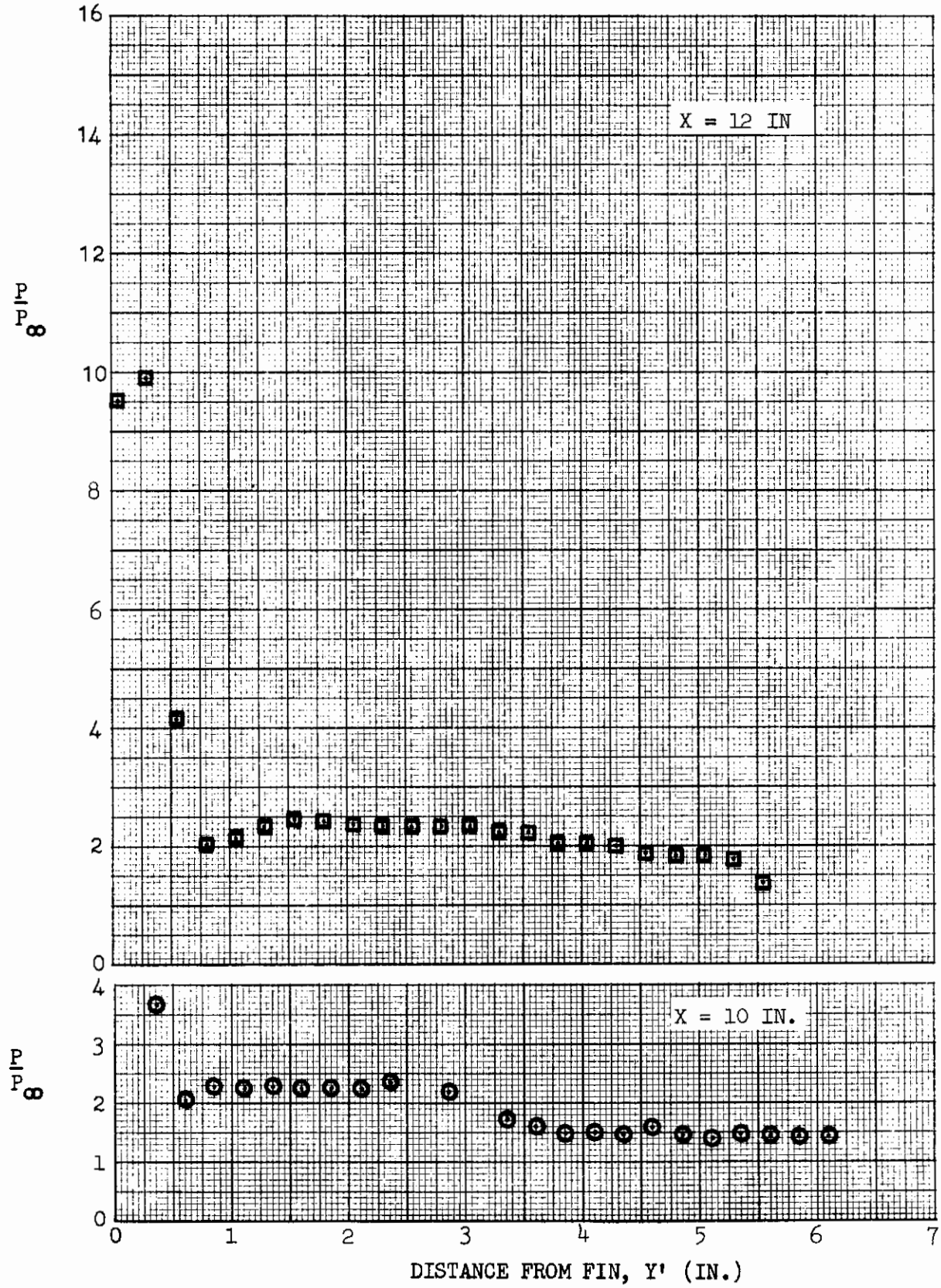

Fig. 27 Pressure Distribution for X_f = 8 in., δ = 15 deg.

δ = 15 deg. Figure 28a shows the experimental melt time distribution normal to the fin in the peak heating region. The data points are faired to determine melt times at each surface node location of the two-dimensional thermal network, which is illustrated in Fig. 3. As described in the Appendix, network dimensions, thermophysical properties, and other pertinent information are input to the data reduction program, which solves for the heat transfer coefficient distribution. Figure 28b compares program calculations with semi-infinite slab theory. As shown, lateral heating effects are small, with the peak heating rate determined by the computer program about eight percent higher than the value based on one-dimensional heat conduction.

Thermophysical property data for Teflon were obtained from Reference 7. Because Stycast properties tend to vary from batch to batch, thermal conductivity and thermal diffusivity tests were performed on a sample of the material used to fabricate the Stycast inserts. These measurements, plotted in Fig. 29, were used for data reduction, along with nominal specific heat and density values from Reference 8. The following table summarizes the thermophysical properties which were used for data reduction.

	Teflon	Stycast
ρ (lb/ft^3)	135	140
c (Btu/lb-$^\circ$F)	0.24	0.27
k (Btu/hr-ft-$^\circ$F)	0.15	0.75

As shown in Fig. 30, the specific heat of Teflon is affected by a room-temperature transition in crystal structure. The specific heat is not well defined for temperatures between 65° and 90°F, but is much larger than the nominal value of 0.24 Btu/lb-$^\circ$F which was used for data reduction. As a result, data from Teflon inserts with initial temperature less than 90°F are probably low and should be considered qualitative. Except for the undisturbed flat plate heating data shown in Fig. 8, none of the Teflon data with initial temperature below 90°F are included in this report. With the exception of four runs, all heat transfer tests were performed using either 150°F or 200°F Tempilaq. Consequently, little error results from the assumption of constant thermophysical properties. Of the four exceptions, only two runs, using 400°F Tempilaq on Teflon inserts, produced useful data. The computer program described in Section 2.3 was used to reduce data from these two runs in order to account for the effects of temperature-dependent thermophysical properties (Ref. 7).

For temperatures between 90–400°F Teflon thermophysical properties appear to be repeatable and accurately known. Stycast thermal conductivity measurements performed by two independent Lockheed organizations (Fig. 29) agree with NASA-Langley nominal values, based on measurements from 16 samples (Ref. 8) within 6 percent. The largest uncertainty appears to be in the specific heat of Stycast, where the nominal value of 0.27 Btu/lb-$^\circ$F is the data mean from 19 samples (Ref. 8). Based on the scatter of data from the literature the estimated accuracies for the thermophysical properties are: Teflon ρ (one percent), Teflon k (seven percent), Teflon c (five percent), Stycast ρ (two percent), Stycast k (eight percent), and Stycast c (ten percent).

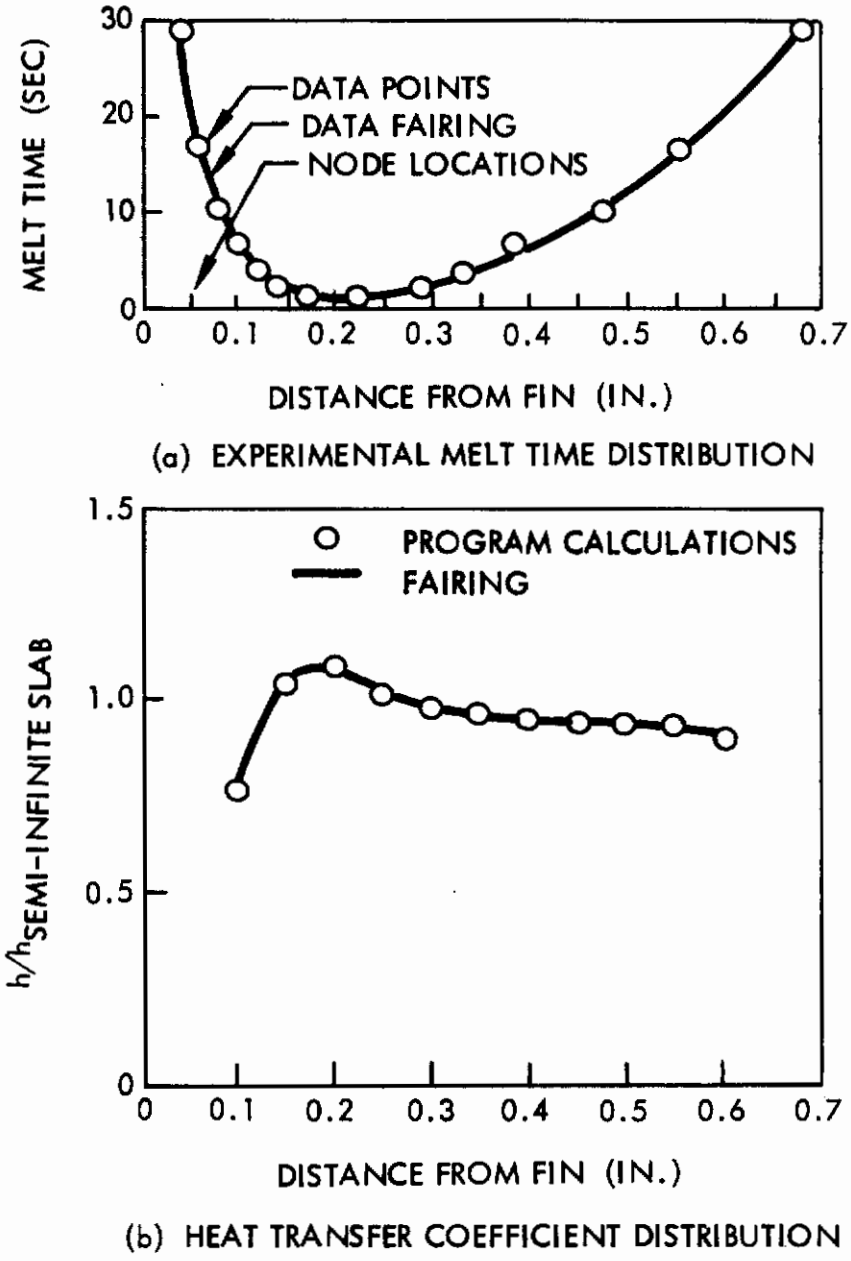

Fig. 28 Data Reduction for Run 338 Using Program I

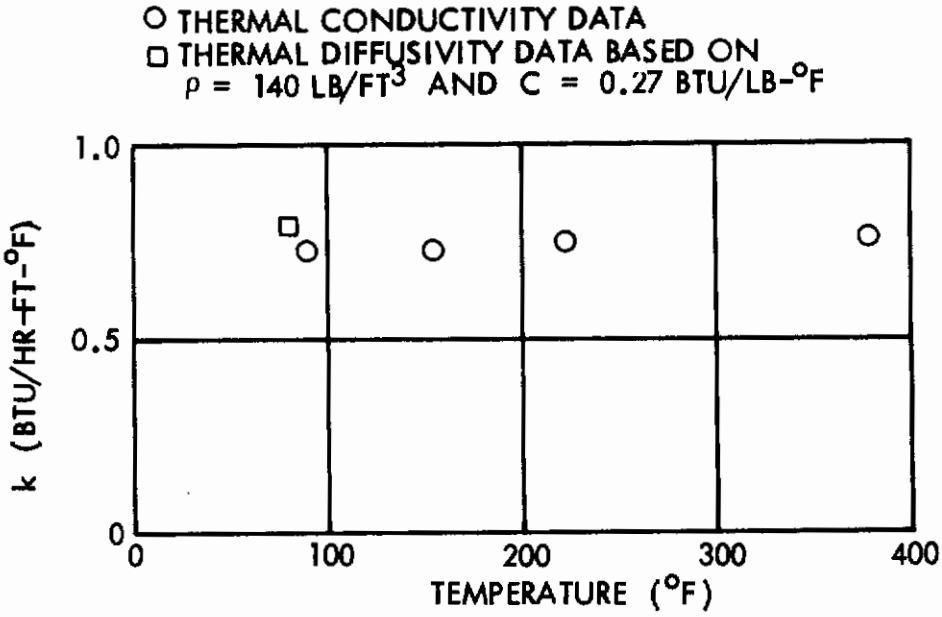

Fig. 29 Stycast Thermal Conductivity

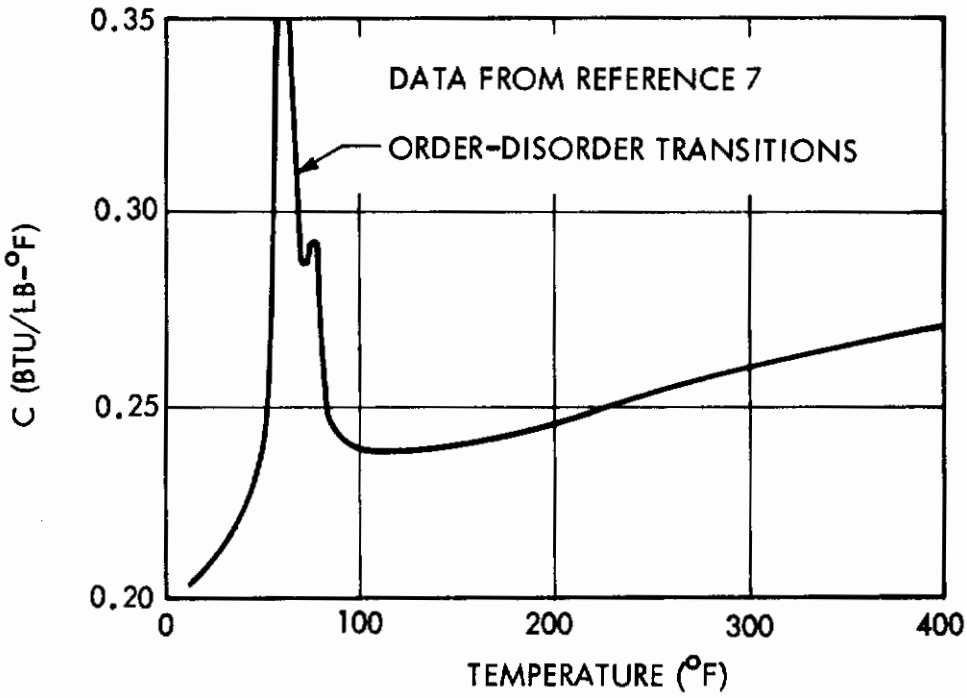

Fig. 30 Teflon Specific Heat

In general, coating melt patterns are well defined on the Stycast insert but are obscure on the Teflon inserts. Because of the poor resolution of melt patterns, data were reduced for only 26 of the 43 runs made using Teflon inserts. A second problem experienced with the Teflon inserts is that the 0.04 in. and 0.06 in. sheets buckled along the high heating region for fin deflections above 5 degrees. The effect of this failure on the data is unknown because the time when buckling occurred cannot be determined from the test film. The local buckling did not affect subsequent tests because the damaged region was covered as the fin angle was progressively increased.

Figure 31 compares heat transfer coefficient distributions along the line of peak heating (see Fig. 48) from various Teflon and Stycast inserts. The Stycast data are consistently higher than the Teflon data, and heating rates from the 0.25 in. inserts are generally slightly higher than data from the thinner inserts, which are backed with polyurethane foam. Part of the latter discrepancy is attributed to inaccuracies in estimating the thermal capacitance of the adhesive used to bond the insert to the foam. For data reduction the insert thickness was increased by 0.002 in., the estimated equivalent thermal capacitance of the adhesive. Because of problems associated with the room-temperature transition in crystal structure, poor resolution of melt patterns, and buckling of the thin inserts, the Teflon data quality is considered to be poor. The Stycast data quality is considered to be good and, in case of disagreement between the Teflon and Stycast data, the latter are used in this report.

Figures 32 through 40 show the heat transfer coefficient distributions on the flat plate for each of the shock interference model primary test attitudes. Most of the heating contours are a composite of data from two or more runs, which were identical except for the test insert and coating melt temperature. The coefficients are in Btu/ft^2 sec $^\circ$F and are based on a laminar flow adiabatic wall temperature for Pr = 0.725, i.e., $T_{aw} = f(i_{aw})$ where $i_{aw} = i_\infty + \sqrt{0.725}\ V_\infty^2 / 2gJ$.

Because no phase-change coatings with melt temperature below 150°F were used during this program, little melting occurred upstream of the shockwave. Consequently, model span effects were not identified and the heating distributions plotted in Figures 32 through 40 include data from both the 8-in. and 12-in. wide inserts. In all cases the interaction region peak heat transfer coefficient was determined from tests utilizing the Stycast inserts. The experimental heating data have been adjusted, by the ratio of flat plate heat transfer coefficients, to a common flow condition, viz., P_0 = 300 psia and T_0 = 2100°R. Freestream flow properties are V_∞ = 5040 ft/sec, P_∞ = 0.855 lb/ft^2, T_∞ = 102.4°R, M_∞ = 10.15, and Re_∞/ft = 0.296 x 10^6. Figure 8 shows the theoretical flat plate heat transfer coefficient distribution based on these properties. The adiabatic wall temperature is 1822°R.

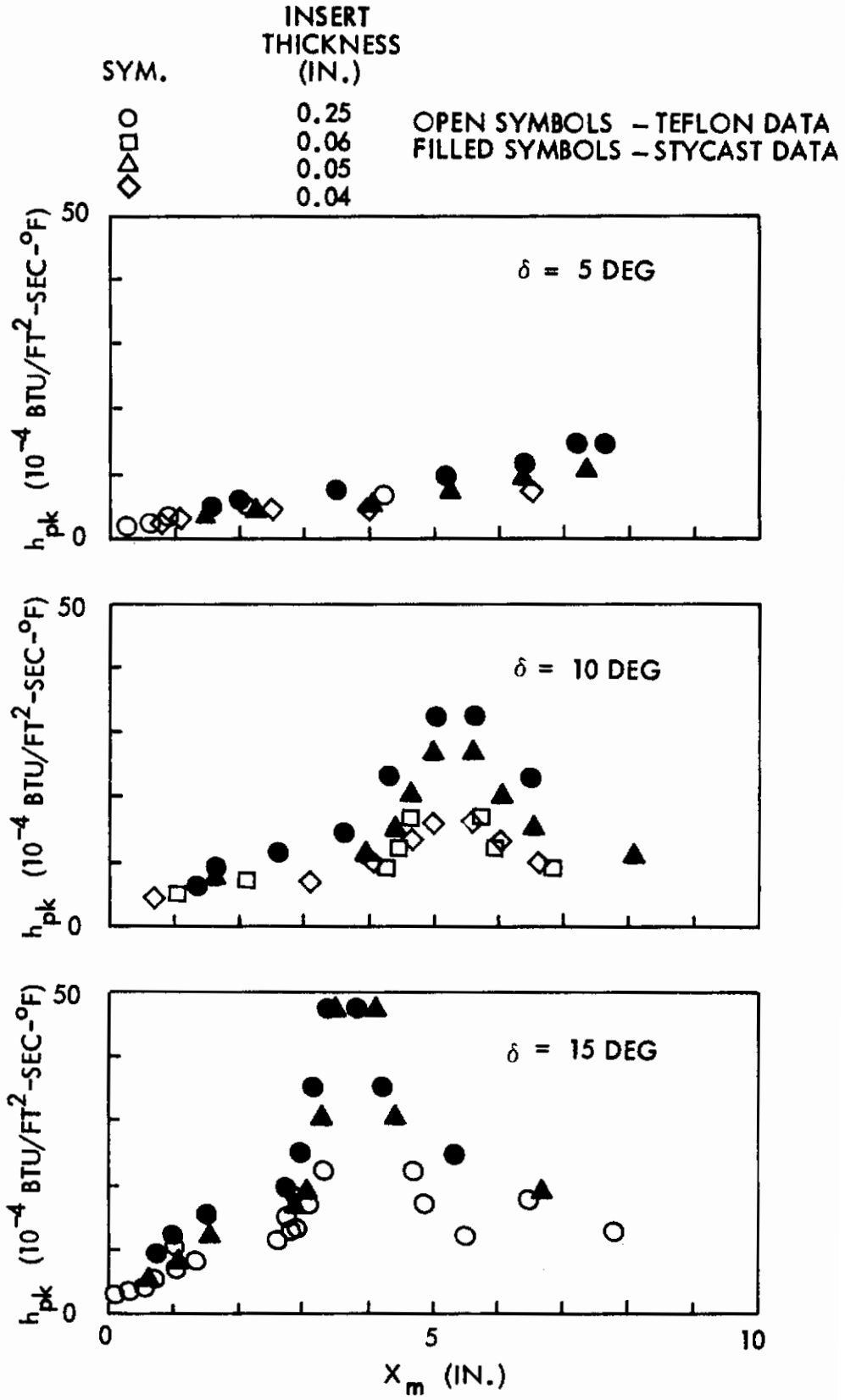

Fig. 31 Comparison of Stycast and Teflon Peak Heating Data for X_f = 8 in.

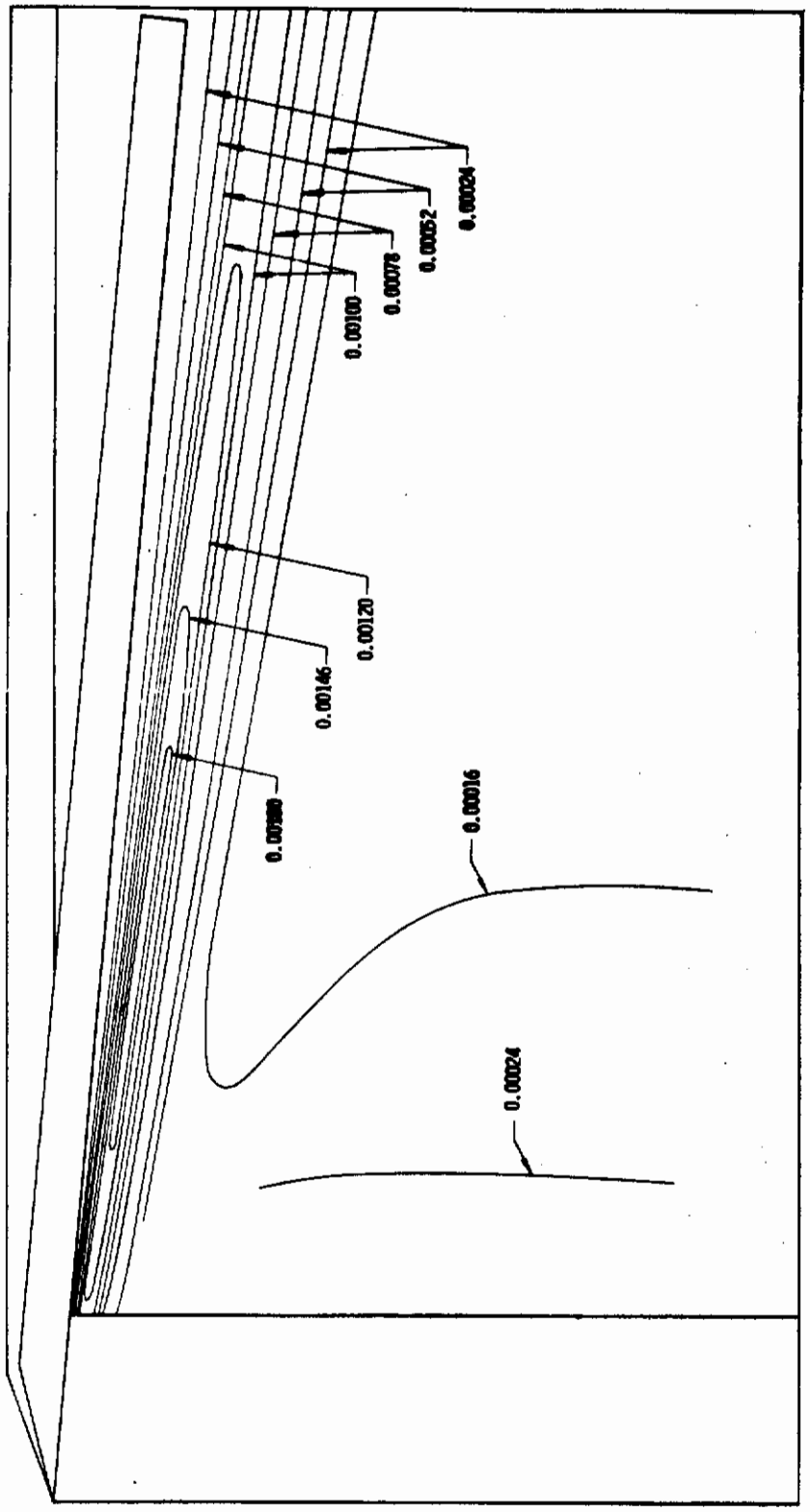

Fig. 32 Heat Transfer Coefficient Distributions for X_f = 0 in., δ = 5 deg.

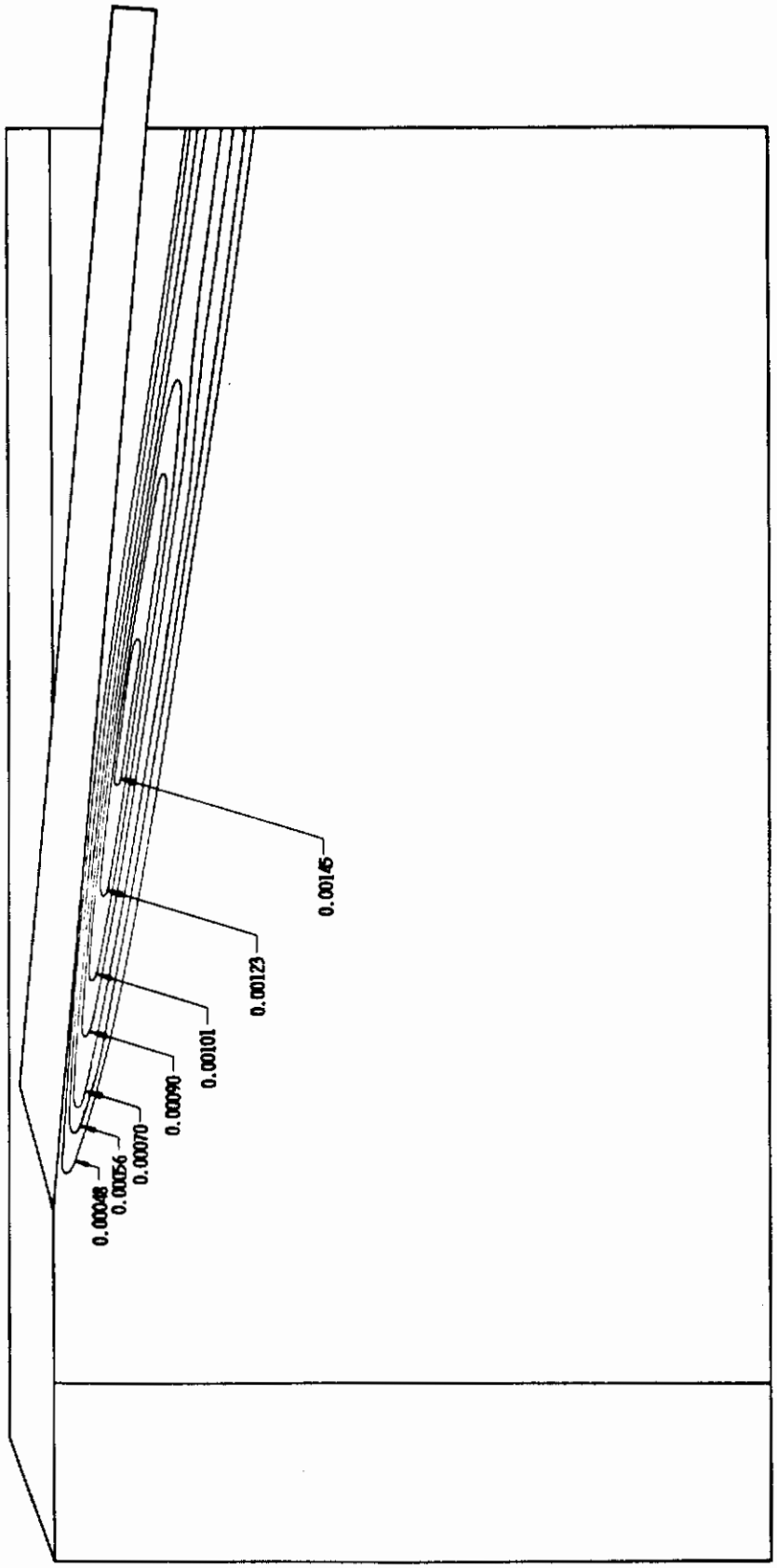

Fig. 33 Heat Transfer Coefficient Distributions for X_f = 4 in., δ = 5 deg.

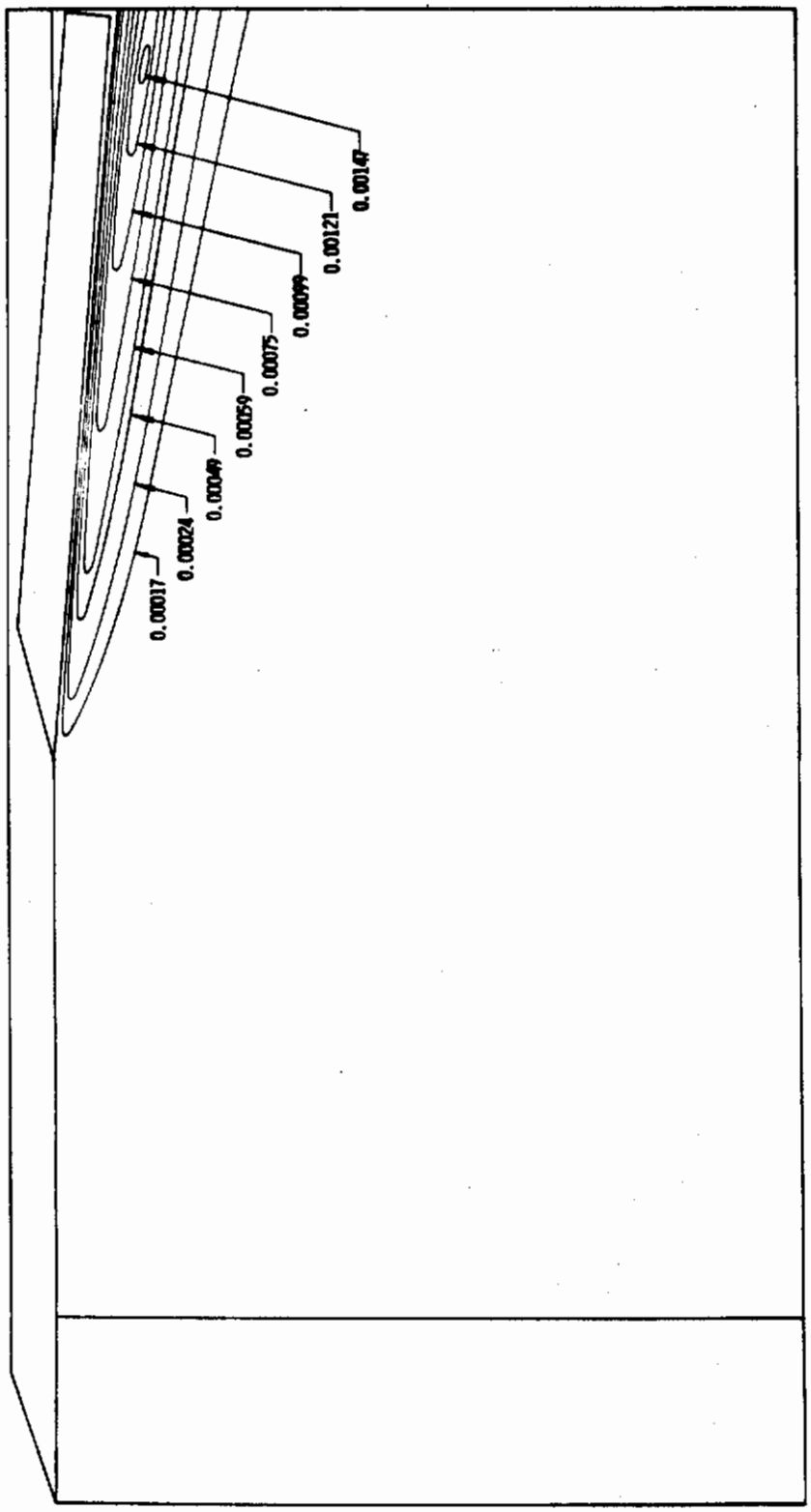

Fig. 34 Heat Transfer Coefficient Distributions for X_f = 8 in., δ = 5 deg.

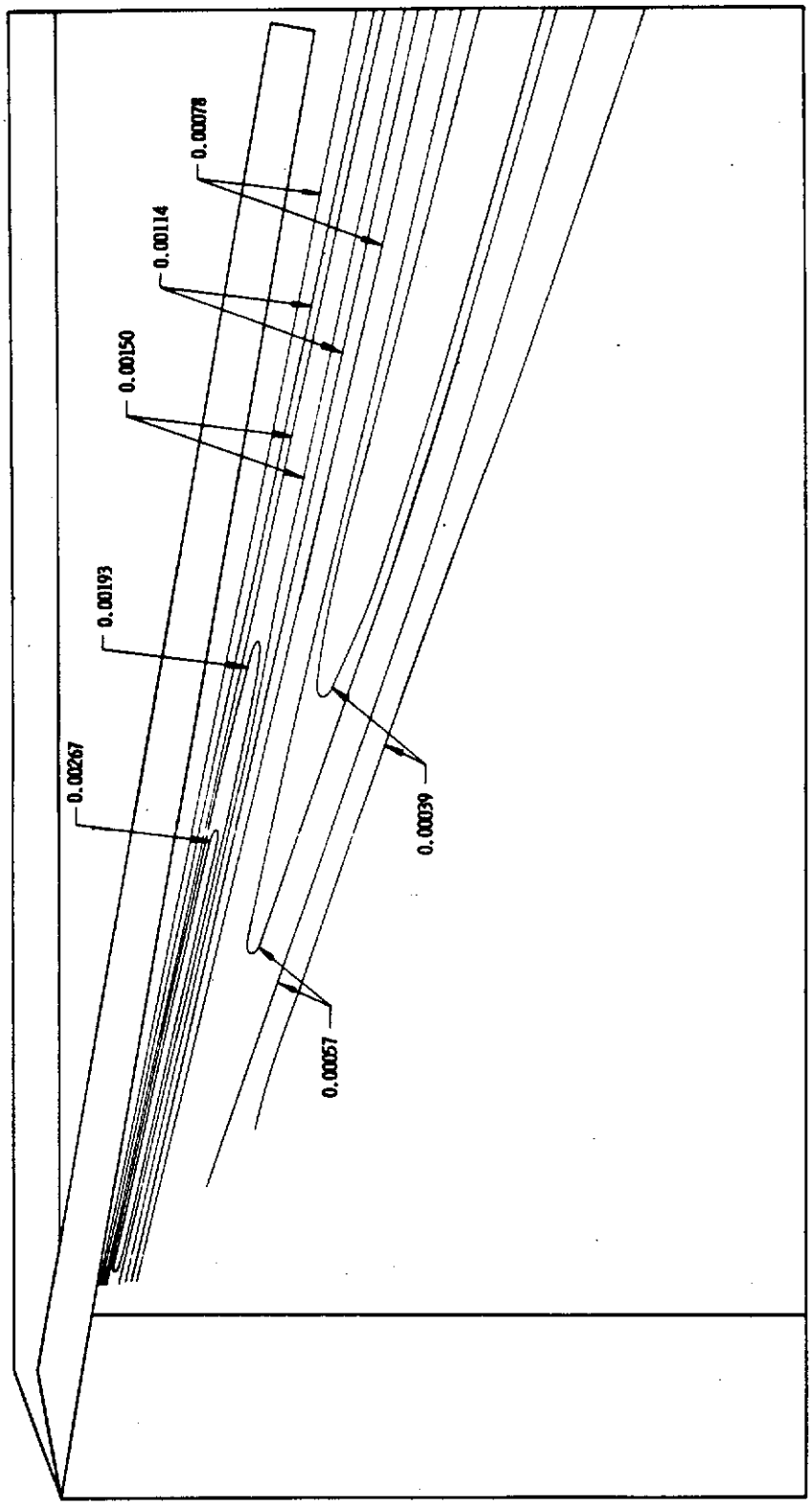

Fig. 35 Heat Transfer Coefficient Distributions for X_f = 0 in., δ = 10 deg.

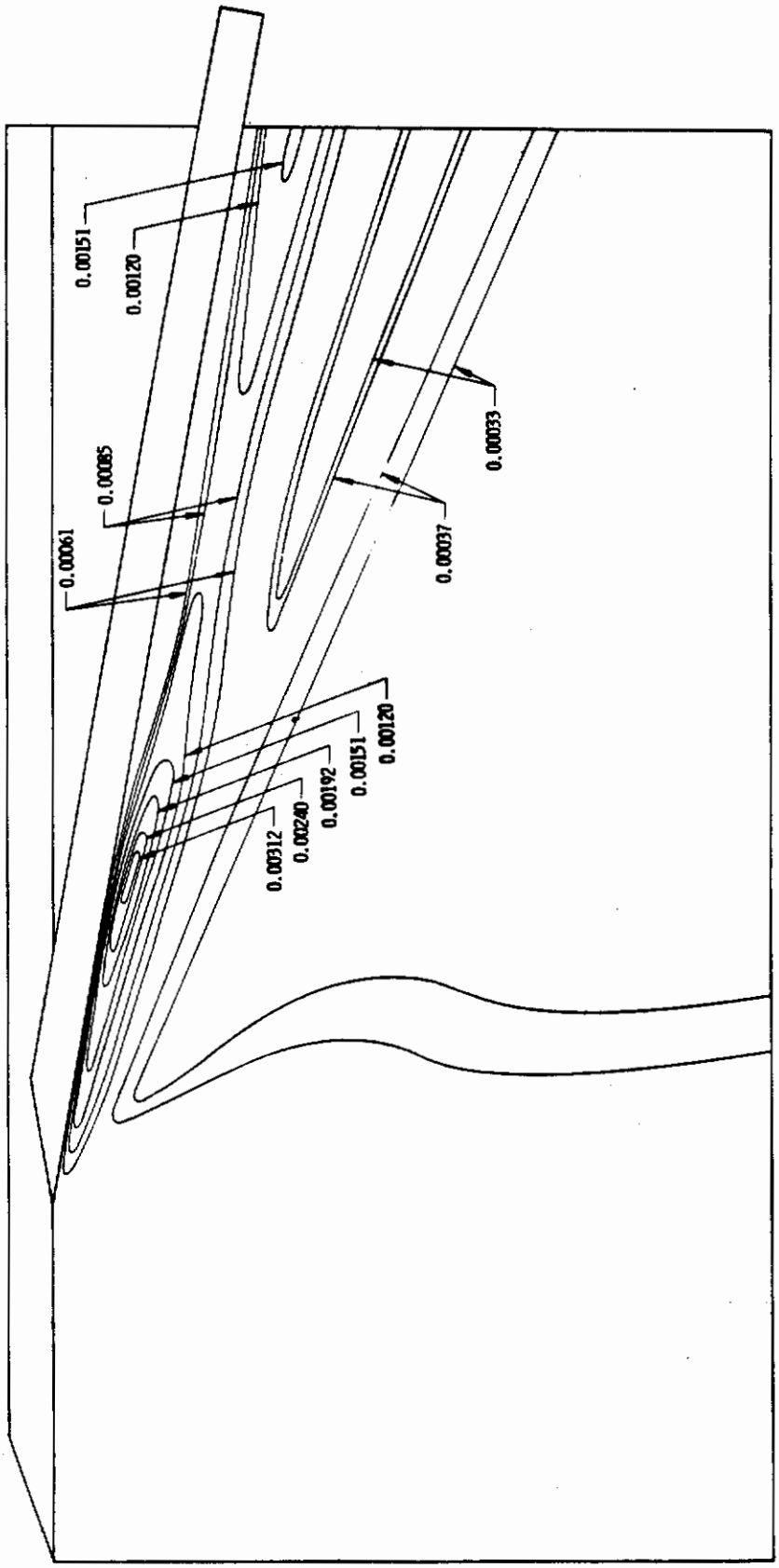

Fig. 36 Heat Transfer Coefficient Distributions for X_f = 4 in., δ = 10 deg.

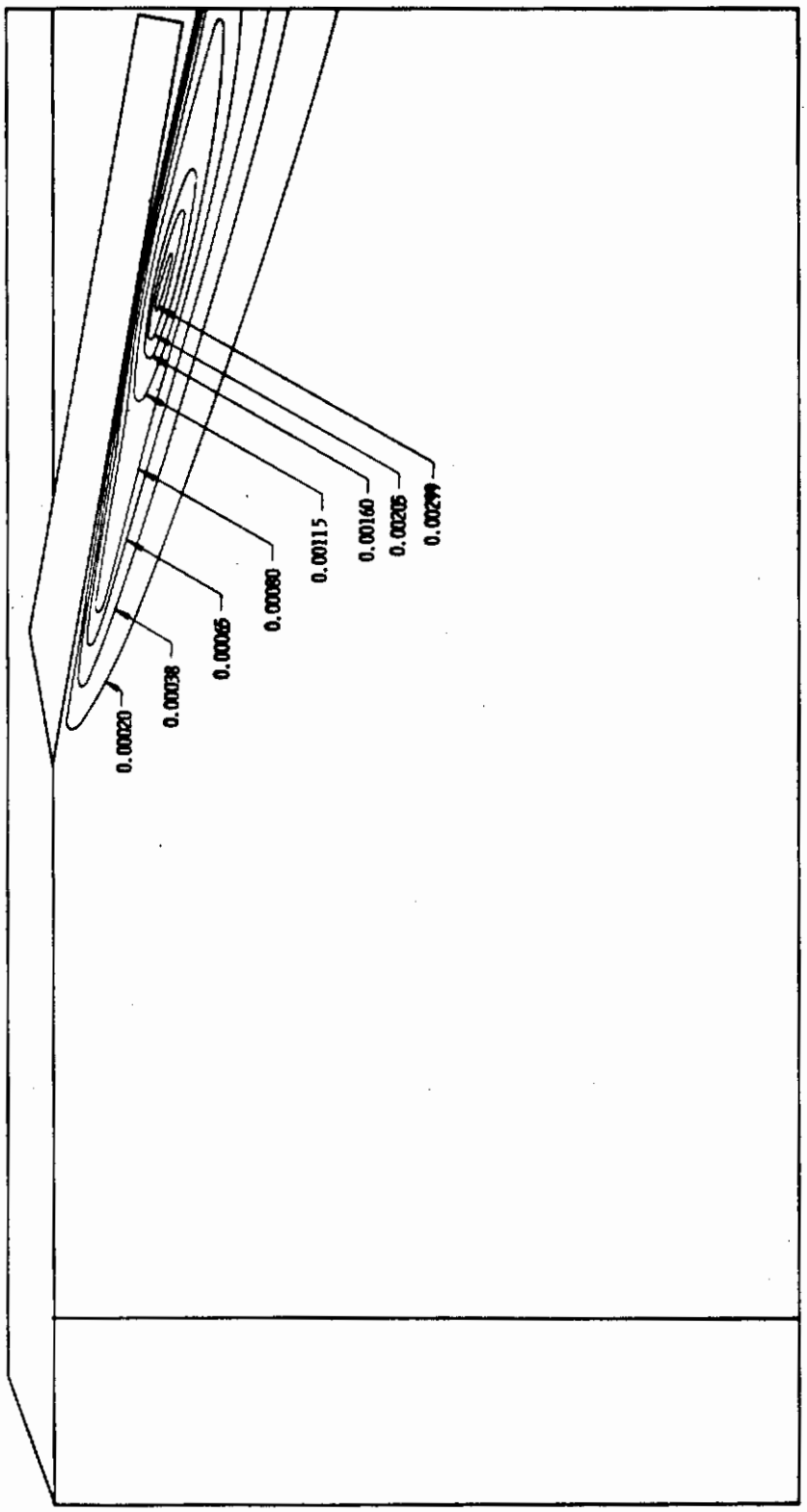

Fig. 37 Heat Transfer Coefficient Distributions for X_f = 8 in., δ = 10 deg.

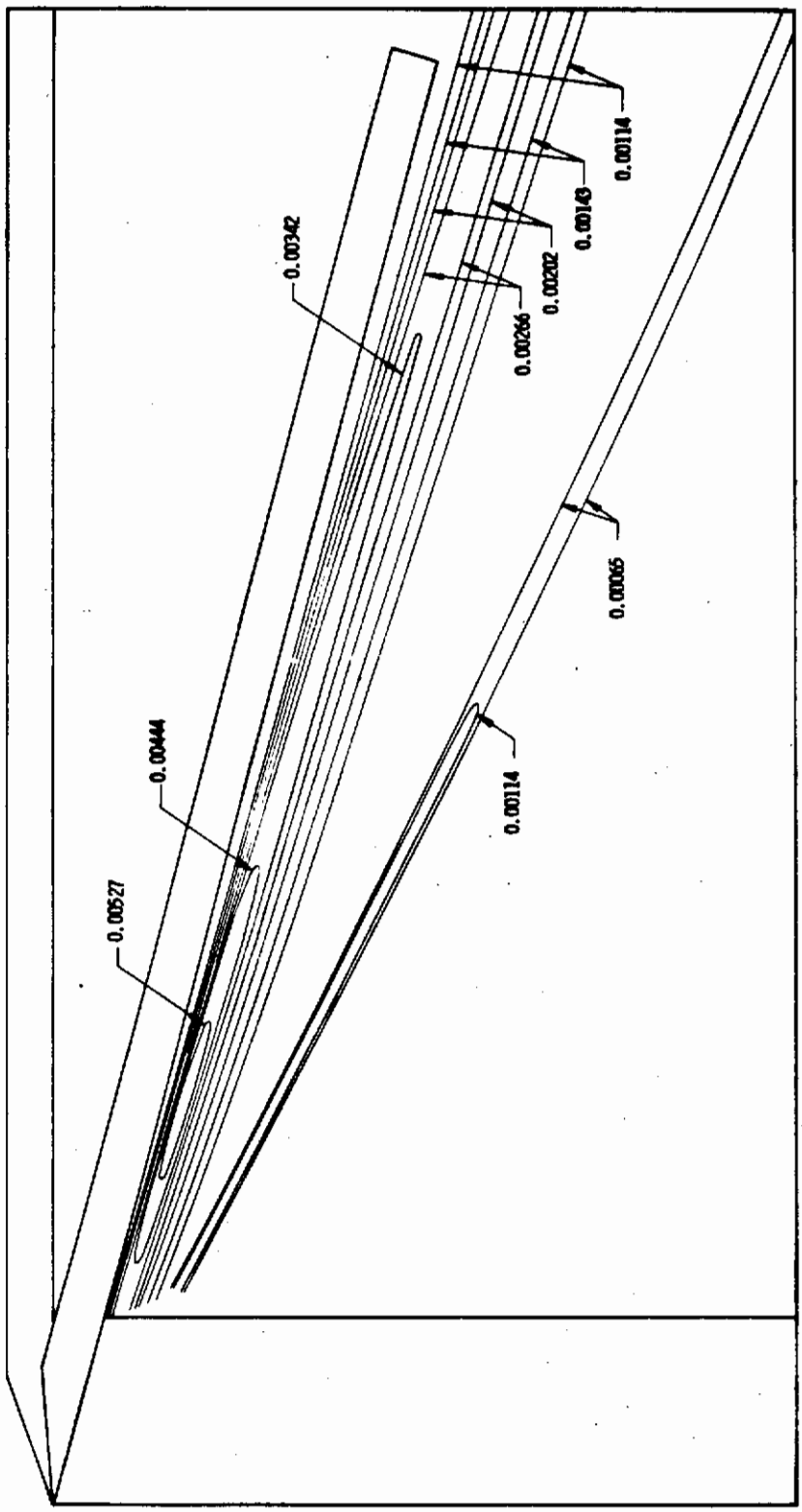

Fig. 38 Heat Transfer Coefficient Distributions for $X_f = 0$ in., $\delta = 15$ deg.

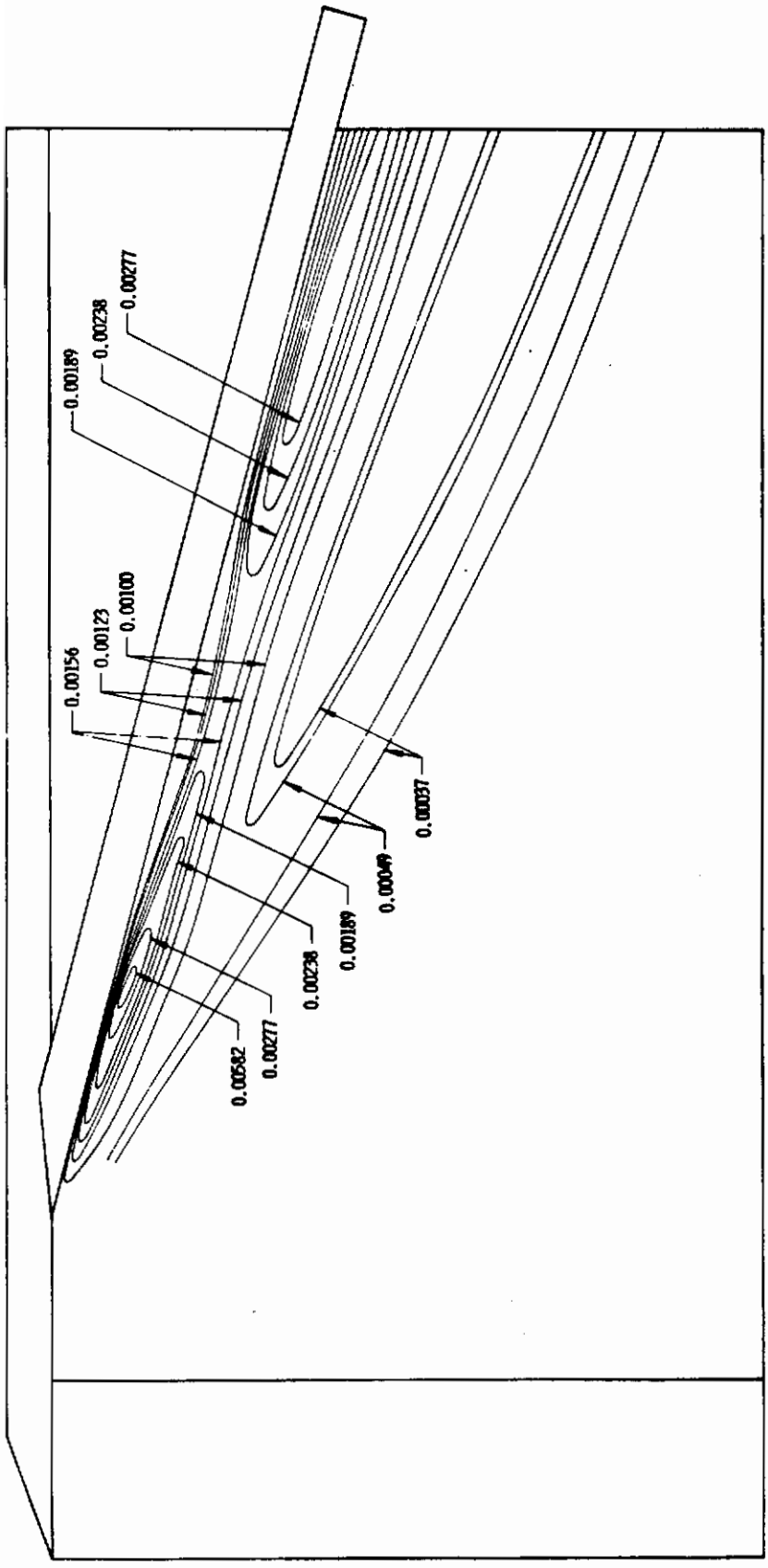

Fig. 39 Heat Transfer Coefficient Distributions for X_f = 4 in., δ = 15 deg.

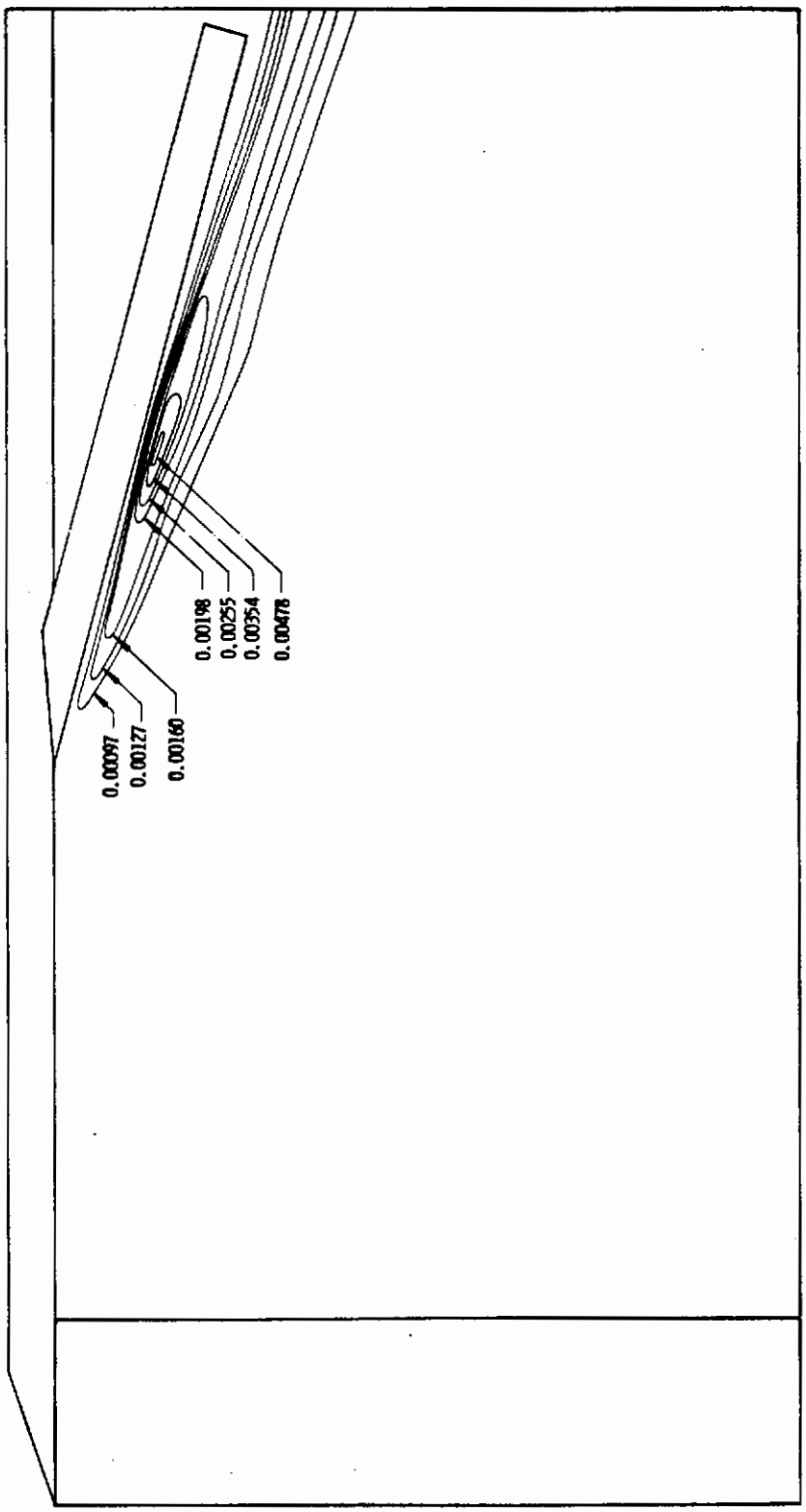

Fig. 40 Heat Transfer Coefficient Distributions for X_f = 8 in., δ = 15 deg.

Section IV

INTERFERENCE REGION PRESSURE AND HEAT TRANSFER DATA CORRELATIONS

Three-dimensional shockwave-boundary layer interactions involve a complex viscous-inviscid coupling process which has precluded development of adequate analytical models to describe the interaction flow field. As a result, estimates of interference region pressure and heat transfer distributions are based largely on semi-empirical correlations of wind tunnel data.

Figure 41a is a schematic of the flow field produced by a shockwave from a fin impinging on a flat plate. The flow model is adapted from the Charwat-Redekopp model based on extensive flow field surveys on asymmetrical intersecting wedges (Ref. 9). High pressure from the impinging shock feeds upstream in the subsonic portion of the boundary layer, causing it to turn away from the surface and separate. Turning of the upstream flow produces the shockwave labeled A in Figure 41a. The flow field downstream of the shock is characterized by a strong inner shock joined by a conical corner flow region. Flow field surveys indicate the presence of vortices emanating from the corner vertex. The pressure rises to a plateau in region 1, then increases to the reattachment value in region 3. Heat transfer is minimum in the separated region (2) and reaches a maximum near the location of peak pressure gradient in region 3.

Figure 41b illustrates surface flow features observed from a photograph of the oil flow test on the shock interference model with 15-deg fin deflection. Regions of vortex scrubbing, oil accumulation, and the onset of separation are identified. Oil flow data shown in Figure 41b and similar data reported by Stainback-Weinstein (Ref. 10), coupled with flow directions of the melted phase-change coating, suggest the presence of the three vortices sketched on Figure 41a.

1. PRESSURE CORRELATIONS

Figures 42 through 47 compare the shock interference model pressure data with theoretical methods for estimating undisturbed pressures upstream of the interaction, plateau pressures in the separated region, and maximum pressures behind the shock. Pressure distributions on the flat plate and fin are predicted by Creager's method (Ref. 4) which is based on the assumption that viscous and inviscid contributions to surface pressure are independent and can be linearly added. With viscous-induced pressures determined by the Lees-Probstein second order weak interaction theory (Ref. 11) the expression for surface pressure on a flat plate is:

$$\frac{P}{P_e} = 1 + \gamma d_e \bar{\chi}_e + \frac{\gamma(\gamma+1)}{4} d_e^2 \bar{\chi}_e^2 + 0.0705 \frac{M_\infty^2 C_d^{2/3}}{\left(\frac{X}{D}\right)^{2/3}} \frac{P_\infty}{P_e} \qquad (4)$$

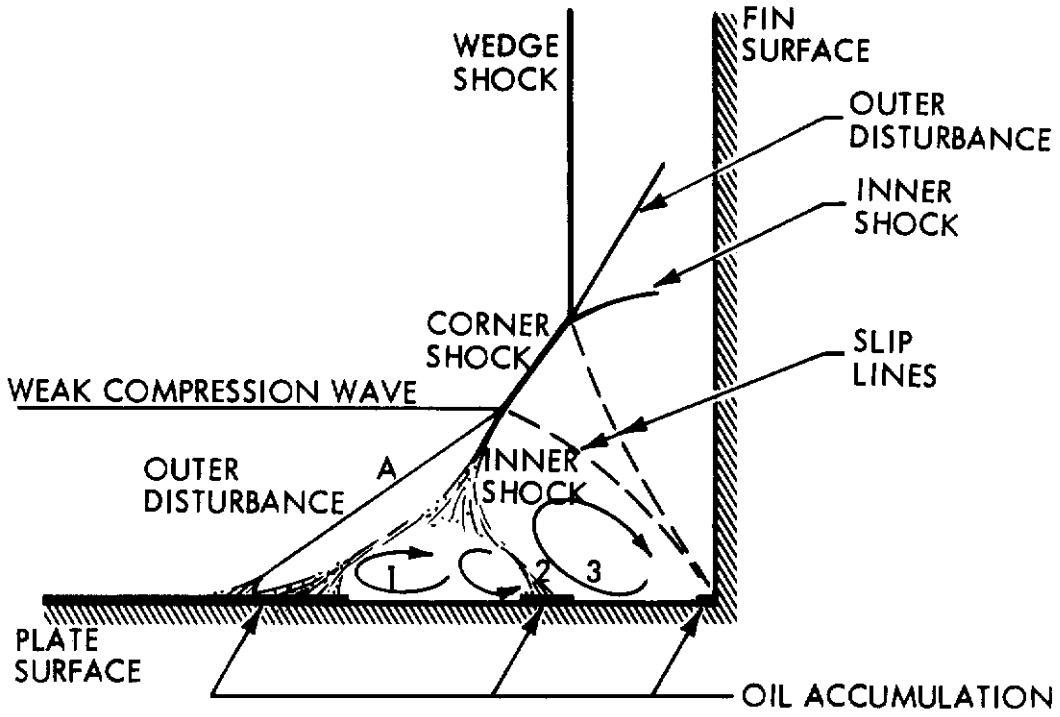

(a) Flow Model

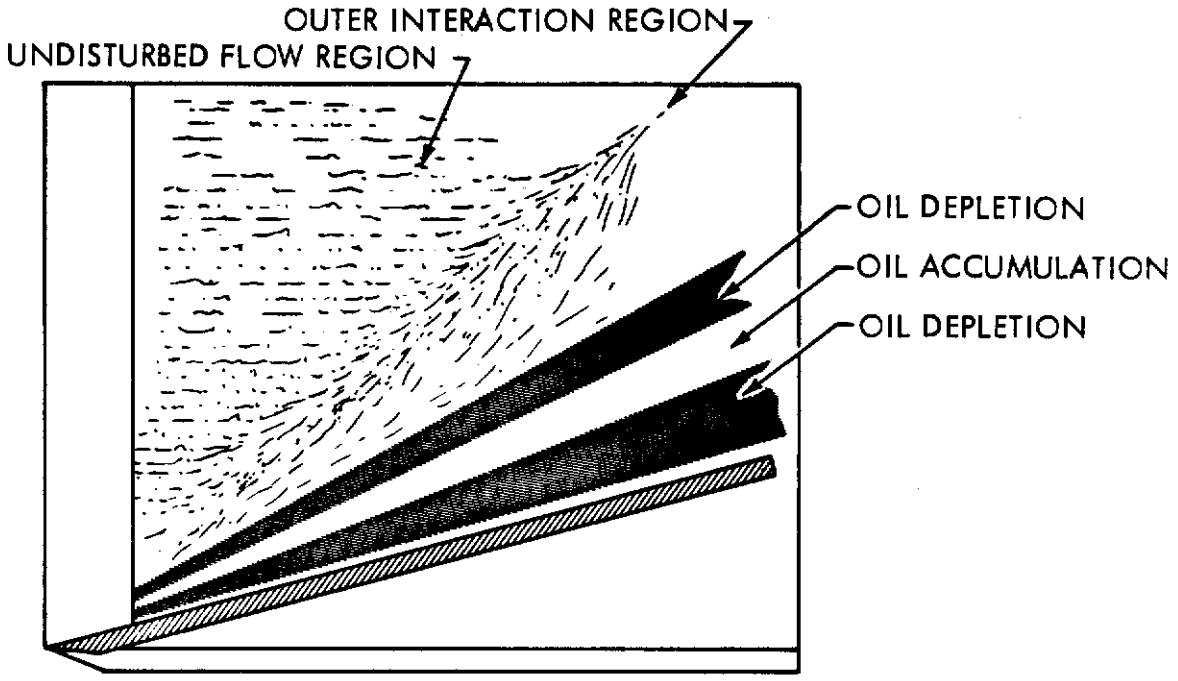

(b) Surface Flow Features from Oil Flow Test with X_f = 0 in., δ = 15 deg.

Fig. 41 Interaction Region Flow Field

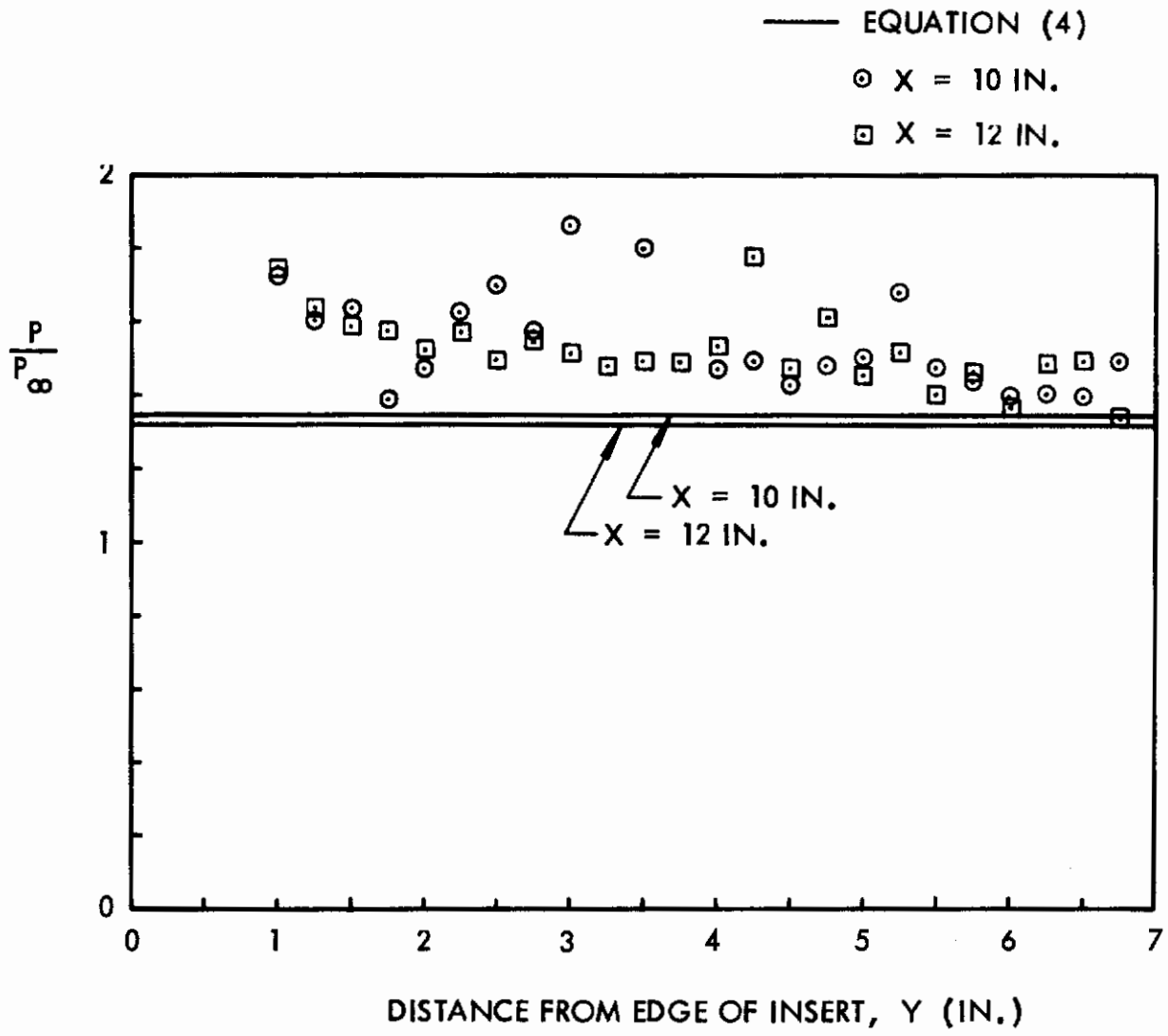

Fig. 42 Correlation of Undisturbed Flat Plate Pressure Data

where

$$d_e = \frac{0.968}{M_e^2} \frac{T_w}{T_e} + 0.145 \ (\gamma - 1)$$

and

$$\overline{\chi}_e = \frac{M_e^3 \sqrt{C_e}}{\sqrt{Re_{ex}}}$$

Reference conditions are based on inviscid, sharp wedge properties. A wall temperature of 600°R and leading edge radius of 0.0005 in. were assumed for theory evaluation.

Figure 42 compares pressure data from the test without side fins with Equation (4). Since the instrumented plate is at zero angle-of-attack, the reference conditions are based on freestream properties. At X = 10 in., the viscous-induced pressure ratio, represented by terms containing χ_e, is 0.30. The bluntness-induced pressure ratio, represented by the last term in Equation (4), is 0.02. As shown, Equation (4) underpredicts the undisturbed flat plate pressure data by 10 to 20 percent. Measurement errors probably contribute significantly to this discrepancy since two pressures in the 0.4 mm Hg range must be measured to determine the experimental pressure ratio P/P_∞. Further, run time was limited to about 90 sec which, in spite of special precautions taken to evacuate the pressure tubing prior to each run, may have been insufficient to stabilize pressures. The tubing length-to-diameter is about 2300. In addition, sizable errors in theory evaluation may result from the assumptions of a constant surface temperature of 600°R and leading edge radius of 0.0005 in., and use of blast wave theory beyond its range of applicability to estimate bluntness-induced pressures.

Oil flow data from the shock interference model were generally disappointing and, with the exception of the data shown in Figure 41, few details of surface flow patterns can be inferred from the test film. Nevertheless, these data were used, in conjunction with surface pressure distributions at model stations 10 and 12 in., to estimate the location of the flow separation line. This information was used to determine the Mach number and Reynolds number at the beginning of the interaction, and thus generate the plateau pressure correlation shown in Figure 43. The experimental plateau pressures are based on the constant-pressure region just downstream of the separation line. Data are compared with the Erdos-Pallone theory (Ref. 12), which is modified for three-dimensional flow by multiplying the plateau pressure coefficient by the square root of the sine of the fin angle (Ref. 13), i.e.:

$$C_{p,pl} = 1.47 \sqrt{\frac{2C_{fo} \sin \delta}{\left(M_o^2 - 1\right)^{0.5}}} \qquad (5)$$

The skin friction coefficient just upstream of the interaction, C_{fo}, was computed by the reference temperature method, i.e.,

$$C_{fo} = \frac{0.664}{\sqrt{Re_{xo}}} \sqrt{C^*}$$

where

$$C^* = \frac{\mu^* T_o}{\mu_o T^*}$$

and

$$T^* = 0.5 \left(T_w + T_o\right) + 0.22\, r \left(\frac{\gamma - 1}{2}\right) M_o^{\,2}\, T_o$$

As shown in Figure 43, plateau pressures are consistently lower than predicted. The discrepancy is not as large as it appears, however, because the numerator in the ordinate contains the term $(P_{pl} / P_o) - 1$ and the plateau-to-upstream pressure ratio is small, ranging from 1.15 to 1.70.

Figure 44 compares peak pressures in the interaction region with theory. The theory labeled "single compression (invicid)" is oblique shock theory based on an isolated sharp wedge exposed to the airstream. The theory labeled "single compression (viscous)" is identical except that viscous and bluntness effects are included, i.e., pressures are predicted by Equation (4). The method labeled "double compression" considers the flow compression due to viscous effects on the flat plate, followed by a compression to peak pressure using an effective turning angle. To apply this solution the Mach number upstream of the interaction, M_o, is computed using the experimental pressure ratio, P_o / P_∞. Then, using oblique shock theory, an equivalent wedge turning angle, δ_{pl}, is determined as a function of M_o and the experimental plateau pressure rise, P_{pl} / P_o. Next, the plateau region Mach number, M_{pl}, is determined as a function of M_o and δ_{pl}. Maximum pressure in the interaction region is then determined as a function of M_{pl} and an effective turning angle of $(\delta - \delta_{pl})$, i.e., separation is assumed to turn the flow away from the fin at an angle corresponding to the equivalent wedge angle of the plateau region. The double compression solution was applied by Gulbran et al (Ref. 13) in an attempt to correlate peak pressures on a shock interference model.

As shown in Figure 44, the peak pressure data exhibit two significant trends: (1) pressures decrease as the fin is moved aft, and (2) the experimental-to-theoretical pressure ratio decreases as the fin angle increases. The generally poor agreement with oblique shock theory is inconsistent with results obtained by Neumann and Burke (Ref. 14), who show this solution to be in good agreement with Mach 6, 8, and 10 data on a similar model configuration.

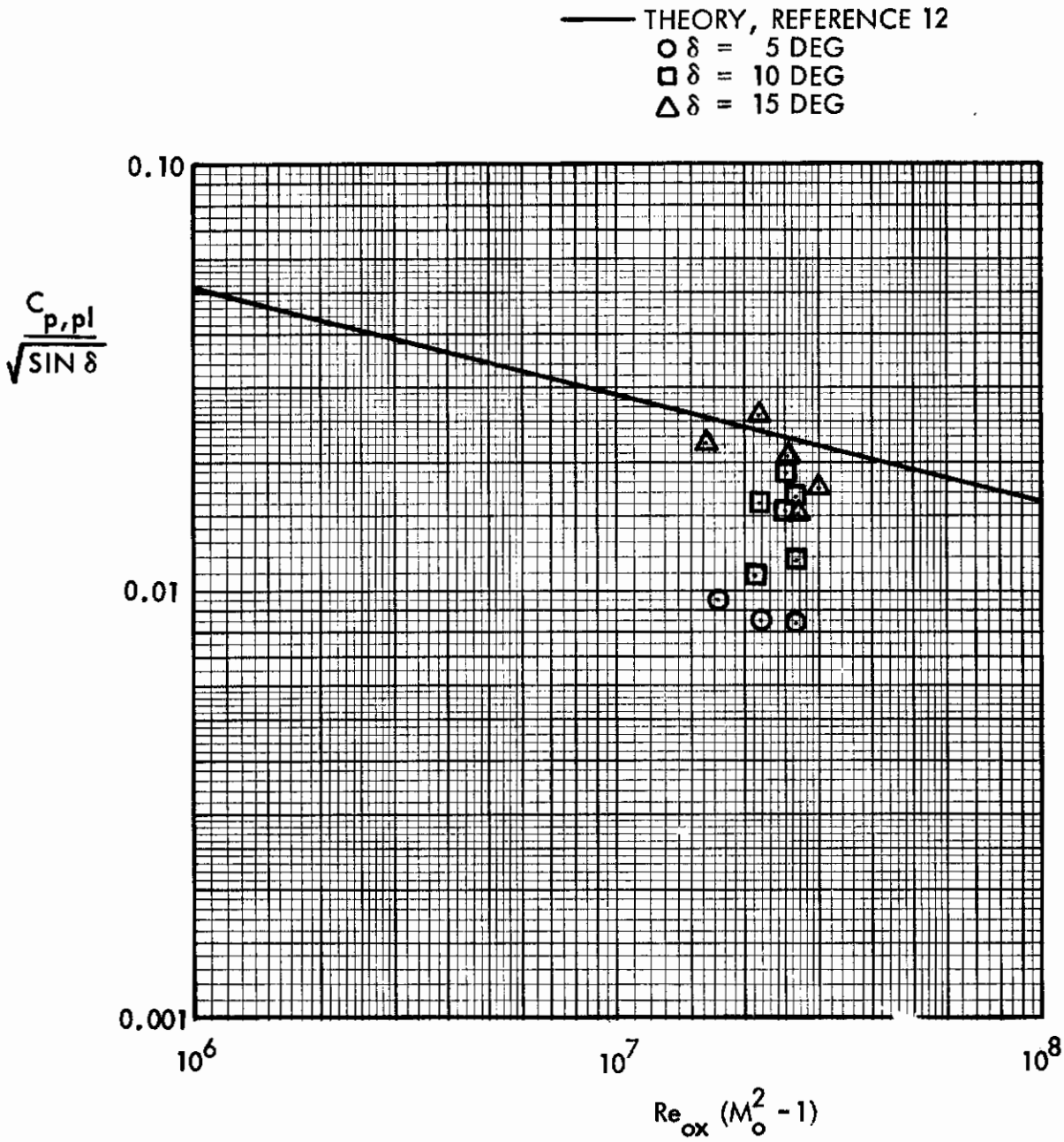

Fig. 43 Correlation of Plateau Pressures

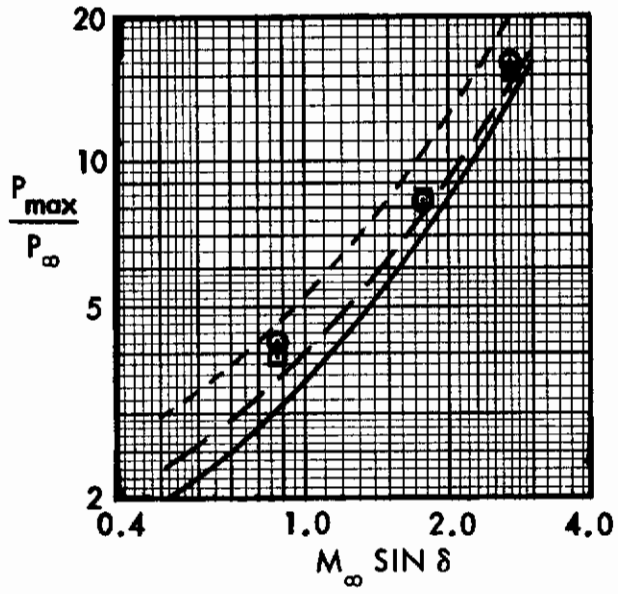

O X = 10 IN.
□ X = 12 IN.

OBLIQUE SHOCK THEORY
——— SINGLE COMPRESSION (INVISCID)
— — SINGLE COMPRESSION (VISCOUS)
- - - - DOUBLE COMPRESSION

X_f = 0 IN.

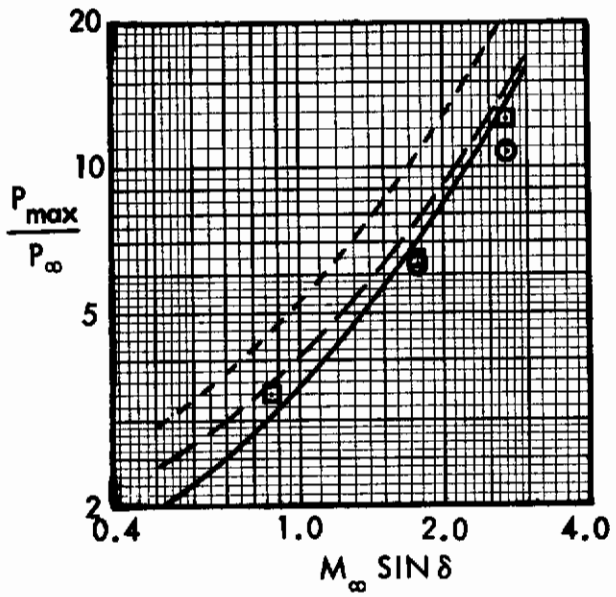

X_f = 4 IN.

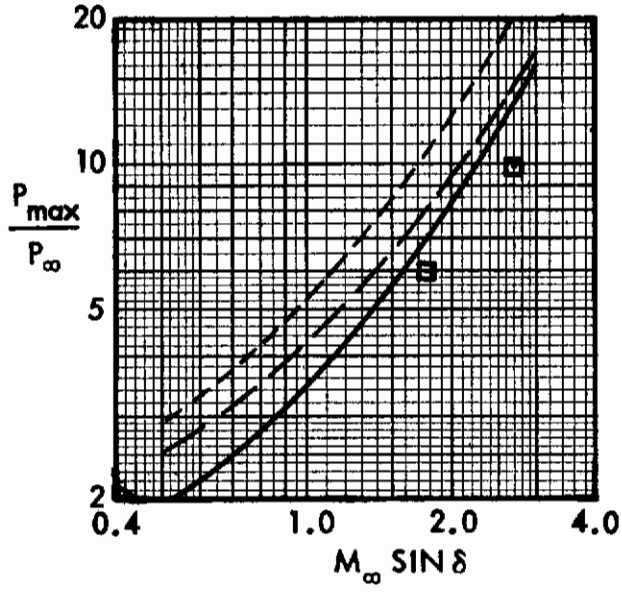

X_f = 8 IN.

Fig. 44 Correlation of Peak Pressures

Figures 45 through 47 compare pressure distributions at X = 12 in. with the theoretical procedures discussed above. Pressures upstream of the interaction and downstream of the fin shock are based on Equation (4). Upstream of the interaction, the reference conditions used for theory evaluation are freestream properties. Downstream of the fin shock, the reference conditions are inviscid, sharp wedge properties. The fin shock location is also based on inviscid, sharp wedge flow. Plateau pressures are based on the Erdos-Pallone solution (Eq. 5), with the separation line estimated from the oil flow and static pressure data. In general, pressures upstream of the interaction are underpredicted and pressures in the separated region are overpredicted. Pressures behind the fin shock are underpredicted when the fin leading edge is coincident with the plate leading edge, but are overpredicted when the fin is moved aft.

2. HEAT TRANSFER CORRELATIONS

Figure 48 is a three-dimensional schematic of the interference region heating distributions observed during the present test program. Peak heating rates occur along a ray angle slightly downstream of the inviscid fin shock location. Along this ray, the heating magnitude fluctuates, with the peak occurring several inches aft of the fin leading edge. As indicated in Figure 48, some data suggest the presence of a second heating peak downstream of the first. The second peak was observed when the fin was placed aft of the plate leading edge, and may be a result of boundary layer transition in the interaction region.

Figure 49 shows the location of maximum heating in the interaction region as a function of fin attitude. Increasing the fin angle tends to move the peak heating point forward and closer to the fin. The location of the peak heating ray relative to the inviscid shock angle, θ_{pk}/θ_s, is slightly less than the value of 0.785 which Neumann and Burke observed from Mach 6 and 8 data (Ref. 14).

Regardless of fin attitude, peak heating occurs from 3 to 7 in. aft of the fin leading edge. This "initial distance" effect was also noted during previous test programs (e.g., Refs. 10, 14, and 15). Watson and Weinstein (Ref. 15) suggested a correlation of the initial distance in terms of the hypersonic interaction parameter χ_∞. Oil flow photographs on a corner flow model tested in a Mach 20 helium tunnel indicated that the initial distance corresponds to a χ_∞ value of about 4. Peak heating locations plotted in Figure 49 correspond to χ_∞ values, based on distance from the fin leading edge, ranging from 2.3 to 3.6. Although this is in fair agreement with the Mach 20 results, insufficient data are available to establish a functional relationship between initial distance and χ_∞.

Various attempts have been made to correlate heat transfer data from regions affected by shockwave-boundary layer interactions. Sayano (Ref. 16), Miller (Ref. 17), Gulbran et al (Ref. 13) and Neumann and Burke (Ref. 14) utilize pressure interaction theory in an attempt to develop empirical formulas for peak heating prediction. In its simplest form, pressure interaction theory can be expressed as (Ref. 14):

$$\frac{h_{pk,\,x}}{h_{fp,\,x}} = K \left(\frac{P_{pk,\,x}}{P_{fp,\,x}} \right)^{1-n} \qquad (6)$$

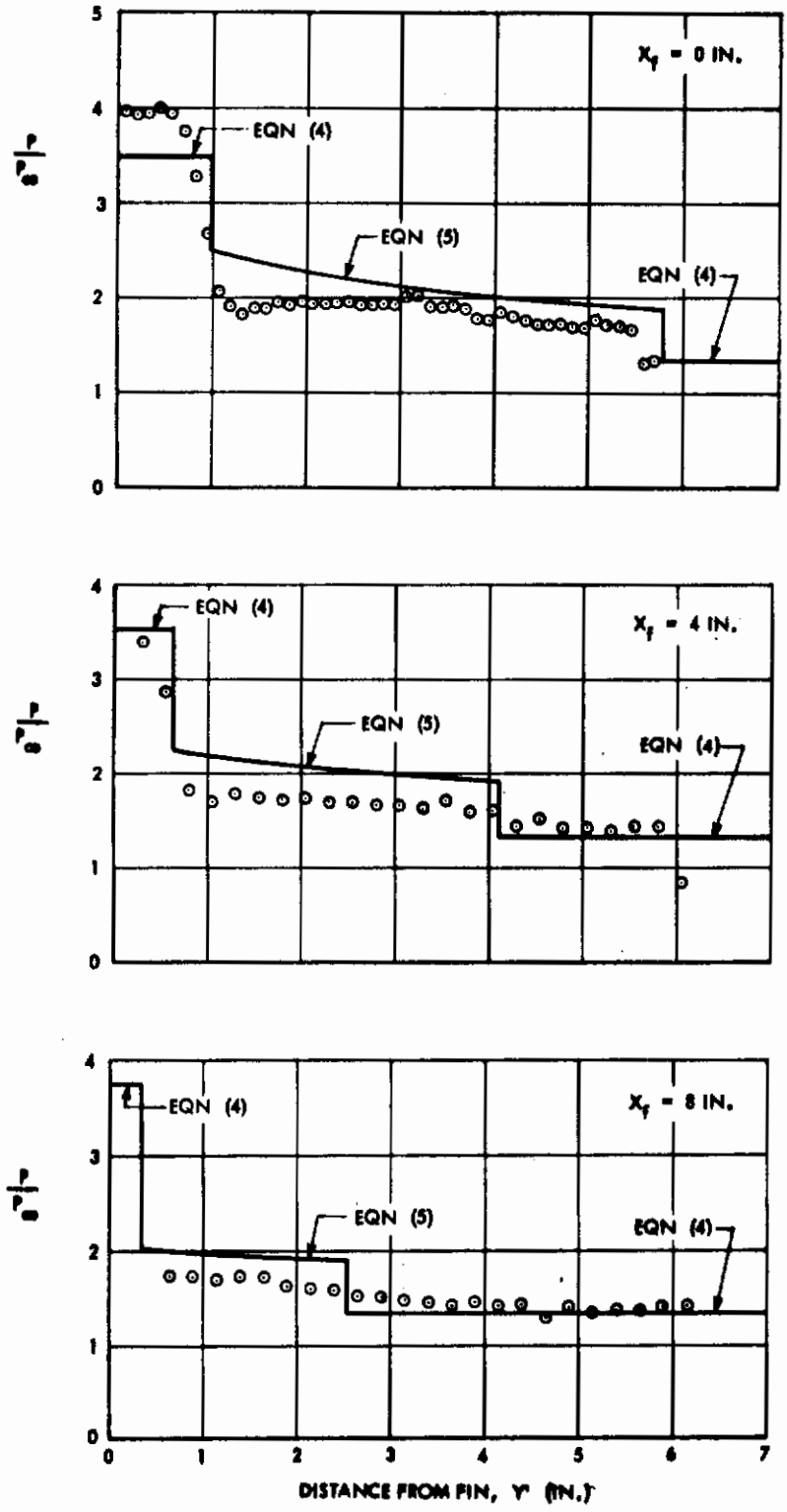

Fig. 45 Correlation of Pressure Distributions at X = 12 in. for δ = 5 deg.

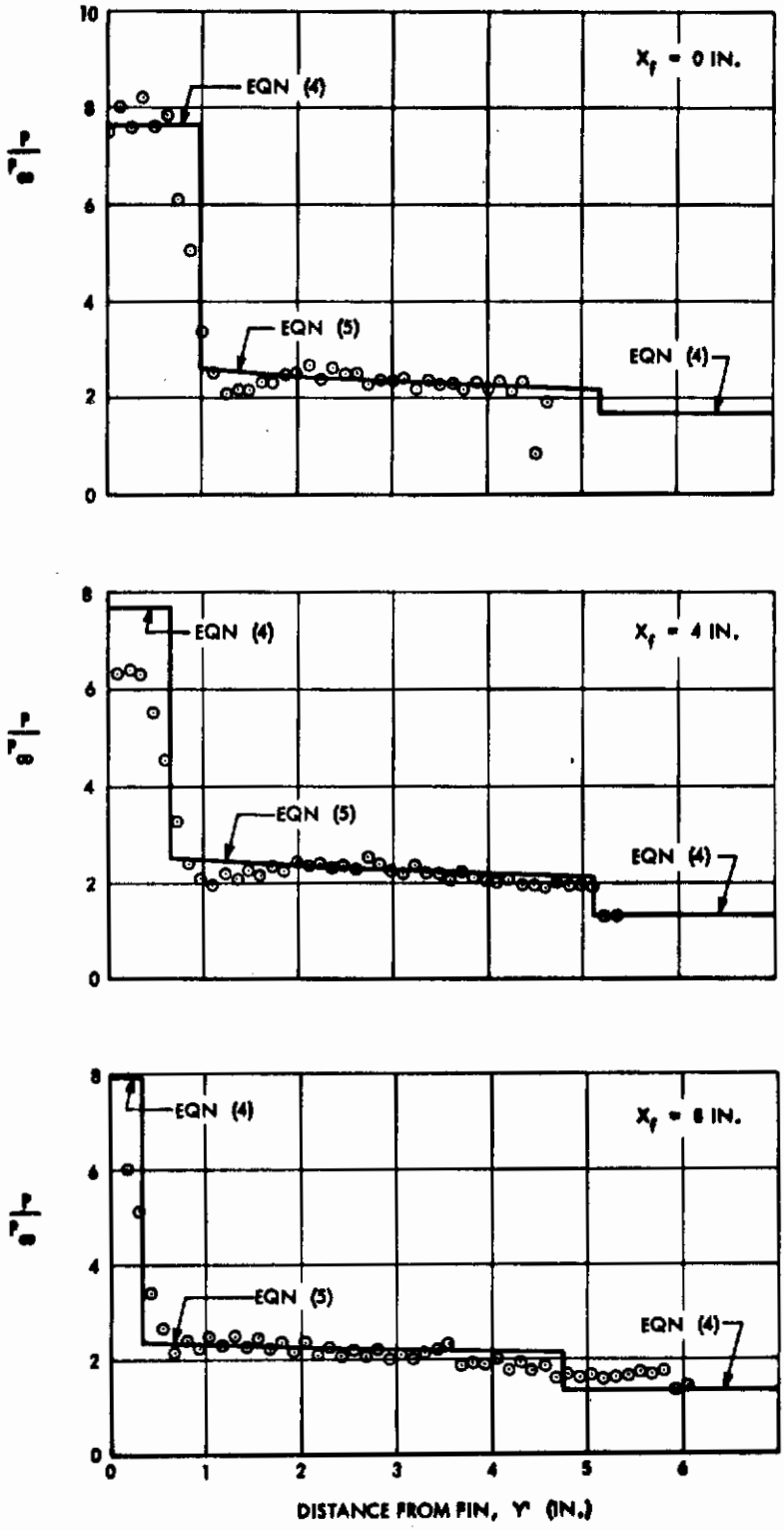

Fig. 46 Correlation of Pressure Distributions at X = 12 in. for δ = 10 deg.

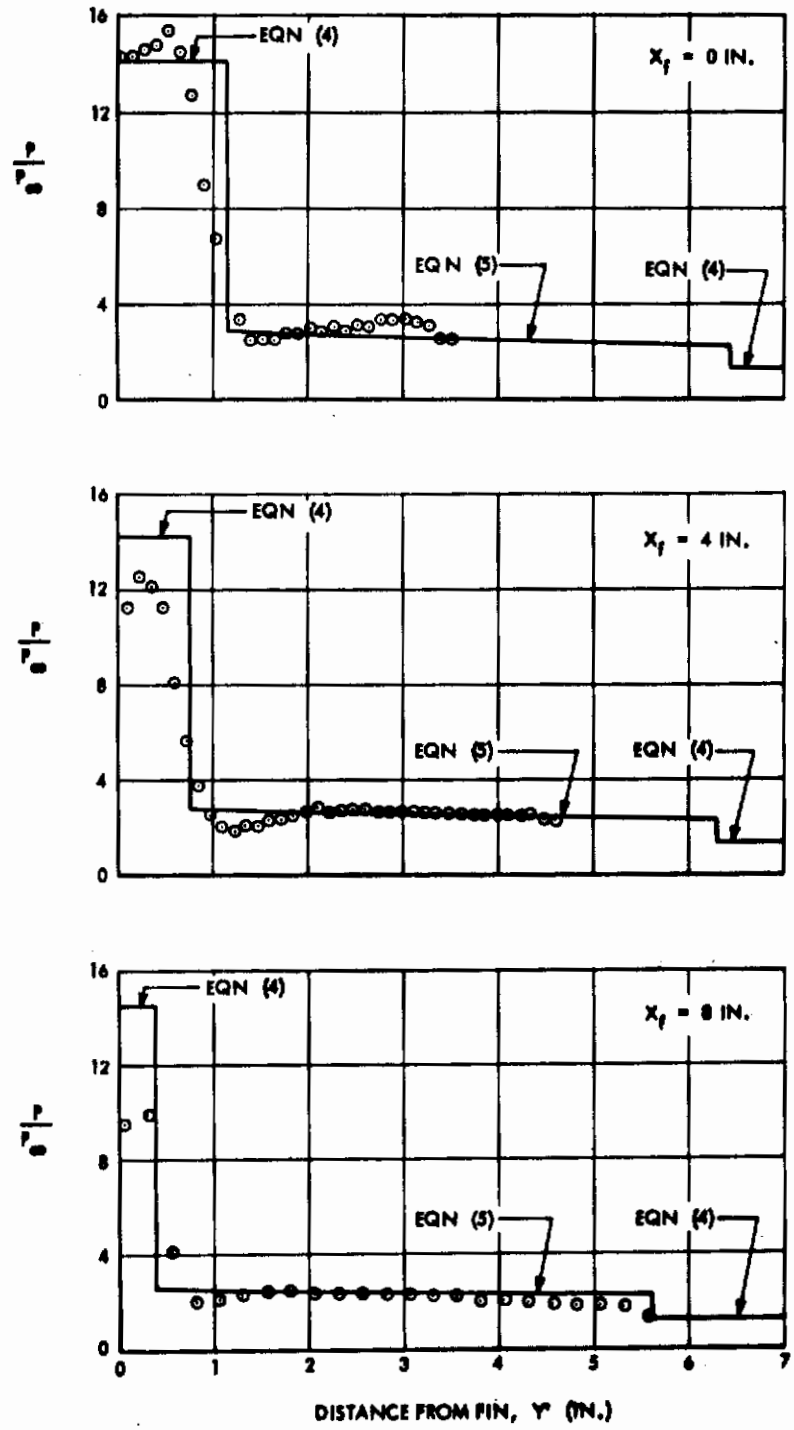

Fig. 47 Correlation of Pressure Distributions at X = 12 in. for δ = 15 deg.

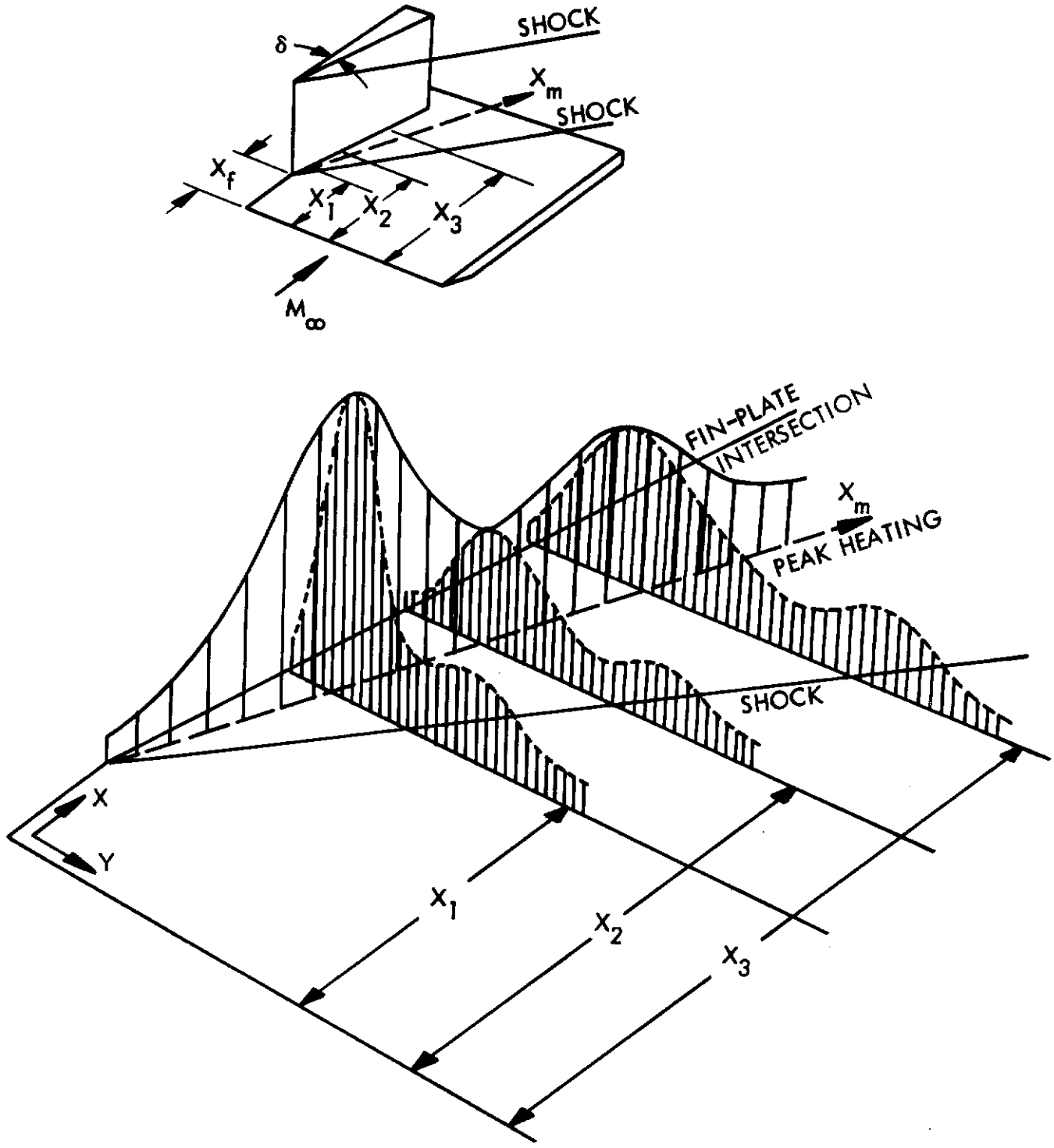

Fig. 48 Schematic of Interaction Region Heating Distributions

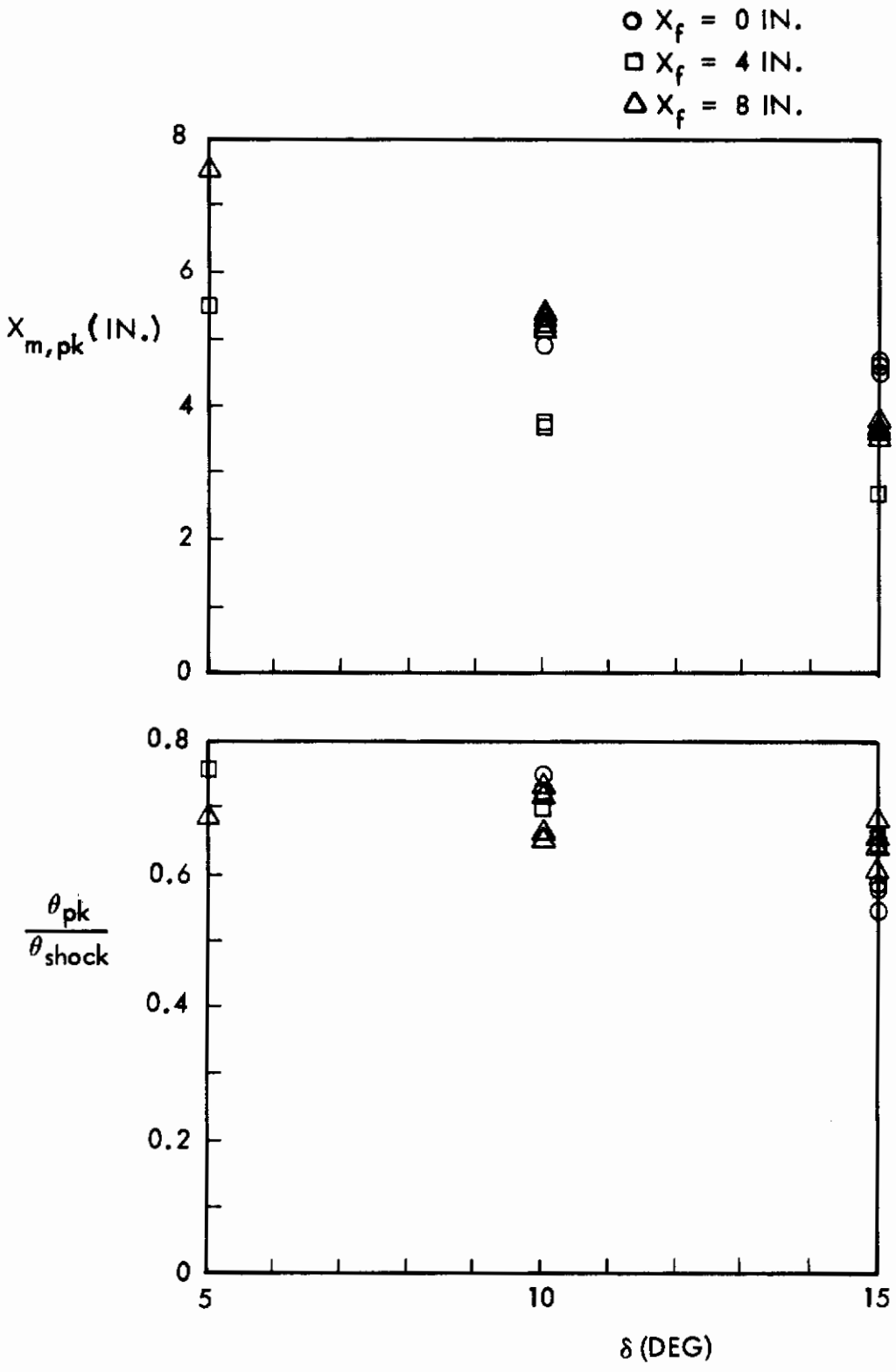

Fig. 49 Peak Heating Locations

where $n = 0.5$ for laminar flow and 0.2 for turbulent flow. The coefficient K is an empirically determined factor. Equation (6) has been used for both two- and three-dimensional shock interaction heating predictions. For two-dimensional turbulent flow $K \cong 1$ (Refs. 14 and 16). Less success has been achieved for two-dimensional interactions when the upstream boundary layer is laminar; however, Neumann (Ref. 18) demonstrates that the boundary layer is easily tripped by the adverse pressure gradient in the interaction region and much of the data considered to be laminar are actually transitional or turbulent.

Neumann and Burke (Ref. 14) utilized pressure interaction theory to develop an empirical formula for predicting peak heating for three-dimensional interactions. They postulate that the three-dimensional shock impingement process initiates a new boundary layer, and the reference length for flat plate heating should be based on the distance between the inviscid fin shock location and the peak heating location. Based on an empirically determined peak heating ray angle, $X_{ref} = 0.215\ X$. Thus, for three-dimensional laminar interactions, Equation (6) becomes

$$\frac{h_{pk,\,x}}{h_{fp,\,x}} = \frac{K}{\sqrt{0.215}} \left(\frac{P_{pk,\,x}}{P_{fp,\,x}} \right)^{0.5} \tag{7}$$

The factor K is assumed to be the correction to the similar solution approach accounting for adverse pressure gradients. Best correlation of peak heating rates was achieved using a value of $K = 1.70$ for Mach 6 data and $K = 1.75$ for Mach 8 data. A limited amount of data indicated that $K \cong 2.0$ for Mach 20 flow (Ref. 18). These values appear reasonable based on the analyses of Bertram and Feller (Ref. 5).

If, as in the present tests, the fin is positioned downstream of the plate leading edge, a distance correction is required in Equation (7). The general expression is

$$\frac{h_{pk,\,x}}{h_{fp,\,x}} = \frac{K}{\sqrt{0.215}} \left(\frac{P_{pk,\,x}}{P_{fp,\,x}} \right)^{0.5} \left(\frac{X}{X - X_f} \right)^{0.5} \tag{8}$$

where X is the longitudinal distance from the plate leading edge to the peak heating location, and X_f is the distance from the plate leading edge to the fin leading edge.

Figures 50, 51, and 52 compare peak heating distributions from the present test program with Equation (8), which was evaluated using experimental peak pressures and theoretical undisturbed flat plate pressures and heat transfer coefficients. Peak heating rates are as much as 60 percent higher than predicted. Furthermore, the heating oscillations indicate that the fin interference phenomenon does not satisfy the self-similar criterion implicit in Equation (8).

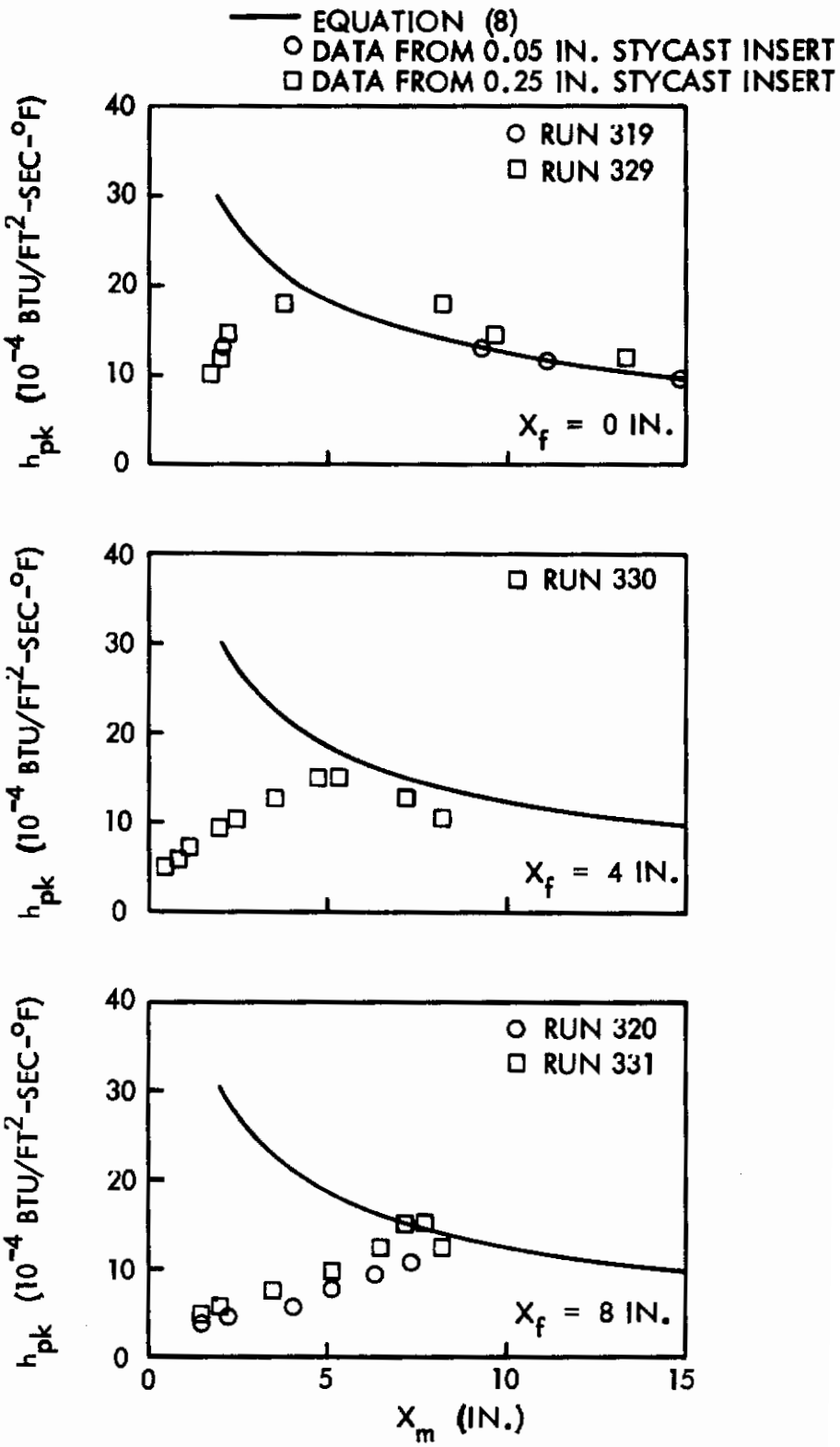

Fig. 50 Correlation of Peak Heating Data for δ = 5 deg.

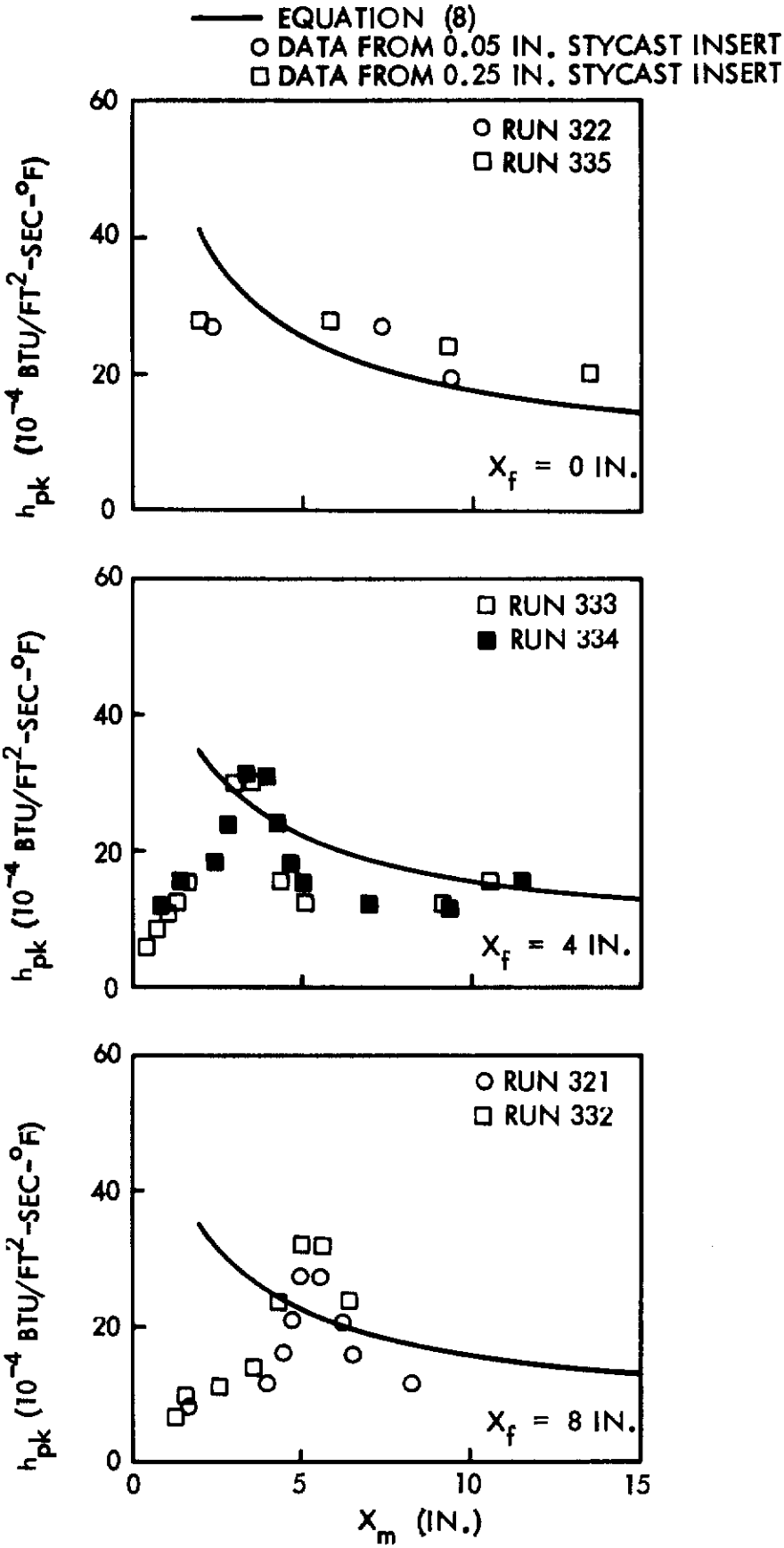

Fig. 51 Correlation of Peak Heating Data for δ = 10 deg.

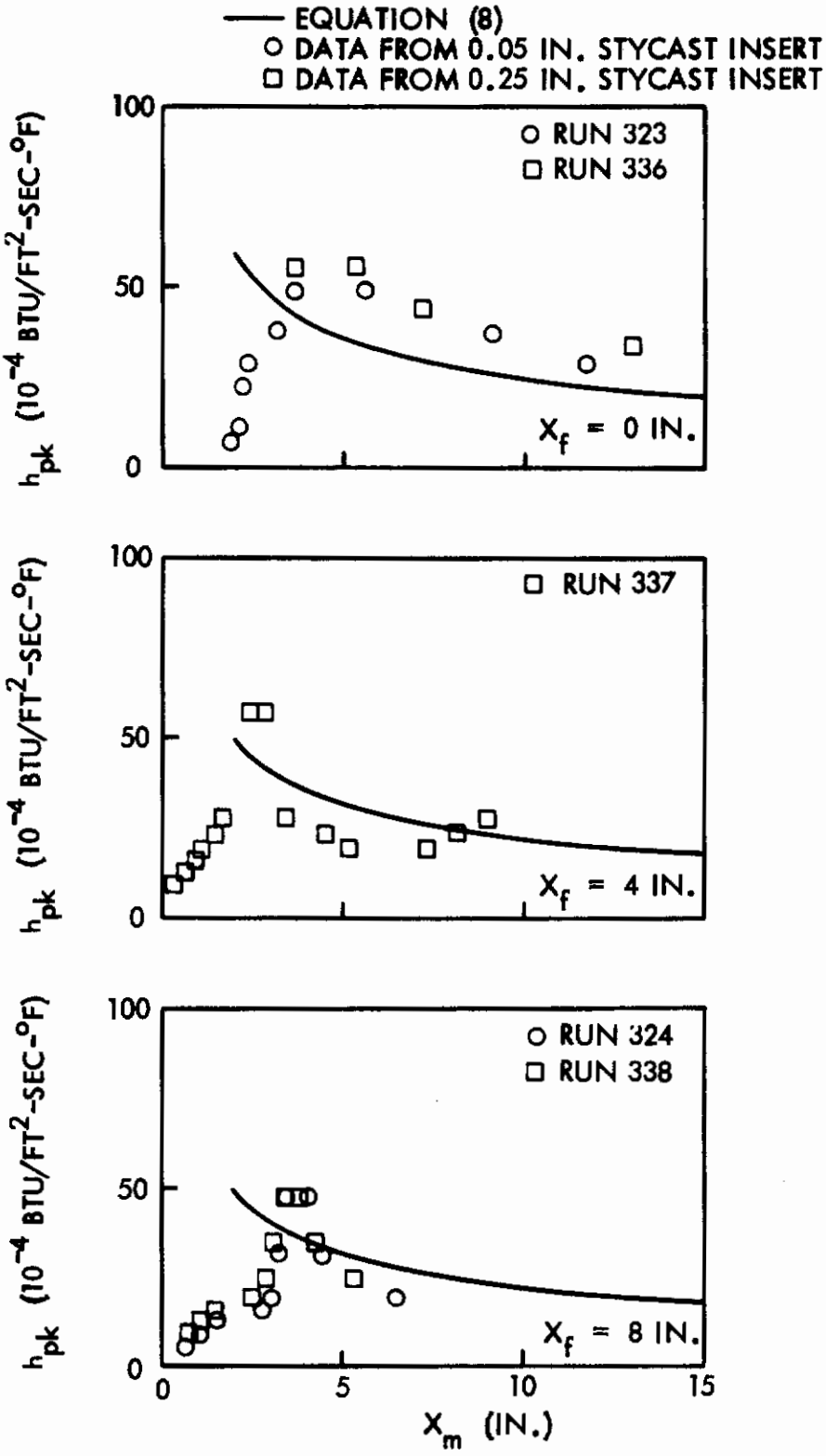

Fig. 52 Correlation of Peak Heating Data for δ = 15 deg.

Figure 53 compares data from the present test program and similar data from the literature with Equation (8). The data are normalized by the square root of the pressure ratio and a reference heat transfer coefficient, h_{ref}, which includes the modified reference length proposed by Neumann and Burke. As shown, the correlation parameter $(h_{pk,x} / h_{ref,x})/(P_{pk,x} / P_{fp,x})^{-0.5}$, which is equal to the coefficient K, varies significantly with streamwise distance. All data show the "initial distance" effect discussed previously, with a distance of 3 in. or more required before the correlation parameter reaches its maximum value.

As shown in Figure 53, peak heating data from the present tests are generally higher than similar data from the literature. However, most of the previous data were obtained using thermocouple-instrumented models and, for most tests, it is doubtful if sufficient instrumentation was located in the highly localized peak heating region to accurately determine peak heating rates.

Analyses of the data shown in Figure 53 have not resulted in functional relationships between the modified pressure interaction parameter and significant variables such as Mach number, Reynolds number, and boundary layer parameters upstream of the interaction. It is apparent, however, that Equation (8) may yield unconservative results if the pressure gradient correction, K, is assumed to range from 1.7 to 2.0, as determined empirically by Neumann and Burke. Consequently, until additional flow field and heat transfer data become available to provide a better understanding of the shockwave-boundary layer interaction phenomenon, it is recommended that peak heating rates be estimated by Equation (8), assuming a value of $K = 3.0$.

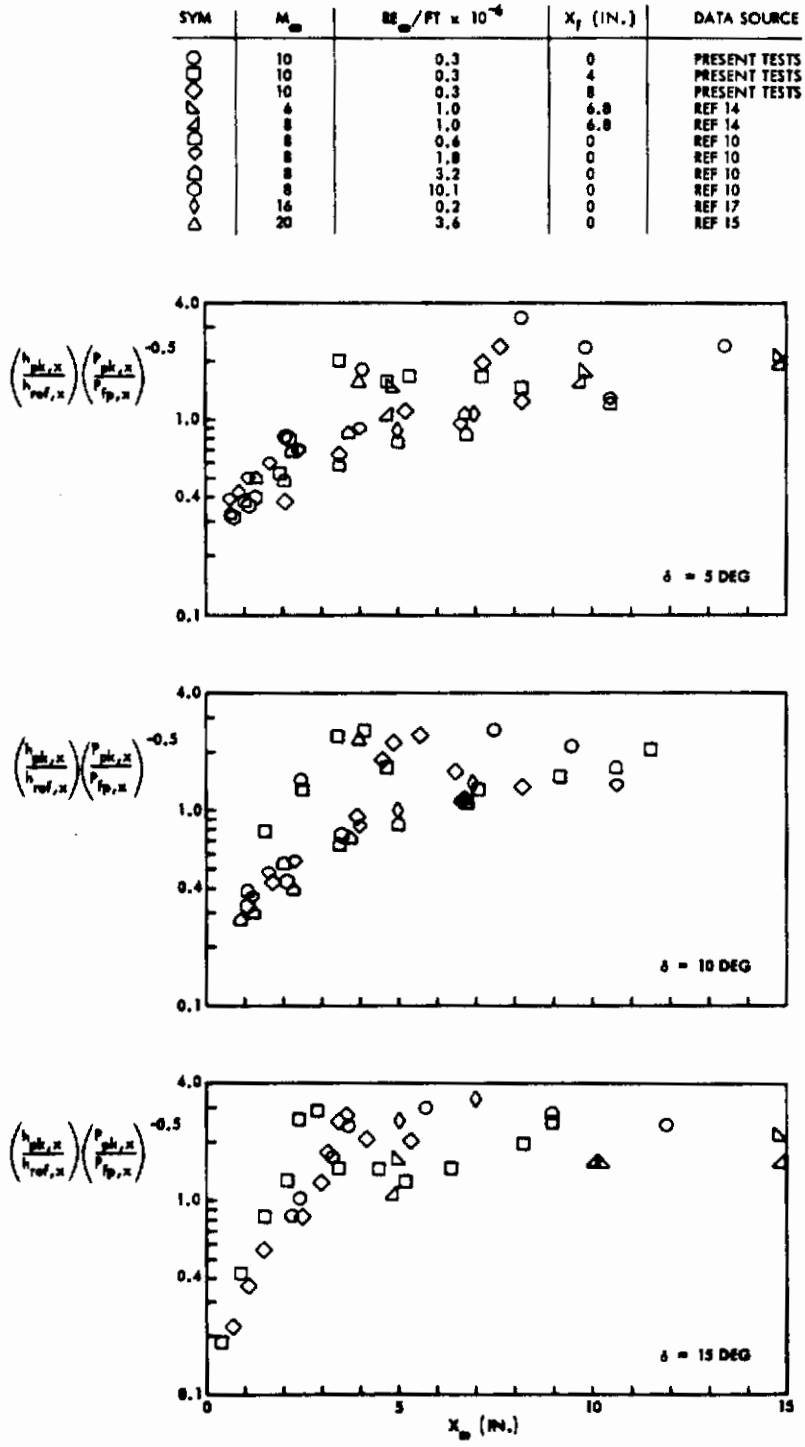

Fig. 53 Peak Heating Data Summary

Section V
CONCLUSIONS AND RECOMMENDATIONS

This study has extended the technique for reducing phase-change coating heat transfer data to the general two-dimensional case of convective heating to one or two sides of a finite-slab with variable thermal properties. The data reduction techniques are validated by comparisons with exact solutions for one-dimensional heat conduction, and by comparing experimental data from the present tests with theory.

A wind tunnel test program conducted in the AFFDL High Temperature Facility has contributed substantially to the data base for three-dimensional shockwave-boundary layer interactions. By use of the temperature-sensitive paint technique, heating distributions in the interaction region have been identified in greater detail than is possible by use of thermocouple-instrumented models.

Pressures upstream of the interaction and in the separated region are slightly underpredicted by the Lees-Probstein viscous interaction theory and the Erdos-Pallone separated flow solution. Pressures downstream of the fin shock are underpredicted by oblique shock theory when the fin leading edge is coincident with the flat plate leading edge, and overpredicted when the fin is moved aft.

Peak heating data from the present tests are generally higher than similar data from the literature. Part of the discrepancy is attributed to problems associated with measuring a highly localized peak heating region using thermocouple-instrumented models. The recommended procedure for estimating peak heating rates in the interaction region is the pressure interaction method of Neumann and Burke, using a value of 3.0 for the pressure gradient coefficient.

Teflon should not be used for phase-change coating heat transfer tests because it undergoes a room-temperature transition in crystal structure which results in an unpredictable variation in specific heat.

APPENDIX

DATA REDUCTION PROGRAM LISTINGS

Tables 2 and 3 are listings of the computer programs developed to reduce phase-change coating heat transfer data (see Section 2.3). The programs are written in Fortran IV and are operational on the U1108 computer at LMSC. Program variables are identified in Table 4. Where possible, identical names are used for Programs I and II.

Input data for Program I, which determines the surface heat transfer coefficient distribution on a slab which is convectively heated on one side and adiabatic on the backface, is illustrated below. The first two data input cards list the number of problems to be solved and the model thermal properties. Data input for each problem follow, in groups of two cards per problem. The data input sequence and column assignments are illustrated below:

NP = Number of problems to be solved

RHO = density, lb/ft^3

A, B, C = Coefficients in specific heat equation $c = A+BT+CT^2$, Btu/lb ^oF

D, E, F = Coefficients in thermal conductivity equation $k = D+ET+FT^2$, Btu/ft hr ^oF

NX = number of nodes in the X direction (parallel to the heated surface)

NY = number of nodes in the Y direction (normal to the heated surface)

X = width of slab, i.e., distance between node 1 and node NX, inches

Y = depth of slab, inches

TI = initial temperature, ^oF

TPC = coating phase-change temperature, ^oF

TAW = adiabatic wall temperature, ^oF

PRINTI = print interval for surface temperature histories, sec.

TIME ( ) = phase-change times for surface nodes 1 thru NX, sec.

Input data for Program II, which determines the surface heat transfer coefficient distribution on a slab which is convectively heated on both sides, is illustrated below. The first two data input cards list the number of problems to be solved and the model thermal properties. Data input for each problem follow, in groups of four cards per problem. The data input sequence and column assignments are illustrated below:

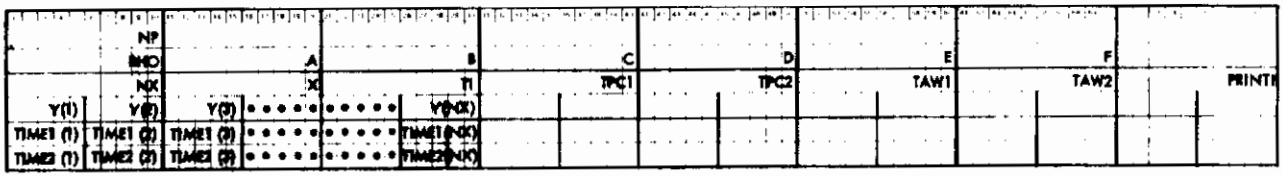

NP = number of problems to be solved

RHO = density, lb/ft^3

A, B, C = coefficients in specific heat equation, $c = A+BT+CT^2$, Btu/lb ^oF

D, E, F = coefficients in thermal conductivity equation, $k = D+ET+FT^2$, Btu/ft hr ^oF

NX = number of nodes in the X direction (parallel to the heated surface)

X = width of slab, i.e., distance between node 1 and node NX, inches

TI = initial temperature, ^oF

TPC1 = coating phase-change temperature for surface 1, ^oF

TPC2 = coating phase-change temperature for surface 2, ^oF

TAW1 = adiabatic wall temperature for surface 1, ^oF

TAW2 = adiabatic wall temperature for surface 2, ^oF

PRINTI = print interval for surface temperature histories, sec

Y ( ) = thickness of slab at each surface node location, inches

TIME 1 ( ) = phase-change times for surface 1 nodes, sec

TIME 2 ( ) = phase-change times for surface 2 nodes, sec

Table 2

LISTING FOR PROGRAM I

```
      DIMENSION C(98),R(184),RC(98),T(98),TOLD(98),H(14),TIME(14),
     1 TIMEC(14),XD(14),HSIS(14),HHSIS(14),EX(14),EXPR(14),TIMECP(14),
     2 NF(14),NFMT1(3),NFMT2(3),NFMT3(3),TS(14)
      DATA NF/84H 1      2      3      4      5      6      7      8      9     1
     10     11     12     13     14     /
      DATA NFMT1/18H(1X,   14     F9.7) /
      DATA NFMT2/18H(1X,   14     F9.0) /
      DATA NFMT3/18H(1X,   14     F9.4) /
      READ (5,100) NC
  100 FORMAT (I10)
      READ (5,101) RHO,A1,A2,A3,B1,B2,B3
  101 FORMAT(1F10.4,6F10.8)
      NP=1
      DO 999 II=1,NC
      READ (5,102) NX,NY,X,Y,TI,TPC,TAW,PRINTI
  102 FORMAT(2I10,6F10.4)
      READ (5,103) TIME
  103 FORMAT(14F5.2)
      IF (NX.GT.14) NX=14
      XN=NX
      IF (NY.LT.4) NY=4
      IF (NX.GT.12.AND.NY.GT.7) NY=7
      IF (NX.GT.11.AND.NY.GT.8) NY=8
      IF (NX.GT.10.AND.NY.GT.9) NY=9
      IF (NY.GT.10) NY=10
      DO 3 I=1,14
      TS(I)=TI
      IF (TIME(I).EQ.0.) TIME(I)=1.
    3 CONTINUE
      TM=(TI+TPC)*.5
      CPI=A1+A2*TM+A3*TM**2
      TCI=(B1+B2*TM+B3*TM**2)/3600.
      XD(1)=0.
      DO 4 I=2,NX
      XD(I)=XD(I-1)+X/(XN-1.)
    4 CONTINUE
      TIMMAX=TIME(1)
      TIMMIN=TIME(1)
      DO 5 I=2,NX
      IF (TIME(I).GT.TIMMAX) TIMMAX=TIME(I)
      IF (TIME(I).LT.TIMMIN) TIMMIN=TIME(I)
    5 CONTINUE
      YMAX=SQRT(5.*TCI*TIMMAX*144./(RHO*CPI))
      IF (Y.EQ.0..OR.Y.GT.YMAX) Y=YMAX
      FOUR=144.*TCI*TIMMIN/(RHO*CPI*Y**2)
      IF(FOUR.GT..5.AND.NY.GT.5) NY=5
      IF(FOUR.GT.1..AND.NY.GT.4) NY=4
      XN=NX
      YN=NY
```

Table 2 (Continued)

```
      TN=XN*YN
      NT=TN
      DO 6 I=1,98
      T(I)=TI
      TOLD(I)=TI
    6 CONTINUE
      TYME=0.
      TPRINT=PRINTI
      ITER=0
C     GUESS HEAT TRANSFER COEFFICIENTS USING SEMI-INFINITE SLAB SOLUTION
      TBAR=(TPC-TI)/(TAW-TI)
      IF(TBAR.LT..03) BETA=.9*TBAR
      IF(TBAR.GE..03.AND.TBAR.LT..08) BETA=1.042*TBAR**1.04
      IF(TBAR.GE..08.AND.TBAR.LT..14) BETA=1.185*TBAR**1.09
      IF(TBAR.GE..14.AND.TBAR.LT..20) BETA=1.338*TBAR**1.15
      IF(TBAR.GE..20.AND.TBAR.LT..30) BETA=1.600*TBAR**1.26
      IF(TBAR.GE..30.AND.TBAR.LT..40) BETA=1.950*TBAR**1.42
      IF(TBAR.GE..40.AND.TBAR.LT..50) BETA=2.490*TBAR**1.70
      IF(TBAR.GE..50.AND.TBAR.LT..60) BETA=2.840*TBAR**1.88
      IF(TBAR.GE..60.AND.TBAR.LT..70) BETA=3.930*TBAR**2.48
      RHOCK=RHO*CPI*TCI
      DO 7 I=1,14
      HSIS(I)=BETA*SQRT(RHOCK/TIME(I))
      TOT=0.2*(Y/12.)**2*RHO*CPI/TCI
      TPCTOT=TIME(I)/TOT
      CORR=1.
      IF (TPCTOT.GT.2.5) CORR=1.41*TPCTOT**-.37
      H(I)=HSIS(I)*CORR
      HHSIS(I)=H(I)/HSIS(I)
    7 CONTINUE
C     COMPUTE RESISTORS AND CAPACITORS   ONLY ONCE IF NOT TEMP-DEPENDENT
    8 IF(TYME.GT.0..AND.A2.EQ.0..AND.A3.EQ.0..AND.B2.EQ.0..AND.B3.EQ.0.)
     1 GO TO 22
      DO 9 I=1,NT
      CP=A1+A2*T(I)+A3*T(I)**2
      C(I)=RHO*CP*X*Y/(144.*(XN-1.)*(YN-2.))
    9 CONTINUE
      DO 10 I=1,NX
      C(I)=0.25*C(I)
      C(I+NX)=0.50*C(I+NX)
      C(I+NX+NX)=0.75*C(I+NX+NX)
      C(I+NT-NX)=0.5*C(I+NT-NX)
   10 CONTINUE
      J=NT-NX+1
      DO 11 I=1,J,NX
      C(I)=0.5*C(I)
      C(I+NX-1)=0.5*C(I+NX-1)
   11 CONTINUE
```

Table 2 (Continued)

```
      J=NT-1
      DO 12 I=1,J
      TAVE=(T(I)+T(I+1))/2.
      TC=(B1+B2*TAVE+B3*TAVE**2)/3600.
      R(I)=X*(YN-2.)/(Y*TC*(XN-1.))
12    CONTINUE
      J=NX-1
      DO 13 I=1,J
      R(I)=4.0*R(I)
      R(I+NX)=2.0*R(I+NX)
      R(I+NX+NX)=4./3.*R(I+NX+NX)
      R(I+NT-NX)=2.*R(I+NT-NX)
13    CONTINUE
      J=100+NT-NX
      DO 14 I=101,J
      TAVE=(T(I-100)+T(I-100+NX))/2.
      TC=(B1+B2*TAVE+B3*TAVE**2)/3600.
      R(I)=Y*(XN-1.)/(X*TC*(YN-2.))
14    CONTINUE
      J=100+NX
      DO 15 I=101,J
      R(I)=0.5*R(I)
      R(I+NX)=0.625*R(I+NX)
      R(I+NX+NX)=0.875*R(I+NX+NX)
      IF(NY.EQ.4) R(I+NT-NX-NX)=.715*R(I+NT-NX-NX)
      IF(NY.GT.4) R(I+NT-NX-NX)=.750*R(I+NT-NX-NX)
15    CONTINUE
      J=101+NT-NX-NX
      DO 16 I=101,J,NX
      R(I)=2.*R(I)
      R(I+NX-1)=2.*R(I+NX-1)
16    CONTINUE
      DO 17 I=NX,NT,NX
      R(I)=9999999.
17    CONTINUE
      RC(1)=C(1)/(1./R(1)+1./R(101)+(H(1)*X)/(24.*(XN-1.)))
      RC(NX)=C(NX)/(1./R(NX-1)+1./R(NX+100)+(H(NX)*X)/(24.*(XN-1.)))
      RC(NT)=C(NT)/(1./R(NT-1)+1./R(100+NT-NX))
      J=NX-1
      DO 18 I=2,J
      RC(I)=C(I)/(1./R(I)+1./R(I-1)+1./R(I+100)+(H(I)*X)/(12.*(XN-1.)))
18    CONTINUE
      J=NX+1
      K=NT-NX
      DO 19 I=J,K
      RC(I)=C(I)/(1./R(I)+1./R(I-1)+1./R(I+100)+1./R(I+100-NX))
19    CONTINUE
```

Table 2 (Continued)

```
      J=NT-NX+1
      K=NT-1
      DO 20 I=J,K
      RC(I)=C(I)/(1./R(I)+1./R(I-1)+1./R(I+100-NX))
   20 CONTINUE
C     DETERMINE MINIMUM R-C PRODUCT AND COMPUTING INTERVAL
      RCMIN=RC(1)
      DO 21 I=2,NT
      IF(RC(I).LT.RCMIN) RCMIN=RC(I)
   21 CONTINUE
   22 DELTIM=0.5*RCMIN
      IF(TYME.GT.0..OR.(DELTIM/TIMMAX).GT..005) GO TO 23
      IF(NY.LE.4) GO TO 23
      NY=NY-1
      YN=NY
      TN=YN*XN
      NT=TN
      GO TO 8
   23 CONTINUE
      IF (DELTIM.GT.TIMMIN/20..AND.TYME.LT.TIMMIN) DELTIM=TIMMIN/20.
      IF (TYME+DELTIM.GT.TPRINT) DELTIM=TPRINT-TYME
C     PERFORM HEAT BALANCES - COMPUTE NEW TEMPERATURES
      J=NX-1
      DO 24 I=2,J
      T(I)=TOLD(I)+DELTIM/C(I)*(H(I)*X*(TAW-TOLD(I))/(12.*(XN-1.))+
     1 (TOLD(I+1)-TOLD(I))/R(I)+(TOLD(I-1)-TOLD(I))/R(I-1)+
     2 (TOLD(I+NX)-TOLD(I))/R(I+100))
   24 CONTINUE
      J=NT-NX+1
      K=NT-1
      DO 25 I=J,K
      T(I)=TOLD(I)+DELTIM/C(I)*((TOLD(I+1)-TOLD(I))/R(I)+
     1 (TOLD(I-1)-TOLD(I))/R(I-1)+(TOLD(I-NX)-TOLD(I))/R(I+100-NX))
   25 CONTINUE
      J=NX+1
      K=NT-NX
      DO 26 I=J,K
      T(I)=TOLD(I)+DELTIM/C(I)*((TOLD(I+1)-TOLD(I))/R(I)+(TOLD(I-1)-
     1 TOLD(I))/R(I-1)+(TOLD(I-NX)-TOLD(I))/R(I+100-NX)+(TOLD(I+NX)-
     2 TOLD(I))/R(I+100))
   26 CONTINUE
      T(1)=TOLD(1)+DELTIM/C(1)*(H(1)*X*(TAW-TOLD(1))/(24.*(XN-1.))+
     1 (TOLD(2)-TOLD(1))/R(1)+(TOLD(1+NX)-TOLD(1))/R(101))
      T(NX)=TOLD(NX)+DELTIM/C(NX)*(H(NX)*X*(TAW-TOLD(NX))/(24.*(XN-1.))+
     1 (TOLD(NX-1)-TOLD(NX))/R(NX-1)+(TOLD(NX+NX)-TOLD(NX))/R(100+NX))
      T(NT)=TOLD(NT)+DELTIM/C(NT)*((TOLD(NT-1)-TOLD(NT))/R(NT-1)+
     1 (TOLD(NT-NX)-TOLD(NT))/R(100+NT-NX))
      KODE=0
```

Table 2 (Continued)

```
      DO 27 I=1,NX
      IF(TOLD(I).LT.TPC.AND.T(I).GE.TPC) TIMEC(I)=TYME+DELTIM*
     1 (TPC-TOLD(I))/(T(I)-TOLD(I))
      IF(T(I).LT.TPC) KODE=1
   27 CONTINUE
      DO 28 I=1,NT
      TOLD(I)=T(I)
   28 CONTINUE
C     AT TIME ZERO LIST THE INPUT DATA AND ALL RESISTORS AND CAPACITORS
      IF(TYME.GT.0.) GO TO 208
      IF (ITER.NE.0) GO TO 208
      WRITE (6,200) NP
  200 FORMAT (///1X,58(1H*),10H  PROBLEM ,I2,2X,58(1H*))
      WRITE (6,201) NX,NY,X,Y,TI,TPC,TAW
  201 FORMAT (9H       NX=,I2,8H      NY=,I2,7H      X=,F6.3,11H IN.      Y=
     1,F6.4,12H IN.      TI=,F5.1,15H DEG.F      TPC=,F5.1,15H DEG.F      T
     2AW=,F6.1,6H DEG.F)
      WRITE (6,202) RHO,A1,A2,A3,B1,B2,B3
  202 FORMAT (14H       DENSITY=,F5.1,12H PCF      CP=,F6.4,1H+,F8.6,2HT+,
     1F8.6,16HT2 BTU/LB F    K=,F10.7,1H+,F10.8,2HT+,F10.8,15HT2 BTU/FT H
     2R F )
      WRITE (6,203) NT,TI
  203 FORMAT (58H                                                    CAPACITORS
     1 1=,I2,10H BASED ON ,F5.1,18H DEG.F , BTU/DEG.F)
      NFMT1(2)=NF(NX)
      NFMT2(2)=NF(NX)
      NFMT3(2)=NF(NX)
      WRITE (6,NFMT1) (C(I),I=1,NT)
      J=NT-1
      WRITE (6,204) J,TI
  204 FORMAT (57H                                                    RESISTORS
     11=,I2,10H BASED ON ,F5.1,22H DEG.F , SEC DEG.F/BTU)
      WRITE (6,NFMT2) (R(I),I=1,J)
      J=100+NT-NX
      WRITE (6,205) J,TI
  205 FORMAT (59H                                                    RESISTORS
     1101=,I3,10H BASED ON ,F5.1,22H DEG.F , SEC DEG.F/BTU)
      WRITE (6,NFMT2) (R(I),I=101,J)
      WRITE (6,206) NT,TI
  206 FORMAT (59H                                                    RC PRODUCT
     1S 1=,I2,10H BASED ON ,F5.1,14H DEG.F , SEC  )
      WRITE (6,NFMT3) (RC(I),I=1,NT)
      WRITE (6,207) NX
  207 FORMAT (86H                                                    SURFACE TE
     1MPERATURE HISTORIES ( T1 THRU T,I2,10H ) , DEG.F )
  208 IF (TYME.EQ.0.) WRITE (6,209) ITER
  209 FORMAT (12H  ITERATION ,I2)
      TYME=TYME+DELTIM
      IF (TYME.EQ.DELTIM) WRITE (6,210) (TS(I),I=1,NX)
  210 FORMAT (119H TIME,SEC  T(1)    T(2)    T(3)    T(4)    T(5)    T(6
     1)    T(7)    T(8)    T(9)   T(10)   T(11)   T(12)   T(13)   T(14)/
     21X,7H   .000,14F8.2)
```

Table 2 (concluded)

```
C       TABULATE SURFACE TEMPERATURE HISTORIES FOR EACH ITERATION
        IF(KODE.EQ.1.AND.ABS(TPRINT-TYME).GT..001) GO TO 29
        WRITE (6,211) TYME,(T(I),I=1,NX)
  211   FORMAT (1X,F7.3,14F8.2)
        TPRINT=TYME+PRINTI
   29   CONTINUE
        IF(KODE.EQ.1) GO TO 8
C       IF ALL SURFACE TEMPS EXCEED THE MELT TEMP DETERMINE THE DIFFERENCE
C       BETWEEN COMPUTED AND EXPERIMENTAL MELT TIMES FOR EACH SURFACE NODE
        DO 30 I=1,NX
        DISCR=(TIMEC(I)-TIME(I))/TIME(I)
        IF(ABS(DISCR).GT..03) KODE=1
   30   CONTINUE
        IF(KODE.EQ.0) GO TO 214
        DO 33 I=1,NX
        IF (ITER.GT.0) GO TO 31
        EX(I)=0.5
        GO TO 32
   31   EX(I)=ALOG10((TIMECP(I)/TIME(I))**EXPR(I))/ALOG10(TIMECP(I)/
       1 TIMEC(I))
        IF (EX(I).GT.5.) EX(I)=5.
        IF (EX(I).LT..2) EX(I)=.2
   32   H(I)=H(I)*(TIMEC(I)/TIME(I))**EX(I)
        TIMECP(I)=TIMEC(I)
        EXPR(I)=EX(I)
        HHSIS(I)=H(I)/HSIS(I)
   33   CONTINUE
        ITER=ITER+1
        IF(ITER.GT.15) GO TO 212
        TYME=0.
        TPRINT=PRINTI
        DO 34 I=1,NT
        T(I)=TI
        TOLD(I)=TI
   34   CONTINUE
        GO TO 8
C       TABULATE FINAL RESULTS
  212   WRITE (6,213) NP,ITER
  213   FORMAT (9H0PROBLEM ,I2,24H DID NOT CONVERGE AFTER ,I2,41H ITERATIO
       1NS - FINAL CALCULATIONS FOLLOW    )
        GO TO 216
  214   WRITE (6,215) NP,ITER
  215   FORMAT (9H0PROBLEM ,I2,17H CONVERGED AFTER ,I2,41H ITERATIONS - FI
       1NAL CALCULATIONS FOLLOW    )
  216   WRITE (6,217) (XD(I),I=1,NX)
        WRITE (6,218) (TIMEC(I),I=1,NX)
        WRITE (6,219) (TIME(I),I=1,NX)
        WRITE (6,220) (H(I),I=1,NX)
        WRITE (6,221) (HHSIS(I),I=1,NX)
  217   FORMAT (20H SURFACE DISTANCE,IN ,14F8.4)
  218   FORMAT (20H CALC MELT TIMES,SEC ,14F8.2)
  219   FORMAT (20H TEST MELT TIMES,SEC ,14F8.2)
  220   FORMAT (20H HTC,BTU/FT SQ SEC F ,14F8.6)
  221   FORMAT (20H H / H SEMI-INF SLAB ,14F8.4)
        NP=NP+1
  999   CONTINUE
        END
```

Table 3

LISTING FOR PROGRAM II

```
      DIMENSION C(98),R(185),RC(98),T(98),TOLD(98),H(28),TIME(28),
     1 TIMEC(28),XD(14),HSIS(28),HHSIS(28),EX(28),EXPR(28),TIMECP(28),
     2 N (14),NFMT1(3),NFMT2(3),NFMT3(3),TS(14),Y(15),TIME1(14),
     3 TIME2(14)
      DATA NF/84H 1      2      3      4      5      6      7      8      9     1
     10     11     12     13     14     /
      DATA NFMT1/18H(1X,  14     F9.7) /
      DATA NFMT2/18H(1X,  14     F9.0) /
      DATA NFMT3/18H(1X,  14     F9.4) /
      READ (5,99) NC
   99 FORMAT (I10)
      NP=1
      READ (5,100) RHO,A1,A2,A3,B1,B2,B3
  100 FORMAT (1F10.4,6F10.8)
      DO 999 I1=1,NC
      READ (5,101) NX,X,TI,TPC1,TPC2,TAW1,TAW2,PRINTI
  101 FORMAT (I10,7F10.4)
      IF (NX.GT.14) NX=14
      NY=7
      XN=NX
      YN=NY
      TN=YN*XN
      NT=TN
      N2=2*NX
      N3=3*NX
      N4=4*NX
      N5=5*NX
      READ (5,102) Y
  102 FORMAT (15F5.4)
      Y(NX+1)=Y(NX)
      READ (5,103) TIME1
      READ (5,103) TIME2
  103 FORMAT(14F5.2)
      DO 1 I=1,NX
      TIME(I)=TIME1(I)
    1 CONTINUE
      J=NX+1
      DO 2 I=J,N2
      K=I-NX
      TIME(I)=TIME2(K)
    2 CONTINUE
      DO 3 I=1,14
      TS(I)=TI
    3 CONTINUE
      TM=(TI+TPC1+TPC2)/3.
      CPI=A1+A2*TM+A3*TM**2
      TCI=(B1+B2*TM+B3*TM**2)/3600.
      XD(1)=0.
```

Table 3 (Continued)

```
      DO 4 I=2,NX
      XD(I)=XD(I-1)+X/(XN-1.)
    4 CONTINUE
      TIMMAX=TIME(1)
      TIMMIN=TIME(1)
      DO 5 I=2,N2
      IF (TIME(I).GT.TIMMAX) TIMMAX=TIME(I)
      IF (TIME(I).LT.TIMMIN) TIMMIN=TIME(I)
    5 CONTINUE
      DO 6 I=1,98
      T(I)=TI
      TOLD(I)=TI
    6 CONTINUE
      TYME=0.
      TPRINT=PRINTI
      ITER=0
C     GUESS HEAT TRANSFER COEFFICIENTS USING SEMI-INFINITE SLAB SOLUTION
      TBAR1=(TPC1-TI)/(TAW1-TI)
      TBAR2=(TPC2-TI)/(TAW2-TI)
      IF(TBAR1.LT..03) BETA1=.9*TBAR1
      IF(TBAR2.LT..03) BETA2=.9*TBAR2
      IF(TBAR1.GE..03.AND.TBAR1.LT..08) BETA1=1.042*TBAR1**1.04
      IF(TBAR2.GE..03.AND.TBAR2.LT..08) BETA2=1.042*TBAR2**1.04
      IF(TBAR1.GE..08.AND.TBAR1.LT..14) BETA1=1.185*TBAR1**1.09
      IF(TBAR2.GE..08.AND.TBAR2.LT..14) BETA2=1.185*TBAR2**1.09
      IF(TBAR1.GE..14.AND.TBAR1.LT..20) BETA1=1.338*TBAR1**1.15
      IF(TBAR2.GE..14.AND.TBAR2.LT..20) BETA2=1.338*TBAR2**1.15
      IF(TBAR1.GE..20.AND.TBAR1.LT..30) BETA1=1.600*TBAR1**1.26
      IF(TBAR2.GE..20.AND.TBAR2.LT..30) BETA2=1.600*TBAR2**1.26
      IF(TBAR1.GE..30.AND.TBAR1.LT..40) BETA1=1.950*TBAR1**1.42
      IF(TBAR2.GE..30.AND.TBAR2.LT..40) BETA2=1.950*TBAR2**1.42
      IF(TBAR1.GE..40.AND.TBAR1.LT..50) BETA1=2.490*TBAR1**1.70
      IF(TBAR2.GE..40.AND.TBAR2.LT..50) BETA2=2.490*TBAR2**1.70
      IF(TBAR1.GE..50.AND.TBAR1.LT..60) BETA1=2.840*TBAR1**1.88
      IF(TBAR2.GE..50.AND.TBAR2.LT..60) BETA2=2.840*TBAR2**1.88
      IF(TBAR1.GE..60.AND.TBAR1.LT..70) BETA1=3.930*TBAR1**2.48
      IF(TBAR2.GE..60.AND.TBAR2.LT..70) BETA2=3.930*TBAR2**2.48
      RHOCK=RHO*CPI*TCI
      DO 7 I=1,NX
      HSIS(I)=BETA1*SQRT(RHOCK/TIME(I))
      HSIS(I+NX)=BETA2*SQRT(RHOCK/TIME(I+NX))
      TDT=.2*(Y(I)/24.)**2*RHO*CPI/TCI
      TPCTD1=TIME(I)/TDT
      TPCTD2=TIME(I+NX)/TDT
      COR1=1.
      COR2=1.
      IF(TPCTD1.GT.2.5) COR1=1.41*TPCTD1**-.37
      IF(TPCTD2.GT.2.5) COR2=1.41*TPCTD2**-.37
      H(I)=HSIS(I)*COR1
      H(I+NX)=HSIS(I+NX)*COR2
```

Table 3 (Continued)

```
      HHSIS(I)=H(I)/HSIS(I)
      HHSIS(I+NX)=H(I+NX)/HSIS(I+NX)
    7 CONTINUE
C     COMPUTE RESISTORS AND CAPACITORS   ONLY ONCE IF NOT TEMP-DEPENDENT
    8 IF(TYME.GT.0..AND.A2.EQ.0..AND.A3.EQ.0..AND.B2.EQ.0..AND.B3.EQ.0.)
     1 GO TO 22
      K=NT-NX+1
      DO 10 I=1,K,NX
      L=I+NX-1
      F=1.
      IF(I.EQ.(NX+1).OR.I.EQ.(NT-N2+1)) F=2.
      IF(I.EQ.(N2+1).OR.I.EQ.(NT-N3+1)) F=3.
      IF(I.EQ.(N3+1))                   F=4.
      N=1
      DO 9 J=I,L
      CP=A1+A2*T(J)+A3*T(J)**2
      C(J)=RHO*CP*X*Y(N)/(2304.*(XN-1.))*F
      TAVE=(T(J)+T(J+1))/2.
      TC=(B1+B2*TAVE+B3*TAVE**2)/3600.
      R(J)=32.*X/(TC*(XN-1.)*(Y(N)+Y(N+1)))/F
      N=N+1
    9 CONTINUE
   10 CONTINUE
      K=101+NT-N2
      DO 12 I=101,K,NX
      L=I+NX-1
      F=1.
      IF(I.EQ.(NX+101).OR.I.EQ.(NT+101-N3)) F=1.25
      IF(I.EQ.(N2+101).OR.I.EQ.(NT+101-N4)) F=1.75
      N=1
      DO 11 J=I,L
      TAVE=(T(J-100)+T(J+NX-100))/2.
      TC=(B1+B2*TAVE+B3*TAVE**2)/3600.
      R(J)=Y(N)*(XN-1.)/(8.*TC*X)*F
      N=N+1
   11 CONTINUE
   12 CONTINUE
      J=NT-NX+1
      DO 13 I=1,J,NX
      C(I)=.5*C(I)
      C(I+NX-1)=.5*C(I+NX-1)
   13 CONTINUE
      DO 14 I=NX,NT,NX
      R(I)=9999999.
   14 CONTINUE
      J=101+NT-N2
      DO 15 I=101,J,NX
      R(I)=2.*R(I)
      R(I+NX-1)=2.*R(I+NX-1)
   15 CONTINUE
```

Table 3 (Continued)

```
      RC(1)=C(1)/(1./R(1)+1./R(101)+(H(1)*X)/(24.*(XN-1.)))
      RC(NX)=C(NX)/(1./R(NX-1)+1./R(100+NX)+(H(NX)*X)/(24.*(XN-1.)))
      RC(NT-NX+1)=C(NT-NX+1)/(1./R(NT-NX+1)+1./R(101+NT-N2)+(H(NX+1)*X)/
     1 (24.*(XN-1.)))
      RC(NT)=C(NT)/(1./R(NT-1)+1./R(100+NT-NX)+(H(N2)*X)/(24.*(XN-1.)))
      J=NX-1
      DO 16 I=2,J
      RC(I)=C(I)/(1./R(I)+1./R(I-1)+1./R(I+100)+(H(I)*X)/(12.*(XN-1.)))
   16 CONTINUE
      J=NT-NX+2
      K=NT-1
      DO 17 I=J,K
      RC(I)=C(I)/(1./R(I)+1./R(I+1)+1./R(I+100-NX)+(H(I+N2-NT)*X)/
     1 (12.*(XN-1.)))
   17 CONTINUE
      J=NX+1
      K=NT-NX
      DO 18 I=J,K
      RC(I)=C(I)/(1./R(I)+1./R(I-1)+1./R(I+100)+1./R(I+100-NX))
   18 CONTINUE
C     DETERMINE MINIMUM R*C PRODUCT AND COMPUTING INTERVAL
      RCMIN=RC(1)
      DO 21 I=2,NT
      IF(RC(I).LT.RCMIN) RCMIN=RC(I)
   21 CONTINUE
   22 DELTIM=0.5*RCMIN
      IF (DELTIM.GT.TIMMIN/20..AND.TYME.LT.TIMMIN) DELTIM=TIMMIN/20.
      IF (TYME+DELTIM.GT.TPRINT) DELTIM=TPRINT-TYME
C     PERFORM HEAT BALANCES - COMPUTE NEW TEMPERATURES
      J=NX-1
      DO 24 I=2,J
      T(I)=TOLD(I)+DELTIM/C(I)*(H(I)*X*(TAW1-TOLD(I))/(12.*(XN-1.))+
     1 (TOLD(I+1)-TOLD(I))/R(I)+(TOLD(I-1)-TOLD(I))/R(I-1)+
     2 (TOLD(I+NX)-TOLD(I))/R(I+100))
   24 CONTINUE
      J=NT-NX+2
      K=NT-1
      DO 25 I=J,K
      T(I)=TOLD(I)+DELTIM/C(I)*(H(I+N2-NT)*X*(TAW2-TOLD(I))/(12.*(XN-1.)
     1)+(TOLD(I+1)-TOLD(I))/R(I)+(TOLD(I-1)-TOLD(I))/R(I-1)
     2 +(TOLD(I-NX)-TOLD(I))/R(I+100-NX))
   25 CONTINUE
      J=NX+1
      K=NT-NX
      DO 26 I=J,K
      T(I)=TOLD(I)+DELTIM/C(I)*((TOLD(I+1)-TOLD(I))/R(I)+(TOLD(I-1)-
     1 TOLD(I))/R(I-1)+(TOLD(I-NX)-TOLD(I))/R(I+100-NX)+(TOLD(I+NX)-
     2 TOLD(I))/R(I+100))
   26 CONTINUE
```

Table 3 (Continued)

```
      T(1)=TOLD(1)+DELTIM/C(1)*(H(1)*X*(TAW1-TOLD(1))/(24.*(XN-1.))+
     1 (TOLD(2)-TOLD(1))/R(1)+(TOLD(1+NX)-TOLD(1))/R(101))
      T(NX)=TOLD(NX)+DELTIM/C(NX)*(H(NX)*X*(TAW1-TOLD(NX))/(24.*(XN-1.))
     1+(TOLD(NX-1)-TOLD(NX))/R(NX-1)+(TOLD(NX+NX)-TOLD(NX))/R(100+NX))
      T(NT)=TOLD(NT)+DELTIM/C(NT)*(H(N2)*X*(TAW2-TOLD(NT))/(24.*(XN-1.))
     1 +(TOLD(NT-1)-TOLD(NT))/R(NT-1)+(TOLD(NT-NX)-TOLD(NT))/
     2 R(100+NT-NX))
      NN=NT-NX+1
      T(NN)=TOLD(NN)+DELTIM/C(NN)*(H(NX+1)*X*(TAW2-TOLD(NN))/(24.*(XN-1.
     1 ))+(TOLD(NN+1)-TOLD(NN))/R(NN)+(TOLD(NN-NX)-TOLD(NN))/R(100+NN-NX
     2 ))
      KODE=0
      DO 27 I=1,NX
      IF(TOLD(I).LT.TPC1.AND.T(I).GE.TPC1) TIMEC(I)=TYME+DELTIM*
     1 (TPC1-TOLD(I))/(T(I)-TOLD(I))
      IF(T(I).LT.TPC1) KODE=1
      IF(TOLD(I+NT-NX).LT.TPC2.AND.T(I+NT-NX).GE.TPC2) TIMEC(I+NX)=TYME+
     1 DELTIM*(TPC2-TOLD(I+NT-NX))/(T(I+NT-NX)-TOLD(I+NT-NX))
      IF(T(I+NT-NX).LT.TPC2) KODE=1
   27 CONTINUE
      DO 28 I=1,NT
      TOLD(I)=T(I)
   28 CONTINUE
C     AT TIME ZERO LIST THE INPUT DATA AND ALL RESISTORS AND CAPACITORS
      IF(TYME.GT.0.) GO TO 208
      IF (ITER.NE.0) GO TO 208
      WRITE (6,198) NP
  198 FORMAT (///1X,58(1H*),10H  PROBLEM ,I2,2X,58(1H*))
      WRITE (6,199) NX,NY,X,TI,TPC1,TPC2,TAW1,TAW2
  199 FORMAT (9H       NX=,I2,6H   NY=,I2,5H   X=,F6.3,10H IN.   TI=,F5.1
     1,10H F   TPC1=,F5.1,10H F   TPC2=,F5.1,10H F   TAW1=,F5.0,10H F
     2TAW2=,F5.0,2H F)
      WRITE (6,200) RHO,A1,A2,A3,B1,B2,B3
  200 FORMAT (14H       DENSITY=,F5.1,12H PCF     CP=,F6.4,1H+,F8.6,2HT+,
     1F8.6,16HT2 BTU/LB F   K=,F10.7,1H+,F10.8,2HT+,F10.8,15HT2 BTU/FT H
     2R F )
      WRITE (6,201) (XD(I),I=1,NX)
  201 FORMAT (80H                                                  NETWORK
     1 DIMENSIONS (INCHES)         /3H X=,14F8.4)
      WRITE (6,202) (Y(I),I=1,NX)
  202 FORMAT (3H Y=,14F8.4)
      WRITE (6,203) NT,TI
  203 FORMAT (58H                                                CAPACITORS
     1 1=,I2,10H BASED ON ,F5.1,18H DEG.F , BTU/DEG.F)
      NFMT1(2)=NF(NX)
      NFMT2(2)=NF(NX)
      NFMT3(2)=NF(NX)
      WRITE (6,NFMT1) (C(I),I=1,NT)
      J=NT-1
      WRITE (6,204) J,TI
```

Table 3 (Continued)

```
 204  FORMAT (57H                                                    RESISTORS
     11=,I2,10H BASED ON ,F5.1,22H DEG.F , SEC DEG.F/BTU)
      WRITE (6,NFMT2) (R(I),I=1,J)
      J=100+NT-NX
      WRITE (6,205) J,TI
 205  FORMAT (59H                                                    RESISTORS
     1101=,I3,10H BASED ON ,F5.1,22H DEG.F , SEC DEG.F/BTU)
      WRITE (6,NFMT2) (R(I),I=101,J)
      WRITE (6,206) NT,TI
 206  FORMAT (59H                                                    RC PRODUCT
     1S 1=,I2,10H BASED ON ,F5.1,14H DEG.F , SEC  )
      WRITE (6,NFMT3) (RC(I),I=1,NT)
      WRITE (6,207)
 207  FORMAT(85H                                    SURFACE TEMPERATURE HIS
     1TORIES,SIDES 1 AND 2, DEG.F           )
 208  IF (TYME.EQ.0.) WRITE (6,209) ITER
 209  FORMAT (12H  ITERATION ,I2)
      TYME=TYME+DELTIM
      IF (TYME.EQ.DELTIM) WRITE (6,210)
 210  FORMAT (119H TIME(SEC) X(1)     X(2)     X(3)     X(4)     X(5)     X(6
     1)     X(7)     X(8)     X(9)    X(10)    X(11)    X(12)    X(13)    X(14))
C     TABULATE SURFACE TEMPERATURE HISTORIES FOR EACH ITERATION
      IF (TYME.EQ.DELTIM)WRITE (6,211)(TS(I),I=1,NX)
 211  FORMAT (8H     .000,14F8.2)
      IF (TYME.EQ.DELTIM)WRITE (6,212)(TS(I),I=1,NX)
 212  FORMAT (8H         ,14F8.2)
      IF(KODE.EQ.1.AND.ABS(TPRINT-TYME).GT..001) GO TO 29
      WRITE (6,213) TYME,(T(I),I=1,NX)
 213  FORMAT (1X,F7.3,14F8.2)
      J=NT-NX+1
      WRITE (6,214) (T(I),I=J,NT)
 214  FORMAT (8X,14F8.2)
      TPRINT=TYME+PRINTI
 29   CONTINUE
      IF(KODE.EQ.1) GO TO 8
C     IF ALL SURFACE TEMPS EXCEED THE MELT TEMP DETERMINE THE DIFFERENCE
C     BETWEEN COMPUTED AND EXPERIMENTAL MELT TIMES FOR EACH SURFACE NODE
      DO 30 I=1,N2
      DISCR=(TIMEC(I)-TIME(I))/TIME(I)
      IF(ABS(DISCR).GT..03) KODE=1
 30   CONTINUE
      IF(KODE.EQ.0) GO TO 217
      DO 33 I=1,N2
      IF (ITER.GT.0) GO TO 31
      EX(I)=0.5
      GO TO 32
 31   EX(I)=ALOG10((TIMECP(I)/TIME(I))**EXPR(I))/ALOG10(TIMECP(I)/
     1 TIMEC(I))
      IF (EX(I).GT.5.) EX(I)=5.
      IF (EX(I).LT..2) EX(I)=.2
```

Table 3 (Concluded)

```
 32   H(I)=H(I)*(TIMEC(I)/TIME(I))**EX(I)
      TIMECP(I)=TIMEC(I)
      EXPR(I)=EX(I)
      HHSIS(I)=H(I)/HSIS(I)
 33   CONTINUE
      ITER=ITER+1
      IF (ITER.GT.15) GO TO 215
      TYME=0.
      TPRINT=PRINTI
      DO 34 I=1,NT
      T(I)=TI
      TOLD(I)=TI
 34   CONTINUE
      GO TO 8
C     TABULATE FINAL RESULTS
 215  WRITE (6,216) NP,ITER
 216  FORMAT (9HOPROBLEM ,I2,24H DID NOT CONVERGE AFTER ,I2,41H ITERATIO
     1NS - FINAL CALCULATIONS FOLLOW    )
      GO TO 219
 217  WRITE (6,218) NP,ITER
 218  FORMAT (9HOPROBLEM ,I2,17H CONVERGED AFTER ,I2,41H ITERATIONS - FI
     1NAL CALCULATIONS FOLLOW    )
 219  WRITE (6,220)
      WRITE (6,221) (   XD(I),I=1,NX)
      WRITE (6,222) (    Y(I),I=1,NX)
      WRITE (6,223) (TIMEC(I),I=1,NX)
      WRITE (6,224) ( TIME(I),I=1,NX)
      WRITE (6,225) (    H(I),I=1,NX)
      WRITE (6,226) (HHSIS(I),I=1,NX)
      WRITE (6,227)
      J=NX+1
      WRITE (6,221) (   XD(I),I=1,NX)
      WRITE (6,222) (    Y(I),I=1,NX)
      WRITE (6,223) (TIMEC(I),I=J,N2)
      WRITE (6,224) ( TIME(I),I=J,N2)
      WRITE (6,225) (    H(I),I=J,N2)
      WRITE (6,226) (HHSIS(I),I=J,N2)
 220  FORMAT(8H SIDE 1 )
 221  FORMAT(20H SURFACE DISTANCE,IN ,14F8.4)
 222  FORMAT(20H LOCAL THICKNESS ,IN ,14F8.4)
 223  FORMAT(20H CALC MELT TIMES,SEC ,14F8.2)
 224  FORMAT(20H TEST MELT TIMES,SEC ,14F8.2)
 225  FORMAT(20H HTC,BTU/FT SQ SEC F ,14F8.6)
 226  FORMAT(20H H / H SEMI-INF SLAB ,14F8.4)
 227  FORMAT(8H SIDE 2 )
      NP=NP+1
 999  CONTINUE
      END
```

Table 4

DATA REDUCTION PROGRAM VARIABLES

A1, A2, A3	Constants in specific heat equation $c = A1 + A2\ T + A3\ T^2$
B1, B2, B3	Constants in thermal conductivity equation $k = B1 + B2\ T + B3\ T^2$
BETA	Parameter in semi-infinite slab theory, $h\sqrt{t}/\sqrt{\rho\ ck}$
C	Thermal capacitance, Btu/^{o}F
CORR, COR1, COR2	Approximate correction to semi-infinite slab theory to account for finite-slab effects
CP	Specific heat, Btu/lb^{o}F
CPI	Specific heat based on average temperature TM, Btu/lb^{o}F
DELTIM	Computing interval, sec
DISCR	Discrepancy between input and computed phase-change time
EX	Exponent in assumption $H(TIMEC)^{EX}$ = constant
EXPR	Exponent EX used during previous computing cycle
FOUR	Fourier number (TC) (TIMMIN)/(RHO) (CPI) (Y^2)
H	Heat transfer coefficient, Btu/ft^2 sec ^{o}F
HHSIS	Heat transfer coefficient ratio H/HSIS
HSIS	Heat transfer coefficient determined by application of semi-infinite slab theory, Btu/ft^2 sec ^{o}F
ITER	Iteration number
KODE	Code, = 0 if problem is solved; = 1 if unsolved
NC	Number of problems to be run consecutively
NF, NFMT1, NFMT2, NFMT3	Output format variables
NP	Problem number
NT, TN	Total number of nodes (product of NX and NY)

Table 4 (Continued)

NX, XN	Number of nodes in X direction
NY, YN	Number of nodes in Y direction
PRINTI	Print interval for surface temperature histories, sec
R	Thermal resistance, sec $^{o}F/Btu$
RC	Equivalent resistance - capacitance product, sec
RCMIN	Minimum RC product
RHO	Material density, lb/ft^3
RHOCK	Density-specific heat-conductivity product, Btu^2/ft^4 sec $^{o}F^2$
T	Temperature, ^{o}F
TAVE	Average temperature of two adjacent nodes, ^{o}F
TAW, TAW1, TAW2	Adiabatic wall temperature, ^{o}F
TBAR, TBAR1, TBAR2	Parameter in semi-infinite slab theory $(T_{pc}-T_i)/(T_{aw}-T_i)$
TC	Thermal conductivity, Btu/ft hr ^{o}F
TCI	Conductivity based on average temperature TM, Btu/ft hr ^{o}F
TDT	Thermal diffusion time, $0.2\ Y^2$ (RHO) (CPI)/(TCI), sec
TI	Initial slab temperature, ^{o}F
TIME, TIME1, TIME2	Experimental melt time, sec
TIMEC	Computed melt time, sec
TIMECP	Computed melt time during previous cycle, sec
TIMMAX	Maximum experimental melt time, sec
TIMMIN	Minimum experimental melt time, sec
TM	Average of initial and phase-change temperature, ^{o}F

Table 4 (Concluded)

TN	Same as NT
TOLD	Temperature computed during previous cycle, ^{o}F
TPC, TPC1, TPC2	Coating phase-change temperature, ^{o}F
TPCTDT, TPCTD1, TPCTD2	Ratio TIME/TDT
TPRINT	Next print time, sec
TS	Initial surface temperature (same as TI), ^{o}F
TYME	Problem time, i.e., time from start of heating, sec
X	Width of slab, i.e., distance between nodes 1 and NX, in.
XN	Same as NX
XD	Distance from node 1 measured parallel to heated surface, in.
Y	Depth of slab, in.
YMIN	Minimum depth of slab for negligible backface temperature rise, in.
YN	Same as NY

REFERENCES

1. Jones, R. A., & Hunt, J. L., Use of Fusible Temperature Indicators for Obtaining Quantitative Aerodynamic Heat-Transfer Data, NASA TR R-230, February 1966

2. Schultz, H. D., Computer Programs for Phase-Change Coating Heat Transfer Data Reduction, LMSC-A993384, September 1971

3. Eckert, E. R. G., Survey on Heat Transfer at High Speeds, WADC TR 54-70, April 1954

4. Creager, M. O., The Effect of Leading Edge Sweep and Surface Inclination on the Hypersonic Flow Field Over a Blunt Flat Plate, NASA Memo 12-26-58A, January 1959

5. Bertram, M. and Feller, W., A simple Method for Determining Heat Transfer, Skin Friction, and Boundary Layer Thickness for Hypersonic Laminer Boundary Layer Flows in a Pressure Gradient, NASA Memo 5-24-59L, June 1959

6. Schultz, H. D. and Baker, R. C., Pressure and Heat Transfer Measurements in Regions of Three-Dimensional Shockwave-Boundary Layer Interactions, LMSC-D157341, March 1972

7. Wentink, T., High Temperature Behavior of Teflon, AVCO-Everett Research Report-55, July 1959

8. Dunavant, J. C., "Variation of Stycast Thermophysical Properties," Paper presented at NASA Space Shuttle Aerothermodynamics/Configuration Working Group Meeting, NASA Ames Research Center, June 1971

9. Charwat, A. F. and Redekopp, L. G., "Supersonic Interference Flow Along the Corner of Intersecting Wedges," AIAA Journal, March 1967

10. Stainback, P. C. and Weinstein, L. M., Aerodynamic Heating in the Vicinity of Corners at Hypersonic Speeds, NASA TN D-4130, November 1967

11. Hayes, W. D. and Probstein, R. F., Hypersonic Flow Theory, Academic Press, 1959

12. Erdos, J. and Pallone, A., "Shock-Boundary Layer Interaction Flow Separation," Proceedings of the 1962 Heat Transfer and Fluid Mechanics Institute, Stanford University Press, 1962

13. Gulbran, C. E., Redeker, E., Miller, D.S. and Strack, S. L., Heating In Regions of Interfering Flow Fields, Part I: Two- and Three-Dimensional Laminar Interactions at Mach 8, AFFDL TR-65-49; Part I, July 1965

14. Neumann, R. D. and Burke, F. L., The Influence of Shock Wave - Boundary Layer Effects on the Design of Hypersonic Aircraft, AFFDL TR-68-152, March 1969

15. Watson, R. D. and Weinstein, L. M., "A Study of Hypersonic Corner Flow Interactions," AIAA Paper 70-227, January 1970

16. Sayano, S., Heat Transfer in Shock Wave-Turbulent Boundary Layer Interaction Regions," Douglas Report SM-42567, November 1962

17. Miller, D. S., Hijman, R., Redeker, E., Janssen, W. C. and Muller, C. R., "A Study of Shock Impingement on Boundary Layers at Mach 16," Proceeding of the 1962 Heat Transfer and Fluid Mechanics Institute, Stanford University Press, 1962

18. Neumann, R. D., Recent Notes and Data on Interference Heating, AFFDL TM 71-16, August 1971

19. Schneider, P. J., Temperature Response Charts, John Wiley & Sons, 1963

20. Beckwith, I., Similar Solutions for the Compressible Boundary Layer on a Yawed Cylinder with Transpiration Cooling, NASA TR R-42, 1959

21. Thomas, A.C., et al, Advanced Reentry Systems Heat Transfer Manual For Hypersonic Flight, AFFDL TR-65-195, October 1966

Unclassified
Security Classification

DOCUMENT CONTROL DATA - R & D

(Security classification of title, body of abstract and indexing annotation must be entered when the overall report is classified)

1. ORIGINATING ACTIVITY *(Corporate author)* Lockheed Missiles & Space Co., Inc. Sunnyvale, California	2a. REPORT SECURITY CLASSIFICATION Unclassified 2b. GROUP

3. REPORT TITLE

Experimental and Analytical Investigation of Temperature Sensitive Paints

4. DESCRIPTIVE NOTES *(Type of report and inclusive dates)*

Final Report

5. AUTHOR(S) *(First name, middle initial, last name)*

Howard D. Schultz

6. REPORT DATE June 1972	7a. TOTAL NO. OF PAGES 92	7b. NO. OF REFS 21
8a. CONTRACT OR GRANT NO. F33615-71-C-1635 b. PROJECT NO. 1366 c. d.	9a. ORIGINATOR'S REPORT NUMBER(S) 9b. OTHER REPORT NO(S) *(Any other numbers that may be assigned this report)* AFFDL-TR-72-52	

10. DISTRIBUTION STATEMENT

Approved for public release, distribution unlimited

11. SUPPLEMENTARY NOTES	12. SPONSORING MILITARY ACTIVITY Air Force Flight Dynamics Laboratory Air Force Systems Command Wright-Patterson AFB, Ohio

13. ABSTRACT

This report presents the results of a study which consisted to two principal phases: (1) an analytical investigation to extend the validity of the temperature-sensitive coating technique for aerodynamic heating measurement to areas in which known theories do not apply, and (2) a combined analytical and experimental study to develop methods of predicting areas of high thermal gradients in an interfering flow field.

Two data reduction computer programs were developed to treat the general two-dimensional case of a finite-slab convectively heated on one or both sides. These programs provide an inverse solution to the two-dimensional transient heat conduction equation with surface heating gradients and variable thermal properties.

A three-dimensional shock interference wind tunnel model was designed, fabricated and tested in the AFFDL High Temperature Facility. The model is basically a sharp flat plate, instrumented for pressure and phase-change coating heat transfer measurements, with a shock generator fin mounted perpendicular to the plate along the edge. Tests were performed at a nominal Mach number of 10 and Reynolds number of 0.3×10^6 per foot.

By use of the temperature-sensitive coating technique, heating distributions in the interaction region have been identified in greater detail than is possible by use of thermocouple-instrumented models. Pressure and heating data are compared with theory and a procedure for estimating peak heating rates in the interaction region is recommended.

DD FORM 1 NOV 65 1473

Unclassified
Security Classification

14. KEY WORDS	LINK A		LINK B		LINK C	
	ROLE	WT	ROLE	WT	ROLE	WT
Aerodynamic Heat Transfer						
Shockwave – Boundary Layer Interaction						